To the Graduate Council:

I am submitting herewith a dissertation written by Laurel Anne Morton entitled "Tungsten Alkyl Alkylidyne and *Bis*(Alkylidene) Complexes. Their Unusual Inter-Conversion and Reactions with Phosphines, Dioxygen and Water." I have examined the final electronic copy of this dissertation for form and content and recommend that it be accepted in partial fulfillment of the requirements for the degree of Doctor of Philosophy, with a major in Chemistry.

Ziling (Ben) Xue
Major Professor

We have read this dissertation
and recommend its acceptance:

Craig E. Barnes

Charles D. Feigerle

X. Peter Zhang

John R. Collier

Accepted for the Council:

Anne Mayhew
Vice Chancellor and Dean
of the Graduate School

(Original signatures are on file with official student records.)

TUNGSTEN ALKYL ALKYLIDYNE AND *BIS*(ALKYLIDENE) COMPLEXES. THEIR UNUSUAL INTER-CONVERSION AND REACTIONS WITH PHOSPHINES, DIOXYGEN AND WATER

A Dissertation

Presented for the

Doctor of Philosophy Degree

The University of Tennessee, Knoxville

Laurel Anne Morton

August 2005

DEDICATION

This dissertation is dedicated to my loving husband, Sam, for his constant patience and understanding, and to my immediate family: Mom, Dad, Kim, Shannon, and Sara, for their unending love and support. I would not have made it through the past few years of graduate studies without their support.

ACKNOWLEDGEMENTS

There are numerous people whom I would like to thank that have, in some way or another, had an impact on my life during my doctoral studies. First and foremost, I would like to thank my research advisor, Professor Zi-Ling (Ben) Xue, for his immense help and patience with me over the past few years. He was an excellent mentor and advisor and has really gone above and beyond what I expected from a research advisor. I do not think I could have finished without his constant support and encouragement.

I would like to acknowledge my committee members: Dr. Craig Barnes, Dr. Peter Zhang, Dr. Charles Feigerle, and Dr. John Collier, for providing much needed guidance and reviews of this work.

The following individuals extended technical support for various aspects of my research at the University of Tennessee, for which I am grateful: Jason Clark and Dr. Hongjun Pan for their help with the 400 MHz NMR instrument, Dr. Chuck Campana at Bruker for his help in solving the crystal structure of the *bis*(alkylidene) complex **3b**, Dr. Al Tuinman for his wonderful mass spectrometry analyses, and finally Dr. John F. C. Turner whose guidance and expertise effected me in so many ways. I will be ever grateful for his technical support and friendship.

I extend thanks as well to the support staff in the chemistry department: Marilyn Ownby, Art Pratt, Rachelle Allen, Kelly Preston, Bill Gurley, Johnny

Jones, John Nelson, Carol Moulton, and Tray Allen. You have all made my life much more enjoyable over the past several years.

Of course I would like to thank all of my co-workers and colleagues, both past and present, for their friendships, for putting up with me, for many helpful discussions about my research, and for making the lab a productive and pleasant environment in which to work. Special thanks goes to Dr. Xianghua (Bruce) Yu for all his help with my crystal structures and many friendly discussions, to Lynn Rodman and Nathan Carrington, whose lunch banter will be missed, to Dr. Jaime Blanton for all her friendly female conversations which were greatly missed after she left, to He (Steve) Qiu and Dr. Shujian (Jim) Chen for the nice laboratory companionship. To former group members, Drs. Tianniu (Rick) Chen and Ruitao (Ray) Wang, you are missed, and I hope we meet again soon. To the newest Xue-group recruits, Jay Chocklett, Michael Bleakley, and Kristie Carter, thank you for the companionship and good luck to you.

I would like to thank other noteworthy colleagues in the chemistry department that for their friendships: Kathleen Giesfeldt and Marco de Jesus, for the much needed afternoon breaks and friendly encounters, and Megan Bragg, who I could always count on when I needed extra NMR time.

I would like to extend warm thanks and gratitude to my undergraduate research advisors and professors at Tennessee Tech for their wonderful tutelage and encouragement to attend graduate school: Dr. Dale Ensor, Dr. Dan Swartling, Dr. Jeff Boles, Dr. Ed Lisic, Dr. Tom Furtsch, Dr. Barbara Jackson, Dr. Scott Northrup, Dr. David Crouse, Dr. Bob Glinski, and Ms. Kathy Rust. Without

my foundation and experiences at TTU I would not have been inspired to be a professor or be where I am today.

Lastly, I am inexpressibly grateful to my family for their loving support and willingness to listen to my endless diatribes. Thanks to my parents, Anne and Mike Ray, for encouraging me to follow my dreams and supporting me through the years. Thanks to my wonderful sisters, Kim, Shannon, and Sara, who have been my best friends growing up and especially now as we are all “grown up” together. I will miss our Saturdays together. I would especially like to thank my husband, Sam, who constantly kept me on track and encouraged me to persevere, even from afar. I would also like to thank my mother and father-in-law, Mary and Sammy Morton, for their phone calls of encouragement; you have become like a second set of parents to me.

This project was supported by the National Science Foundation and the Camille Dreyfus Teacher-Scholar program. Their support is greatly appreciated.

ABSTRACT

This dissertation focuses on the unique chemistry of d^0 alkylidyne and *bis*(alkylidene) complexes with β-silicon atoms. The goals of this dissertation research were to prepare and characterize these new d^0 transition metal complexes, to study their reactivities including thermodynamics and kinetics of the inter-conversion between the alkylidyne and *bis*(alkylidene) complexes, and to explore the mechanism of the reactions of O_2 or water with d^0 alkylidyne complexes.

A summary of the research in this dissertation is provided in Chapter 1. Chapter 2 reports the study of an unusual exchange between new alkyl alkylidyne and *bis*(alkylidene) complexes promoted by phosphine coordination. A novel d^0 tungsten alkylidyne complex $(Me_3SiCH_2)_3W(\equiv CSiMe_3)(PMe_3)$ (**3a**) was prepared from $(Me_3SiCH_2)_3W\equiv CSiMe_3$ (**4a**) and PMe_3, and found to undergo a rare exchange with its *bis*(alkylidene) tautomer $(Me_3SiCH_2)_2W(=CHSiMe_3)_2(PMe_3)$ (**3b**). The thermodynamics of this equilibrium were investigated by variable-temperature ^{31}P NMR to give the thermodynamic parameters ΔH^o and ΔS^o of the exchange. Kinetic studies show that the α-hydrogen exchange between **3a** and **3b** follows first-order reversible kinetics. Activation parameters $\Delta H^{\neq}$ and $\Delta S^{\neq}$ for the forward (**3a** → **3b**) and reverse reactions (**3b** → **3a**) are reported. Reaction of **4a** with PMe_2Ph to give alkyl alkylidyne **5a** and *bis*(alkylidene) **5b** tautomeric mixture has also been studied,

and the exchange here is compared with that involving **3a** and **3b**.

Preparation and characterization of two new alkyl alkylidene alkylidyne complexes, and kinetic studies of their formation are presented in Chapter 3. The **3a** ⇌ **3b** equilibrium mixture under heating in the presence of excess PMe_3 was found to undergo α-hydrogen abstraction and convert to $(Me_3SiCH_2)(Me_3SiCH{=})W(\equiv CSiMe_3)(PMe_3)_2$ (**8a-b**). This reaction follows second-order kinetics – first order with respect to **3** and PMe_3. In the presence of excess PMe_3, pseudo first-order kinetics was observed to give the activation parameters $\Delta H^{\neq}$ and $\Delta S^{\neq}$ for the reaction. Preparation of $(Me_3SiCH_2)(Me_3SiCH{=})W(\equiv CSiMe_3)(PMe_2Ph)_2$ (**9a-b**) is also reported and compared with the formation of **8a-b**.

Chapter 4 describes the synthesis of $(Me_3SiCH_2)_3(Me_3SiC\equiv)W\leftarrow O{=}PMe_3$ (**11**) and its reaction with O_2 to yield an unusual oxo-siloxy complex $O{=}W(OSiMe_3)(CH_2SiMe_3)_3$ (**12**). Unexpected $-SiMe_3$ migration from an alkylidyne to an oxo ligand occurs in the reaction. In the absence of $O{=}PMe_3$, the reaction of $(Me_3SiCH_2)_3W\equiv CSiMe_3$ (**4a**) and O_2 did not yield **12**. **12** was isolated as $(Me_3SiCH_2)_3(Me_3SiC\equiv)W\leftarrow O{=}W(OSiMe_3)(CH_2SiMe_3)_3$ (**13**), an adduct with $(Me_3SiCH_2)_3W\equiv CSiMe_3$ (**4a**). Studies with ^{18}O-labelled $^{18}O_2$ have been conducted to determine whether the oxygen atoms in **12** come from $^{18}O_2$. High-resolution mass spectrometry (HRMS) was used to analyze the products.

Chapter 5 reports the study of the reaction of $(Me_3SiCH_2)_3W\equiv CSiMe_3$ (**4a**) with H_2O and the unexpected formation of CH_4 and **12** in this reaction. The

reaction of **4a** with D_2O showed α-hydrogen scrambling during the reaction and formation of methane isotopomers, which were studied by HRMS. Reactions of $(Me_3SiCH_2)_3(Me_3SiC\equiv)W\leftarrow O{=}PMe_3$ (**11**) with H_2O were also studied, and found to yield the oxo complex **12** as well.

TABLE OF CONTENTS

LIST OF TABLES

LIST OF FIGURES

LIST OF SCHEMES

NUMBERING SCHEME FOR COMPOUNDS IN THE TEXT

1-^{13}C	$(Bu^tCH_2)_3W{\equiv}{}^{13}CBu^t$
1	$(Bu^tCH_2)_3W{\equiv}CBu^t$
2a	$(Bu^tCH_2)_2W({\equiv}CBu^t)(SiBu^tPh_2)$
2b	$(Bu^tCH_2)W(=CHBu^t)_2(SiBu^tPh_2)$
3a	$(Me_3SiCH_2)_3W({\equiv}CSiMe_3)(PMe_3)$
3a'	$(CH_3)_3W({\equiv}CH)(PMe_3)$
3b	$(Me_3SiCH_2)_2W(=CHSiMe_3)_2(PMe_3)$
3b'	$(CH_3)_2W(=CH_2)_2(PMe_3)$
4a	$(Me_3SiCH_2)_3W{\equiv}CSiMe_3$
4a'	$(CH_3)_3W{\equiv}CH$
4b	$(Me_3SiCH_2)_2W(=CHSiMe_3)_2$
4b'	$(CH_3)_2W(=CH_2)_2$
5a	$(Me_3SiCH_2)_3W({\equiv}CSiMe_3)(PMe_2Ph)$
5b	$(Me_3SiCH_2)_2W(=CHSiMe_3)_2(PMe_2Ph)$
6	$(Bu^tCH_2)W({\equiv}C^tBu)(=CH^tBu)(PMe_3)_2$
7	$(Bu^tCH_2)W({\equiv}C^tBu)(=CH^tBu)$(dmpe)
8a	*syn*-$(Me_3SiCH_2)(Me_3SiCH=)W({\equiv}CSiMe_3)(PMe_3)_2$
8b	*anti*-$(Me_3SiCH_2)(Me_3SiCH=)W({\equiv}CSiMe_3)(PMe_3)_2$
9a	*syn*-$(Me_3SiCH_2)(Me_3SiCH=)W({\equiv}CSiMe_3)(PMe_2Ph)_2$

9b *anti*-$(Me_3SiCH_2)(Me_3SiCH{=})W(\equiv CSiMe_3)(PMe_2Ph)_2$

10 $(Bu^tCH_2)_2W(=O)([=CR(SiPhBu^t)]$

11 $(Me_3SiCH_2)_3(Me_3SiC\equiv)W\leftarrow O{=}PMe_3$

12 $O{=}W(OSiMe_3)(CH_2SiMe_3)_3$

13 $(Me_3SiCH_2)_3(Me_3SiC\equiv)W\leftarrow O{=}W(OSiMe_3)(CH_2SiMe_3)_3$

CHAPTER 1

Introduction

1.1. Foreword

A current research focus of synthetic inorganic chemistry is the controlled activation of dioxygen such as single oxygen atom transfer to substrates that mimics biological systems where such reactions are catalyzed enzymatically. Among the types of multiply bonded ligands, oxo complexes were the first discovered and have been most extensively studied. Much work has been done on the chemistry and biochemistry of dioxygen activation and reactivity with d^n transition metal complexes largely to understand oxygenase enzymes and to develop model systems for their functions in biological systems.[1] Oxidation of the metals is often involved in these reactions. The chemistry of dioxygen with d^0 early-transition-metal complexes including those with metal-carbon triple bonds remains a largely unexplored area.

1.1.1. *Fischer and Schrock Carbene and Carbyne Ligands*

The history of the study of metal-carbon multiple bonds and how they are formed is rich. Fischer and coworkers discovered the first carbene complexes in 1964 and the first carbyne complexes in 1973 (Eqs. 1 and 2).[2] Fischer-type carbene and carbyne ligands are often observed in low-oxidation-state metal complexes. Typically, they are found in the chemistry of late transition metals

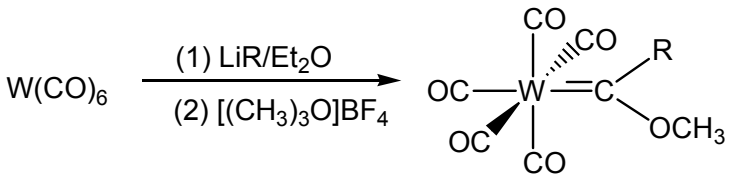

Eq. 1.1

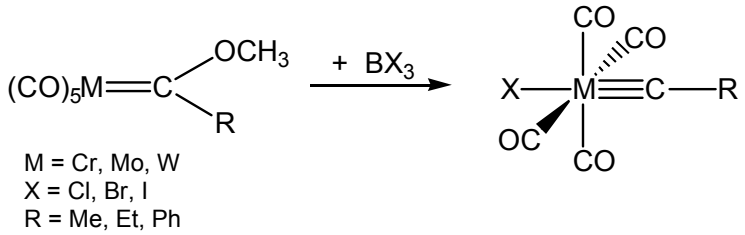

Eq. 1.2

bearing π-acceptor ligands, and the carbene ligands often contain π-donor substituents such as $-OCH_3$. Eqs. 1.1 and 1.2 exemplify these characteristics.

In contrast to the Fischer carbenes, in 1973, an attempt to form pentaneopentyltantalum resulted in the synthesis of the first carbene ligand in a high-oxidation-state metal complex, now known as the Schrock-type alkylidene (Eq. 1.3).[3] In 1978, the first Schrock alkylidyne was reported (Eq. 1.4).[3]

$$(Bu^tCH_2)_3TaCl_2 \xrightarrow{+\ 2\ Bu^tCH_2Li} (Bu^tCH_2)_3Ta{=}CH^tBu \qquad \text{Eq. 1.3}$$

$$WCl_6 \xrightarrow{6\ Bu^tCH_2Li} (Bu^tCH_2)_3W{\equiv}C^tBu \quad (\mathbf{1}) \qquad \text{Eq. 1.4}$$

Schrock-type alkylidene and alkylidyne ligands are typically found in high-oxidation-state early transition metal complexes containing non-π-acceptor ligands and non-π-donor R groups.[4] With the discovery of two new classes of compounds in such a short time-span, the field of organometallic chemistry

underwent a rapid expansion. Fischer and Schrock complexes proved to be useful in many different areas of catalysis, and in doing so widened fundamental understanding of these new classes of compounds. Investigations into the chemistry of compounds that contain metal-carbon multiple bonds have continued steadily since.[5,2b]

1.1.2. *Dioxygen*

Dioxygen has a triplet ground state with two unpaired electrons. Both the unpaired electrons have parallel spins and the half-filled antibonding molecular orbitals of $^3O_2$ can accommodate two additional electrons as shown in Figure 1.1.[6] The direct reaction of $^3O_2$ with singlet compounds to give singlet products is a spin-forbidden process with a very low rate of reaction. One way to circumvent this energy barrier is *via* a free radical pathway.[7] The reaction of a singlet compound with $^3O_2$ forming two doublets (free radicals) is a spin-allowed process. The process is highly endothermic and is observed typically with reactive substrates that form resonance stabilized radicals.

Another method to overcome the high spin conservation barrier is by combining $^3O_2$ with a paramagnetic transition metal ion, as shown in Eq. 1.5.

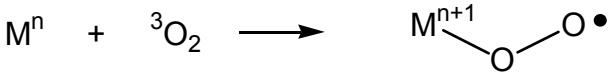

Eq. 1.5

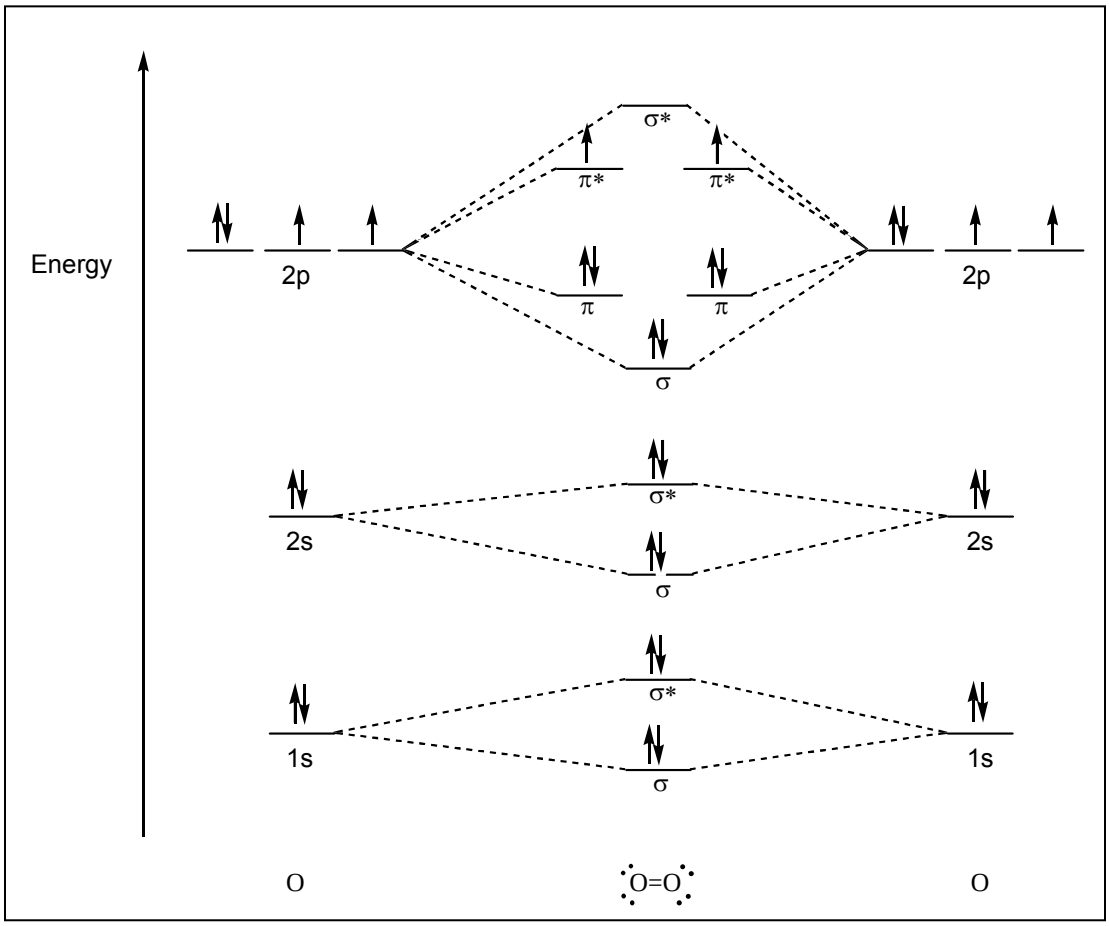

Figure 1.1. A qualitative molecular orbital diagram of dioxygen.

The resulting metal dioxygen complex may react selectively with singlet compounds under moderate conditions. This concept forms the basis for the extensive studies of oxygen activation by metal complexes. Since in most oxidation reactions there is no resonance stabilizer, this mechanism is the most accepted. It has been found that nearly all transition metals will bind dioxygen, resulting in a wide variety of complex formations.

The interaction of metal complexes with dioxygen has been the subject of numerous studies for its importance in many oxidation reactions, especially those involved in biological respiration processes.[7e] A large interdisciplinary effort has been mounted to understand oxygenase enzymes of all kinds by isolating and studying the pure enzymes, and by developing model systems.[7e] The first reported dioxygen complex was Werner's[7e] Co^{III} complex $[\{(NH_3)_5\text{-}Co\}_2O_2]^{4+}$ in 1898. A renewed interest in dioxygen chemistry began in 1936 when Pauling and Coryell discovered that "the oxygen molecule undergoes a profound change in electronic structure on combination with hemoglobin".[7f] It has since been found that nature utilizes metal-oxo complexes in numerous important enzymes. An unprecedented amount of research has focused on the cytochrome P-450 family of enzymes, which contain an oxo-iron porphyrin system and have been found to be involved in a wide range of biological oxidation processes. A second class of oxo-metal based enzymes are the molybdenum- or tungsten-containing "oxo-transferases", which like P-450, are involved in both oxidative and reductive processes. Significant advances have been made in the development of model systems that mimic the enzymatic transformations in the body.[5b]

The mechanism of reactions of organometallic complexes is of fundamental importance to understanding the role of transition metals in catalytic oxidation processes. Little is known, however, about how dioxygen reacts with metal-carbon multiple bonds. The study of transition metal organometallics and their reactions with dioxygen began when Frankland reported the autoxidation of dimethyl zinc in 1853. Forty years later, Demuth and Meyer clearly defined the reaction and its product, zinc peroxide.[8] Studies of reactions between O_2 and early transition metal organometallics began in the early 1970's. Zucchini and coworkers investigated the reaction of O_2 with $Zr(CH_2Ph)_4$ which was found to react two equiv of O_2 per mole.[9a] Brindley and Hodgson studied the reaction of O_2 with titanium, zirconium, dimolybdenum, and tungsten alkyl complexes.[9b] Their measurement of the total absorption of oxygen per alkyl ligand suggested metal alkoxides were the stable end products. Their findings and those that followed supported oxygen insertion into the metal-alkyl and other metal-ligand bonds.

In general, it is now known that oxygen insertion to the alkyl-metal bond gives mainly alkoxides and some peroxides. When the central metal reacts with dioxygen, an oxo complex is often obtained. It is now accepted that most of the oxygenation reactions occur by a radical mechanism to overcome the spin-forbidden energy barrier.[1]

1.1.3. *Reactions of d^0 Transition Metal Complexes with O_2*

Reactions of d^0 transition metal complexes with O_2 have been studied in the synthesis of metal oxide materials used in the microelectronics industry.[10–12] Oxygen insertion into Zr-Si and Zr-R bonds in the reactions of $Cp_2ZrCl(SiMe_3)$, Cp_2ZrRCl, and Cp_2ZrR_2 with O_2 has been reported by Tilley,[10g] Schwartz,[10a] Gibson,[10b] Brindley[10d] and coworkers. The Cp-free complexes $(RO)_2TiMe_2$, $(ArO)_2TaMe_3$, $(ArN=)_2MoMe_2$, and $LY(\mu\text{-}Me)_2AlMe_2$ (L = porphyrin) have been shown to undergo O insertion in their reactions with O_2, as reported by Wolczanski,[11a,b] Rothwell,[11c] Gibson,[11d] Schaverien[11m] and coworkers, respectively. In recent years, reactions of O_2 with d^0 complexes such as $Ta(NR_2)_5$ and $(Et_2N)_3Ta{=}NBu^t$ have been used in the preparation of microelectronic metal oxide thin films as new gate materials.[12] The nature of these CVD reactions is largely unknown, and mechanistic pathways to the microelectronic MO_n materials are not understood.

Reactions of d^0 transition metal complexes with dioxygen have attracted much attention and have been used to make metal oxides, known as high dielectric constant (κ) gate materials, and used as microelectronic gate materials in VLSI devices. High-κ MO_n oxide thin films have been explored to replace SiO_2, a relatively low-κ solid (κ = 3.9), as the next generation of gate materials. These materials have also been utilized as new capacitor materials for DRAM (dynamic random access memory) devices.[13]

Our research has been mostly focused on the fundamental chemistry of d^0 transition metal alkylidyne complexes and their reactions with O_2. Reactions of H_2O with transition metal complexes, an alternative route to MO_n materials, have also been investigated to reveal unique chemistry and provides a comparison to the reactions involving O_2.

1.2. Current Dissertation

The preparation and characterization of novel d^0 tungsten alkyl alkylidyne and *bis*(alkylidene) complexes, mechanistic pathways in the formation of these compounds, and studies of their reactions towards O_2 and H_2O and related chemistry of these complexes are the foci of this Ph.D. dissertation.

1.2.1. *Chapter 2*

Preparation, characterization, and X-ray crystal structure of novel alkyl alkylidyne $(Me_3SiCH_2)_3W(\equiv CSiMe_3)(PMe_3)$ (**3a**), *bis*(alkylidene) $(Me_3SiCH_2)_2W(=CHSiMe_3)_2(PMe_3)$ (**3b**), and studies of the interconversion between alkylidyne **3a** and *bis*(alkylidene) **3b** complexes are reported. An adduct between PMe_3 and alkyl alkylidyne $(Me_3SiCH_2)_3W\equiv CSiMe_3$ (**4a**), $(Me_3SiCH_2)_3W(\equiv CSiMe_3)(PMe_3)$ (**3a**), was found to undergo a rare reversible transformation to its *bis*(alkylidene) tautomer $(Me_3SiCH_2)_2W(=CHSiMe_3)_2(PMe_3)$ (**3b**). The *bis*(alkylidene) tautomer **3b** is favored in the **3a** $\rightleftharpoons$ **3b** [$(Me_3SiCH_2)_3W(\equiv CSiMe_3)(PMe_3) \rightleftharpoons (Me_3SiCH_2)_2W(=CHSiMe_3)_2(PMe_3)$]

equilibrium with K_{eq} ranging from 12.3(0.2) at 278(1) K to 9.37(0.12) at 303(1) K, giving the thermodynamic parameters for the equilibrium: ΔH^{o} = –1.8(0.5) kcal/mol and ΔS^{o} = –1.5(1.7) eu. The α-hydrogen exchange between **3a** and **3b** follows first-order reversible kinetics. The activation parameters are $\Delta H^{\neq}$ = 16.2(1.2) kcal/mol and $\Delta S^{\neq}$ = –22(4) eu for the forward reaction (**3a** $\rightarrow$ **3b**), and $\Delta H^{\neq}$ = 18.0(1.3) kcal/mol and $\Delta S^{\neq}$ = –21(4) eu for the reverse reaction (**3b** $\rightarrow$ **3a**). The role of PMe_3 in the exchange **3a** $\rightleftharpoons$ **3b** has been studied by density functional theory calculations through the collaboration with researchers at the Hong Kong University of Science and Technology. A paper about the chemistry in this chapter has been published in *J. Am. Chem. Soc.* **2004,** *126*, 10208-10209.[14]

1.2.2. *Chapter 3*

Heating the **3a** $\rightleftharpoons$ **3b** equilibrium mixture in the presence of excess PMe_3 caused an α-hydrogen abstraction and conversion to $(Me_3SiCH_2)(Me_3SiCH{=})W(\equiv CSiMe_3)(PMe_3)_2$ (**8a-b**) (Eq. 1.6).

$(Me_3SiCH_2)_3W(\equiv CSiMe_3)(PMe_3)$ (**3a**) $\rightleftharpoons$ $(Me_3SiCH_2)_2W(=CHSiMe_3)_2(PMe_3)$ (**3b**) $\rightarrow$ $(Me_3SiCH_2)(Me_3SiCH{=})W(\equiv CSiMe_3)(PMe_3)_2$ (**8a-b**) Eq. 1.6

This reaction was found to follow second-order kinetics – first order with respect to **3** and PMe_3, respectively. In the presence of excess PMe_3, pseudo first-order kinetics was observed and activation parameters are $\Delta H^{\neq}$ = 27.4(1.5) kcal/mol

and $\Delta S^{\neq}$ = –1(4) eu. Preparation of $(Me_3SiCH_2)(Me_3SiCH=)W(\equiv CSiMe_3)(PMe_2Ph)_2$ (**9a-b**) is also reported and compared with the formation of **8a-b**.

1.2.3. *Chapter 4*

Synthesis of $(Me_3SiCH_2)_3(Me_3SiC\equiv)W\leftarrow O{=}PMe_3$ (**11**), an adduct between $(Me_3SiCH_2)_3W\equiv CSiMe_3$ (**4a**) and $O{=}PMe_3$, is reported in Chapter 4. **11** was found to react with O_2 to give CO_2 and $O{=}W(OSiMe_3)(CH_2SiMe_3)_3$ (**12**) which was isolated as an adduct with **4a,** $(Me_3SiCH_2)_3(Me_3SiC\equiv)W\leftarrow O{=}W(OSiMe_3)(CH_2SiMe_3)_3$ (**13**). In this reaction, the $–SiMe_3$ group in the $\equiv CSiMe_3$ ligand undergoes an unprecedented migration to form the $–OSiMe_3$ ligand in **12**, and the ≡C– atom is oxidized to CO_2. $O{=}PMe_3$ is believed to serve as a mediator for the 1,3-silyl migration, and the mechanism may be radical in nature. Studies with ^{18}O-labelled $^{18}O_2$ have been conducted to determine whether the oxygen atoms in **12** come from $^{18}O_2$. High-resolution mass spectrometry (HRMS) was used to analyze the products.

1.2.4. *Chapter 5*

Reaction of $(Me_3SiCH_2)_3W\equiv CSiMe_3$ (**4a**) with H_2O was studied, and found to yield the oxo complexes **12** as well and CH_4. In this reaction, a silyl migration in the $\equiv CSiMe_3$ ligand was also observed, and the ≡C– atom is converted to CH_4. These studies show that two different alkylidyne complexes, **4a** and **11**, react

with O_2 and H_2O, respectively, to yield the same unusual oxo complex **12**. The reaction of **4a** with D_2O showed α-hydrogen scrambling during the reaction and formation of methane isotopomers, which were studied by HRMS. Reactions of $(Me_3SiCH_2)_3(Me_3SiC\equiv)W\leftarrow O{=}PMe_3$ (**11**) with H_2O were also studied, and found to yield the oxo complex **12** as well.

1.2.5. *Chapter 6*

Based on the work reported in the current dissertation, some future studies are suggested in this chapter.

CHAPTER 2

New Tungsten Alkyl Alkylidyne and *Bis*(alkylidene) Complexes and Kinetic and Thermodynamic Studies of Their Unusual Inter-Conversions

2.1. Introduction

The reactivity of α-hydrogen atoms in alkyl ligands free of β-hydrogen atoms (e.g., Me_3CCH_2 and Me_3SiCH_2) has been studied due to their role in the formation of high-oxidation-state alkylidene and alkylidyne complexes.[3a,5b,5d,15–17] d^0-Alkyl alkylidyne $(RCH_2)_3W{\equiv}CR'$ and alkylidene $(Bu^tCH_2)_3Ta{=}CDBu^t$ complexes are known to undergo α-hydrogen migrations among the α-carbon atoms.[3c,18] In previous work, *bis*(alkylidene) complexes are believed to be intermediates in alkyl-alkylidyne scrambling through α-hydrogen transfer in alkylidyne complexes $(Bu^tCH_2)_3W{\equiv}^{13}CCMe_3$ (**1-^{13}C**) and $(Bu^tCH_2)_3W{\equiv}CSiMe_3$.[18] Such α-hydrogen exchanges in, for example, $(Bu^tCH_2)_3W{\equiv}^{13}CCMe_3$ (**1-^{13}C**) at 60 °C, lead to scrambling of the ^{13}C labeled atom between the alkyl and alkylidene ligands and the formation of $(Bu^tCH_2)_2(Bu^t\text{-}^{13}CH_2)W{\equiv}CBu^t$ (Scheme 2.1a). A statistical distribution of the ^{13}C-labeled α-carbon atoms in $(Bu^t{*}CH_2)_3W{\equiv}{*}CBu^t$ (*C: 25% ^{13}C) is reached in 24 hours.[18c] In other words, the ^{13}C label is present in the α-carbon atoms in the $^{13}CH_2$: $\equiv^{13}C$ groups in a 3 : 1 ratio. Another case of such alkyl-alkylidene scrambling has been reported in d^0 $(Bu^tCH_2)_3W{\equiv}CSiMe_3$,

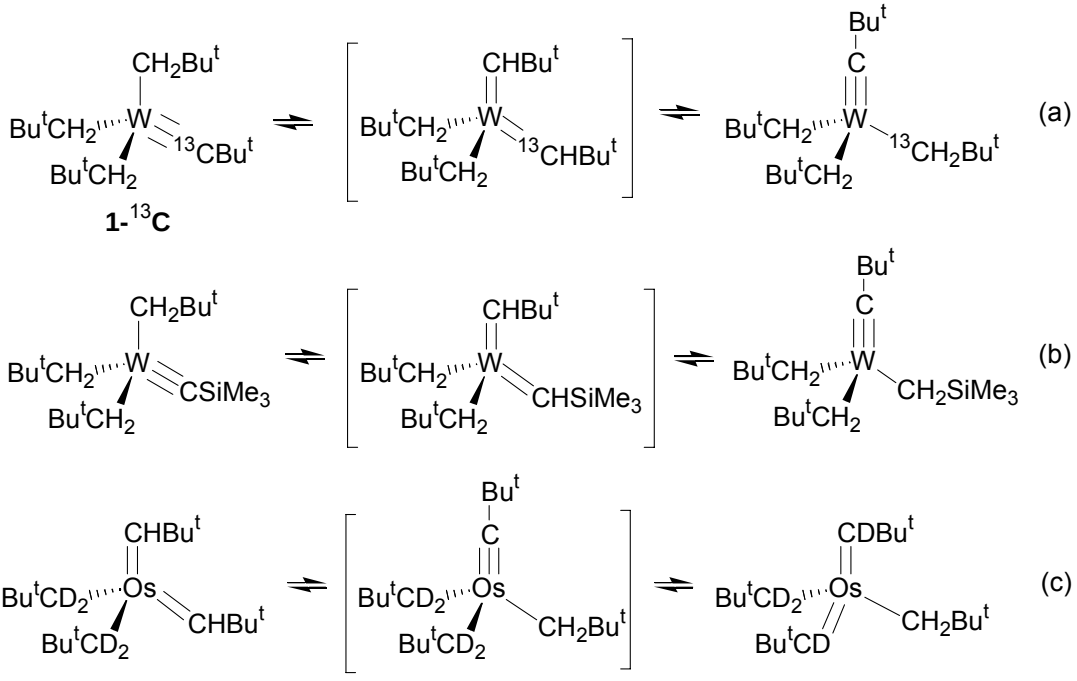

Scheme 2.1. Proposed intermediates in alkylidene/alkylidyne scrambling processes.[18,19]

leading to the formation of $(Bu^tCH_2)_2(Me_3SiCH_2)W{\equiv}CBu^t$ (Scheme 2.1b). Deuterium labeling studies using $(Bu^tCHD)_3W{\equiv}CSiMe_3$ and $(Bu^tCD_2)_3W{\equiv}CSiMe_3$ as well as kinetic studies of the α-hydrogen exchanges are consistent with unimolecular and stepwise transfer of two H atoms in one alkyl ligand to the alkylidyne ligand in $(Bu^tCH_2)_3W{\equiv}CSiMe_3$.[18a] A *bis(*alkylidene) "$(Bu^tCH_2)_2W(=CHSiMe_3)(=CHBu^t)$" was proposed as an intermediate in the transfer (Scheme 1b), although it was not observed.[18a] It is reasonable to assume that there is a similar *bis*(alkylidene) intermediate in the alkyl-alkylidyne scrambling in $(Bu^tCH_2)_3W{\equiv}^{13}CBu^t$ (**1-^{13}C**, Scheme 2.1a).[18c] In the d^2 osmium *bis*(alkylidene) complex $Os(=CHBu^t)_2(CD_2Bu^t)_2$, H/D atoms were found to scramble among the α-carbon atoms (Scheme 2.1c).[19c] This exchange is believed to occur through the alkyl alkylidyne intermediate "$(Bu^tCH_2)_3Os{\equiv}CBu^t$."

Although the exchange of α-hydrogen atoms is a fundamental dynamic process in these archetypical d^0 alkylidene and alkylidyne complexes, there is, to our knowledge, only one direct observation of such an exchange between *bis*(alkylidene) and alkylidyne tautomers.[3b,5c,5d,15a,20,21] Alkylidyne complex $(Me_3CCH_2)_2W(\equiv CCMe_3)(SiBu^tPh_2)$ (**2a**), a *silyl* analog of **1**, was found to be in an equilibrium with its silyl *bis*(alkylidene) tautomer $(Me_3CCH_2)W(=CHCMe_3)_2(SiBu^tPh_2)$ (**2b**) (Eq. 2.1).[22]

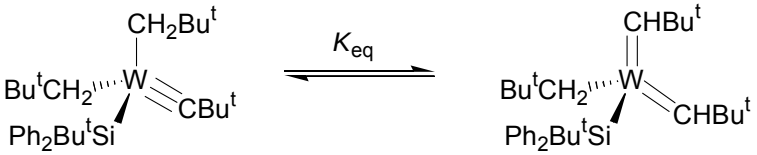

2a **2b** (Eq. 2.1)

$(Bu^tCH_2)W(=CHBu^t)_2(SiBu^tPh_2)$ (**2b**) is one of the rare known d^0 *bis(*neopentylidene) complexes; the only other known examples involve tantalum and niobium d^0 *bis*(neopentylidene) complexes.[16e,19c,23] Theoretical studies reveal that the silyl ligand plays a critical role in the relative stabilities of the d^0 tungsten *bis*(alkylidene) tautomer (**2b**) through the d-p π interaction between the silyl ligand and the electron density in the metal-alkylidyne/alkylidene bonds.[22b]

We recently observed that $(Me_3SiCH_2)_3W(\equiv CSiMe_3)(PMe_3)$ (**3a**), an adduct between PMe_3 and $(Me_3SiCH_2)_3W\equiv CSiMe_3$ (**4a**), undergoes an exchange with its *bis*(alkylidene) tautomer $(Me_3SiCH_2)_2W(=CHSiMe_3)_2(PMe_3)$ (**3b**, Eq. 2.2).[14]

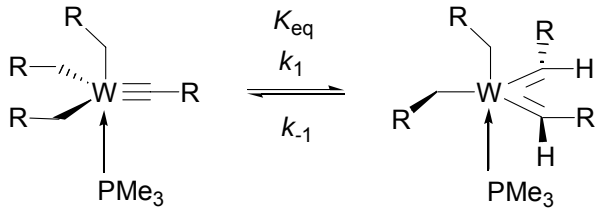

R = $SiMe_3$, **3a** **3b** (Eq. 2.2)

In the *absence* of the phosphine, the *bis*(alkylidene) tautomer "$(Me_3SiCH_2)_2W(=CHSiMe_3)_2$ (**4b**)" was not observed. Unlike the exchange involving *silyl* alkylidyne and *bis*(alkylidene) complexes **2a** and **2b**, this is an

unusual phosphine-induced exchange. Assuming $(Me_3SiCH_2)_3W{\equiv}CSiMe_3$ (**4a**) undergoes an alkyl-alkylidyne scrambling involving "$(Me_3SiCH_2)_2W(=CHSiMe_3)_2$ (**4b**)" as an intermediate similar to that in Scheme 2.1b, the current work suggests that PMe_3 coordination making $(Me_3SiCH_2)_2W(=CHSiMe_3)_2(PMe_3)$ (**3b**) significantly stabilizes **4a** to make its phosphine adduct **3b** observable at room temperature. The synthesis of analogues $(Me_3SiCH_2)_3W(\equiv CSiMe_3)(PMe_2Ph)$ (**5a**) and $(Me_3SiCH_2)_2W(=CHSiMe_3)_2(PMe_2Ph)$ (**5b**) was also studied and the tautomeric mixture was found to undergo a similar equilibrium. Our preparation and characterization of **3a**, **3b**, **5a**, and **5b** as well as thermodynamic and kinetic studies of the **3a** ⇌ **3b** exchange in Eq. 2.2 are reported here.

2.2. Results and Discussion

2.2.1. *Synthesis and Characterization of the Tungsten Alkyl Alkylidyne Complex $(Me_3SiCH_2)_3W(\equiv CSiMe_3)(PMe_3)$ (3a)*

Addition of PMe_3 to a solution of $(Me_3SiCH_2)_3W{\equiv}CSiMe_3$ (**4a**) in toluene-d_8 leads to an immediate color change from yellow to red, and the formation of the PMe_3 adduct $(Me_3SiCH_2)_3W(\equiv CSiMe_3)(PMe_3)$ (**3a**). NMR spectroscopic characterization [^1H, ^{13}C, ^{31}P, ^{29}Si, ^1H-gated-decoupled ^{13}C (Figure 2.1) and HMQC] of **3a** at –50 °C suggests that the PMe_3 ligand coordinates *cis* to the alkylidyne ligand. Two alkyl resonances were observed in the ^1H (in a 1 : 2 ratio), ^{13}C and ^{29}Si NMR spectra of **3a** at –50 °C, as expected from the structure of **3a**

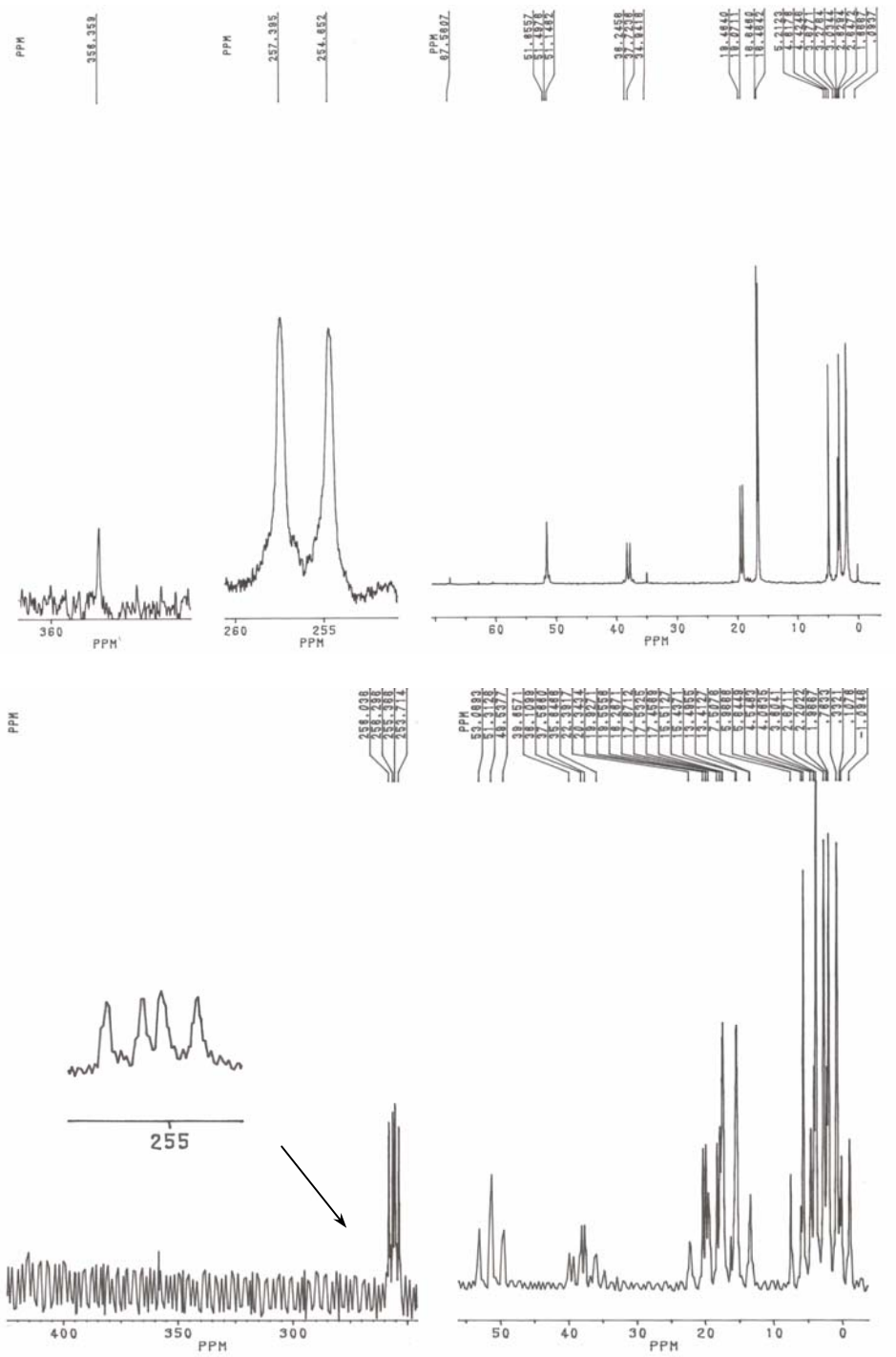

Figure 2.1. Upper: ^{13}C NMR (62.896 MHz) spectrum of a mixture of **3a** and **3b** at 23 °C. Lower: ^{1}H-gated-decoupled ^{13}C NMR (62.896 MHz) spectrum of a mixture of **3a** and **3b** at 23 °C.

in Eq. 2.2. The coupling constant $^2J_{P\text{-}C\text{-}axial}$ of 36.5 Hz for the axial $–CH_2R$ ligand is, as expected, larger than $^2J_{P\text{-}C\text{-}equatorial}$ of 7.2 Hz for the equatorial $–CH_2R$ ligand. The resonance of the alkylidyne C atom in the PMe_3 adduct $(Me_3SiCH_2)_3W(\equiv CSiMe_3)(PMe_3)$ (**3a**) at 358.81 ppm appeared as a doublet ($^2J_{P\text{-}C}$ = 14.5 Hz) in both ^{13}C and ^1H-gated-decoupled ^{13}C NMR spectra, and is down-field shifted from that of $(Me_3SiCH_2)_3W\equiv CSiMe_3$ (**4a**) at 343.27 ppm.

2.2.2. *Synthesis and Characterization of the Tungsten Bis(alkylidene) Complex $(Me_3SiCH_2)_2W(=CHSiMe_3)_2(PMe_3)$ (3b)*

Upon warming the solution of **3a** in toluene-d_8 to room temperature, **3a** was found to undergo alkyl-to-alkylidyne α-hydrogen migration to give *bis*(alkylidene) $(Me_3SiCH_2)_2W(=CHSiMe_3)_2(PMe_3)$ (**3b**), which was characterized by ^1H (Figure 2.2), ^{13}C (Figure 2.3), ^{31}P, ^{29}Si, ^1H-gated-decoupled ^{13}C (Figure 2.1) and HMQC NMR spectroscopy. The two tautomers are found to be in equilibrium (**3a** $\rightleftharpoons$ **3b**). The two alkylidene ligands are inequivalent; the alkylidene C resonances in **3b** are observed *as doublet of doublets* at 256.43 ($^1J_{C\text{-}H}$ = 123.5 Hz) and 254.71 ppm ($^1J_{C\text{-}H}$ = 102.6 Hz) in the ^1H-gated-decoupled ^{13}C NMR spectrum at –50 °C (Figure 2.1). The coupling constants $^2J_{P\text{-}C\text{-}axial}$ and $^2J_{P\text{-}C\text{-}equatorial}$ of 32.3 and 0 Hz for the axial and equatorial $–CH_2R$ ligands, respectively, and $^2J_{P\text{-}C}$ of 11.8 and 12.6 Hz for the two alkylidene ligands suggest that the two alkylidene and one alkyl ligands coordinate *cis* to the PMe_3 ligand. The ^1H NMR resonances of the alkylidene H atoms in **3b** were observed as

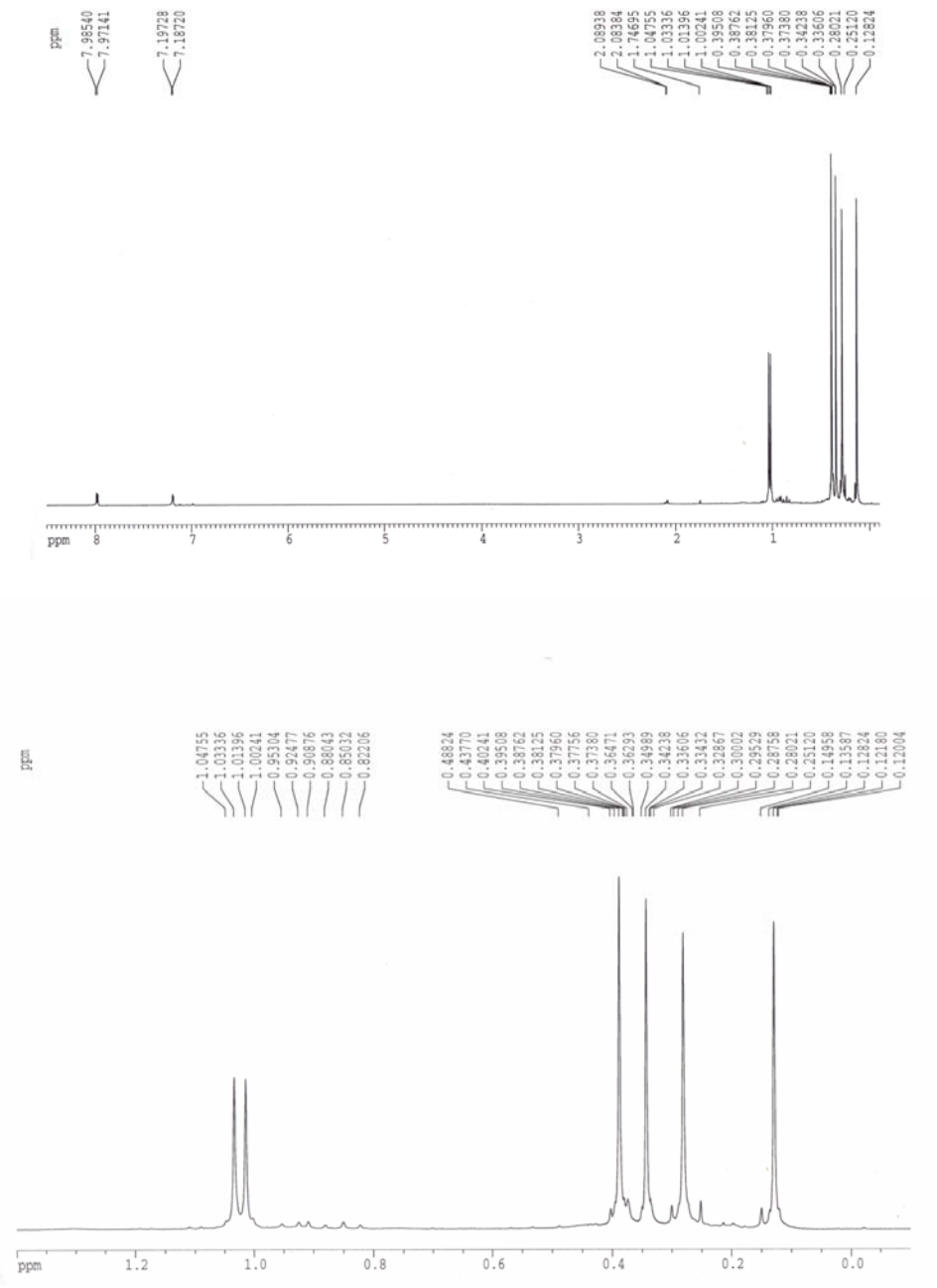

Figure 2.2. Upper: ^{1}H NMR (400.11 MHz) spectrum of $(Me_3SiCH_2)_2W(=CHSiMe_3)_2(PMe_3)$ (**3b**) at –20 °C. Lower: Expansion of the –0.1-1.4 ppm region of the spectrum.

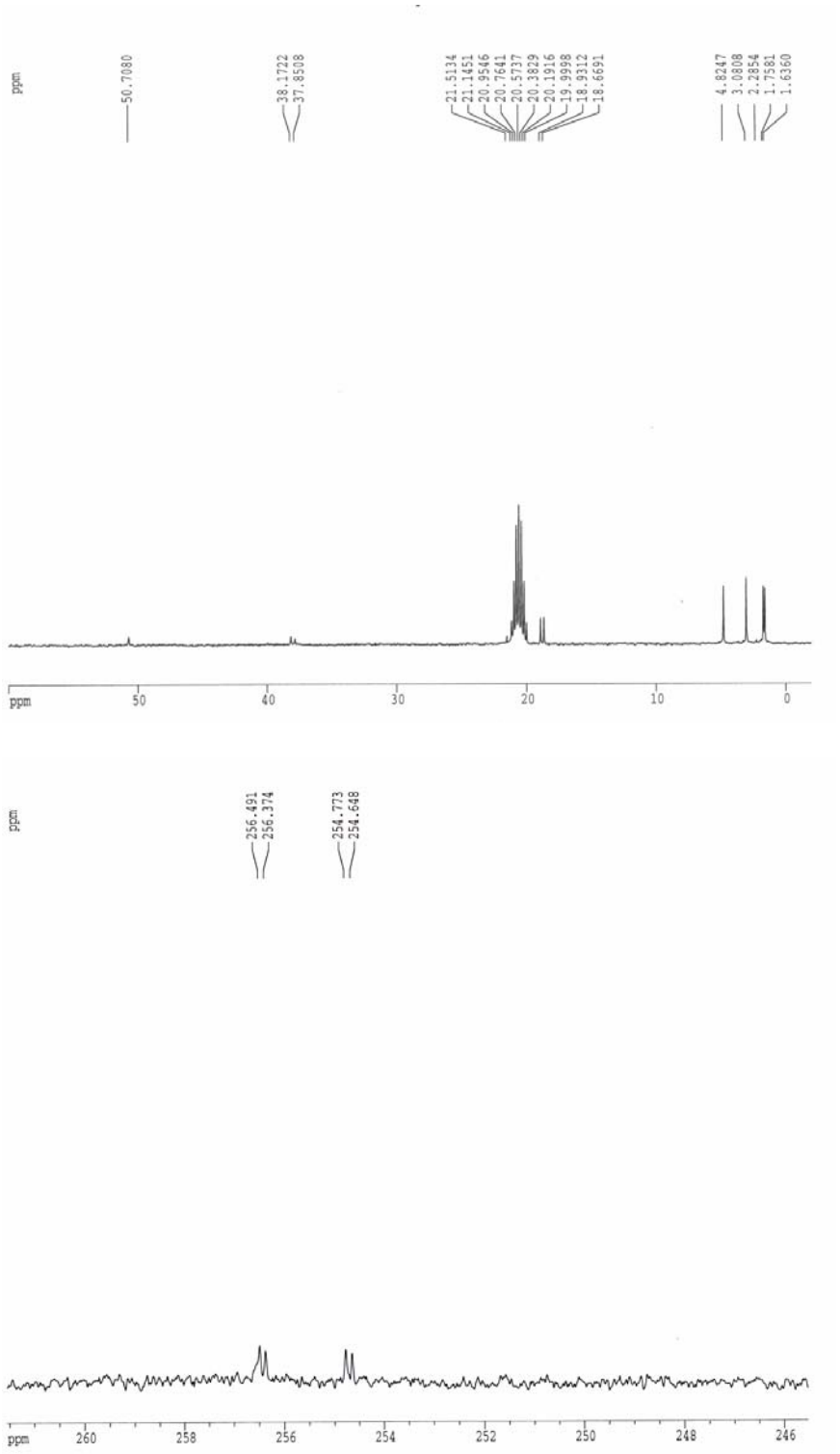

Figure 2.3. ^{13}C NMR (100.63 MHz) spectrum of **3b** at –40 °C. Upper: –2-60 ppm region. Lower: 246-261 ppm region.

doublets at 7.985 ($^3J_{P\text{-}H}$ = 5.6 Hz) and 7.1982 ($^3J_{P\text{-}H}$ = 4.0 Hz) ppm, respectively. The presence of two inequivalent alkylidene ligands suggest that **3b** adopts an *anti, syn* configuration (Eq. 2.2), and it is unlikely that the two ligands are involved in a fast rotation about the W=C bonds. The prochiral W atom in **3a** gives rise to diastereotopic α-hydrogen atoms (CH_aH_b-SiMe$_3$) for the equatorial alkyl ligands observed as doublet of doublets at 0.751 ppm (both $^2J_{Ha-Hb}$ and $^3J_{P-H}$ = 14.4 Hz) and 0.213 ppm ($^3J_{P\text{-}H}$ = 28.2 Hz) in its ^{1}H NMR spectrum at –50 °C (Figure 2.4). The presence of the prochiral W atom in **3b** similarly leads to diastereotopic α-hydrogen atoms (CH_eH_f-SiMe$_3$, Figure 2.5) for the equatorial alkyl ligand observed as doublet of doublets at 0.917 ($^3J_{P\text{-}H}$ = 17.7 Hz, $^2J_{Ha\text{-}Hb}$ = 11.3 Hz) and 0.876 ($^3J_{P\text{-}H}$ = 32.2 Hz) ppm in the ^{1}H NMR spectrum at –50 °C. The chemical shift differences between the diastereotopic H_a and H_b atoms in **3a** (0.538 ppm) is larger than that (0.041 ppm) in **3b**. The chemical shift difference in alkylidyne **3a** is, however, smaller than 4.56 ppm in pseudo-tetrahedral silyl alkylidyne complex $(Me_3CCH_2)_2W(\equiv CSiMe_3)[Si(SiMe_3)_3]$.[20j]

The equilibrium mixture of **3a** and **3b** is stable in solution for several days and cooling the solution to –30 °C yielded crystals of **3b** that were suitable for X-ray diffraction studies. A representation of the molecular structure, crystallographic refinement data, and selected bond distances and angles of **3b** are given in Figure 2.6, and Tables 2.1 and 2.2, respectively. Low-temperature ^{1}H NMR spectra of the crystals showed that the crystals are those of **3b**, indicating that **3b** preferentially crystallized from the mixture. Elemental analysis

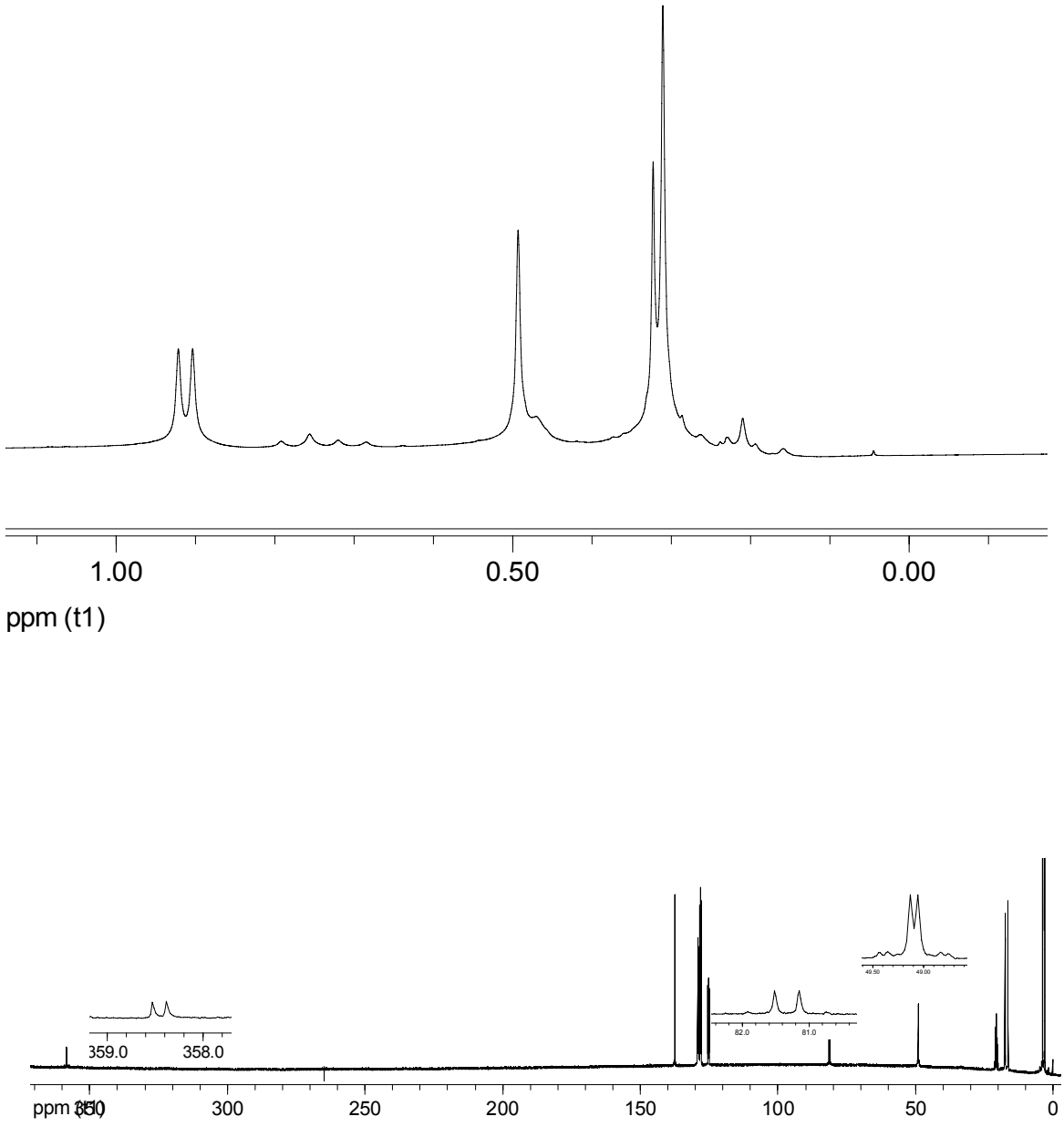

Figure 2.4. Upper: ^{1}H NMR (400.11 MHz) spectrum of **3a** at –50 °C.

Lower: ^{13}C NMR (100.63 MHz) of **3a** at –50 °C.

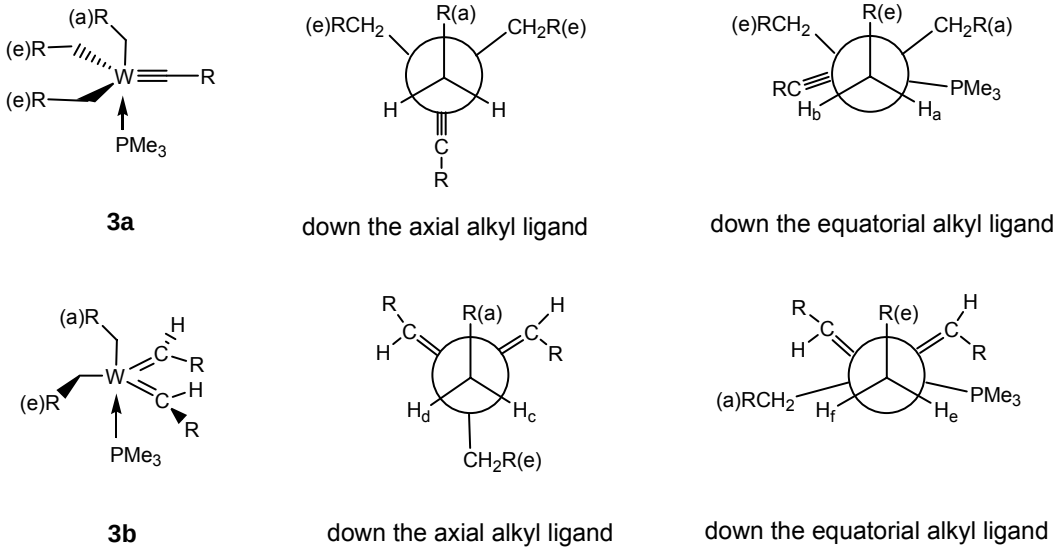

R = $SiMe_3$; (a) = axial; (e) = equatorial

Figure 2.5. Newman projections of **3a** and **3b** showing diastereotopic protons.

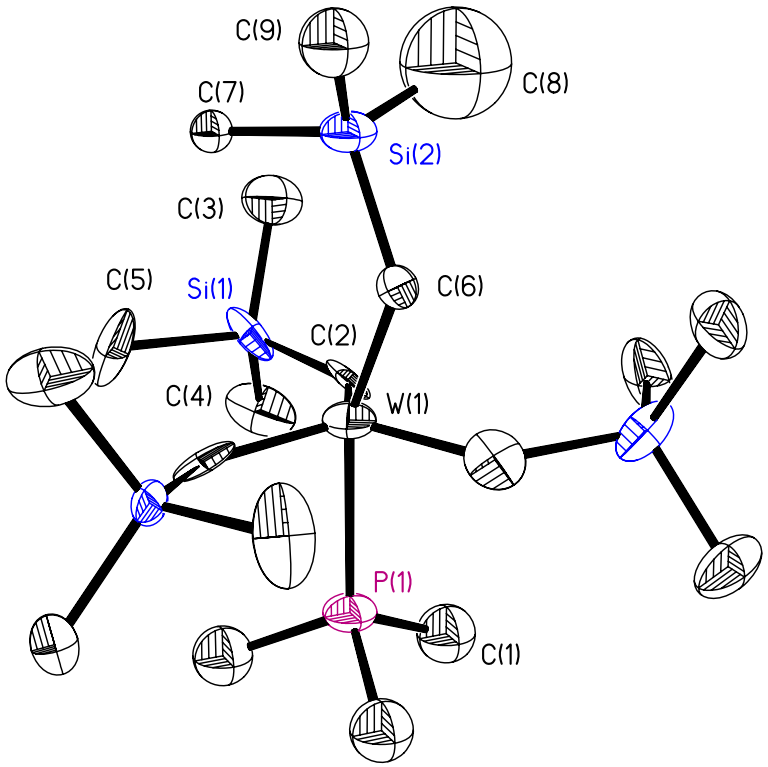

Figure 2.6. An ORTEP view of *bis*(alkylidene) **3b** showing 30% probability thermal ellipsoids. This is a disordered structure. See page 28 for details.

Table 2.1. Crystal data and structure refinement for **3b**

Compound No.	**3b**
Empirical formula (formula weight)	$C_{21}H_{53}O_1P_1Si_5W_1$ (676.90)
Temperature	–100(2) °C
Wavelength	0.71073 Å
Crystal system	Hexagonal
Space group	*P*6(3)
Unit Cell Dimensions	*a* = 12.1310(5) Å α = 90°
	b = 12.1310(5) Å β = 90°
	c = 12.1091(5) Å γ = 120°
Volume	1543.25(11) Å^3
Z	2
Density (calculated)	1.457 g/cm^3
Absorption coefficient	4.000 mm^{-1}
F(000)	692
Crystal size	0.35 × 0.25 × 0.25 mm^3
θ range for data collection	1.68 to 27.42°
Index ranges	$-15 \le h \le 15$, $-15 \le k \le 15$, $-15 \le l \le 15$
Reflections collected	15949

Table 2.1. Continued

Compound No.	**3b**
Independent reflections	2352 [R(int) = 0.0371
Completeness to θ = 27.42°	100.0%
Absorption correction	Semi-empirical from equivalents
Refinement method	Full-matrix least-squares on F^2
Data / restraints / parameters	2352 / 112 / 86
Goodness-of-fit on F^2	1.207
Final R indices [$I > 2\sigma(I)$]	$R1$ = 0.0624, $wR2$ = 0.1235
R indices (all data)	$R1$ = 0.0655, $wR2$ = 0.1255
Absolute structure parameter	0.44(11)
Largest diff. peak and hole	1.881 and −2.401 e.Å^{-3}

[a] $R1 = \Sigma||F_o| - |F_c|| / \Sigma|F_o|$; $wR2 = [\Sigma\, w(F_o^2 - F_c^2)^2 / \Sigma\, w(F_o^2)^2]^{1/2}$;
$w = 1/[\sigma^2(F_o) + (aP)^2 + bP]$; $P = [2F_c^2 + \mathrm{Max}(F_o^2, 0)]/3$

Table 2.2. Selected bond distances (Å) and angles (°) for **3b**

Distances			
W(1)-C(2)	1.964(12) *	Si(1)-C(5)	1.879(10)
W(1)-C(6)	2.041(18)	C(6)-Si(2)	1.889(19)
W(1)-P(1)	2.514(5)	Si(2)-C(9)	1.854(15)
P(1)-C(1)	1.86(2)	Si(2)-C(8)	1.874(16)
C(2)-Si(1)	1.860(13)	Si(2)-C(7)	1.858(15)
Si(1)-C(4)	1.871(13)		
Si(1)-C(3)	1.861(13)		
Angles			
C(2)-W(1)-C(2a)	119.39(14)	C(1)-P(1)-W(1)	115.6(7)
C(6)-W(1)-P(1)	155.3(6)	C(2)-W(1)-P(1)	85.5(5)
C(2)-W(1)-C(6)	112.7(12)	Si(1)-C(2)-W(1)	135.1(7)
C(2a)-W(1)-C(6)	98.7(14)	Si(2)-C(6)-W(1)	128.4(12)
C(5)-Si(1)-C(2)	111.2(6)	C(7)-Si(2)-C(6)	108.9(12)
C(5)-Si(1)-C(3)	108.7(7)	C(7)-Si(2)-C(8)	108.4(11)

***** This is the average of one W=CHR and two W-CH_2R bonds in the disordered structure.

of the crystals is consistent with the composition of **3b**. The X-ray crystal structure of **3b** was found to be severely disordered with a crystallographically imposed 3-fold axis through the Si(2), W(1) and P(1) atoms. The structure was solved with the help from Dr. Charles F. Campana of Bruker AXS, Inc. The C(6) atom was located in three equivalent positions: C(6), C(6a) and C(6b), each with a partial occupancy of 1/3. Only C(6) is shown in the ORTEP view of **3b** (Figure 2.6). **3b** adopts a pseudo trigonal bipyramidal structure with C(6) and P(1) in the axial positions and the C(6)-W(1)-P(1) angle of 155.3(6)°. The axial W(1)-C(6) bond distance of 2.041(18) Å is similar to 2.096(5) Å in $(Bu^tCH_2)_3W{\equiv}CSiMe_3$,[18a] but shorter than 2.112(9) Å and 2.118(9) Å in $(Bu^tCH_2)_2W(=O)[=C(SiMe_3)SiBu^tPh_2]$[22a,c] and 2.258(8) Å in the alkyl alkylidene alkylidyne complex $W(CH_2Bu^t)(=CHBu^t)(\equiv CBu^t)[Me_2P(CH_2)_2PMe_2]$.[24] The 3-fold disorder leads to an average of the three equatorial W-C bond distance [W(1)-C(2)] of 1.964(12) Å. This average is smaller than the W(1)-C(6) bond distance of 2.041(18) Å, suggesting that the two alkylidene W=C bonds are in the equatorial positions. This observation is consistent with the NMR data of **3b** discussed earlier in this section. The equatorial C(2)-Si(1) bond distance of 1.860(13) Å is slightly shorter than the axial C(6)-Si(2) distance of 1.889(19) Å. The W(1)-P(1) bond distance of 2.514(5) Å is similar to those [2.450(3) and 2.577(3) Å] in $W(CH_2Bu^t)(=CHBu^t)(\equiv CBu^t)[Me_2P(CH_2)_2PMe_2]$.[24]

2.2.3. *Synthesis and Characterization of $(Me_3SiCH_2)_3W(\equiv CSiMe_3)(PMe_2Ph)$ (5a) and $(Me_3SiCH_2)_2W(=CHSiMe_3)_2(PMe_2Ph)$ (5b)*

$(Me_3SiCH_2)_3W(\equiv CSiMe_3)(PMe_2Ph)$ (**5a**) and $(Me_3SiCH_2)_2W(=CHSiMe_3)_2(PMe_2Ph)$ (**5b**) were prepared by a procedure similar to that used to prepare complexes **3a** and **3b**. Upon addition of PMe_2Ph to a solution of $(Me_3SiCH_2)_3W(\equiv CSiMe_3)$ (**4a**) in toluene-d_8 at 23 °C, an immediate color change from yellow to orange-red was observed. NMR spectroscopic data at –50 °C, *vide infra*, were consistent with the formation of the PMe_2Ph adduct $(Me_3SiCH_2)_3W(\equiv CSiMe_3)(PMe_2Ph)$ (**5a**). NMR spectroscopic characterization (^1H, ^{13}C, ^{31}P, ^{29}Si, and HMQC) of **5a** suggests that the PMe_2Ph ligand coordinates *cis* to the alkylidyne ligand as in **3a**. Upon warming the solution of **5a** in toluene-d_8 to 23 °C, **5a** was found to undergo alkyl-to-alkylidyne α-hydrogen migration to give *bis*(alkylidene) $(Me_3SiCH_2)_2W(=CHSiMe_3)_2(PMe_2Ph)$ (**5b**), which was characterized by ^1H, ^{13}C, ^{31}P, ^{29}Si, and HMQC NMR spectroscopy. As in **3a** ⇌ **3b**, the two tautomers reach an equilibrium (**5a** ⇌ **5b**) [K_{eq} (303 K) = 4.65(0.11)].

5a and **5b** also exhibit diastereotopic α-hydrogen atoms on the equatorial alkyl ligands, as shown in the Newman projections in Figure 2.7. The ^1H NMR resonances of the alkylidene H atoms in **5b** were observed as doublets at 8.217 ($^3J_{P\text{-}H}$ = 5.3 Hz) and 7.621 ($^3J_{P\text{-}H}$ = 3.6 Hz) ppm, respectively. Similarly, the ^{13}C NMR resonances of the alkylidene ligands in **5b** appeared as doublets at 257.8 and 256.0 ppm, respectively. These observations suggest that, as in **3b**, there

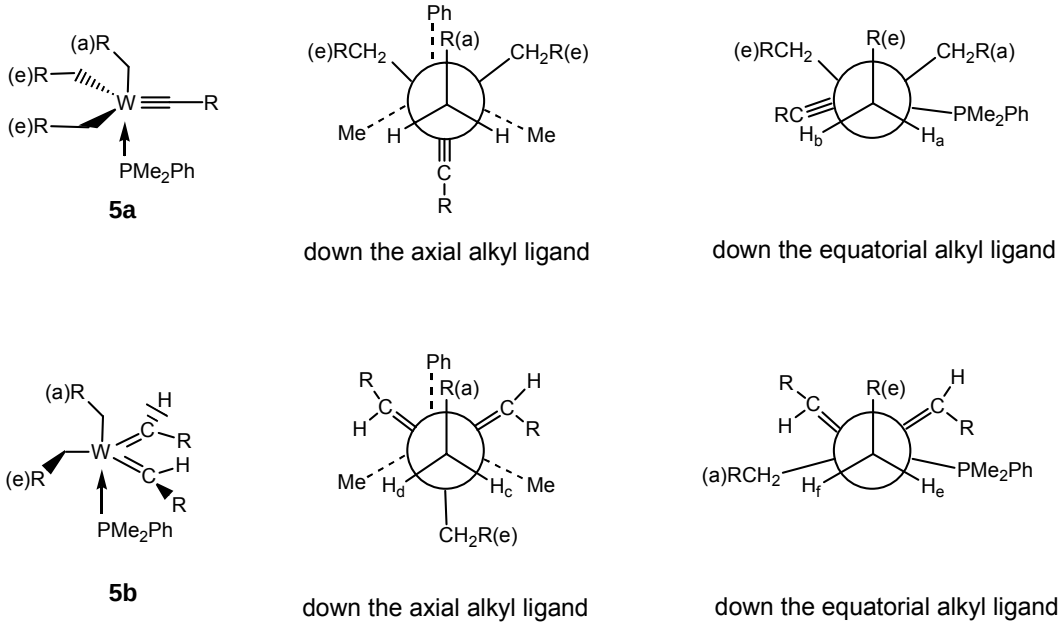

R = $SiMe_3$; (a) = axial; (e) = equatorial

Figure 2.7. Newman projections of **5a** and **5b** showing the diastereotopic protons.

are two inequivalent alkylidene ligands in **5b**. The coupling constants $^2J_{P\text{-}C\text{-}axial}$ and $^2J_{P\text{-}C\text{-}equatorial}$ of 32.2 and 0 Hz for the axial and equatorial $-CH_2R$ ligands, respectively, and $^2J_{P\text{-}C}$ of 12.1 and 11.1 Hz for the two alkylidene ligands suggest that the two alkylidene and one alkyl ligands coordinate *cis* to the PMe_3 ligand. Two inequivalent alkylidene ligands suggest that **5b** adopts an *anti, syn* configuration similar to that of **3b**. The prochiral W atom in **5a** gives rise to diastereotopic α-hydrogen atoms (CH_aH_b-$SiMe_3$) for the equatorial alkyl ligands as doublet of doublets at 0.750 ppm ($^2J_{Ha\text{-}Hb}$ = $^3J_{P\text{-}H}$ = 14.8 Hz) and 0.530 ppm in the ^{1}H NMR spectrum at –50 °C.

The equilibrium mixture of **5a** and **5b** in solution was found thermally unstable. They are converted to $(Me_3SiCH_2)(Me_3SiCH{=})W(\equiv CSiMe_3)(PMe_2Ph)_2$ (**9a-b**), which is discussed in Chapter 3. Repeated attempts to purify **5a-b** through crystallization gave thermally unstable, oily liquids which failed to give satisfactory C elemental analysis, although the H and P elemental analyses were good.[25] The characterization of **5a-b** was thus based on their ^{1}H, ^{13}C, ^{31}P, ^{29}Si, ^{1}H-decoupled ^{13}C, and HMQC NMR spectra.

2.2.4. *Kinetic and Thermodynamic Studies of the 3a ⇌ 3b Exchange*

In the current work, $(Me_3SiCH_2)_3W(\equiv CSiMe_3)(PR_3)$ (**3a** and **5a**), adducts between phosphines PR_3 and alkyl alkylidyne $(Me_3SiCH_2)_3W{\equiv}CSiMe_3$ (**4a**), were found to undergo exchanges with their *bis*(alkylidene) tautomers $(Me_3SiCH_2)_2W(=CHSiMe_3)_2(PR_3)$ (**3b** and **5b**). Given the unusual nature of the

exchange processes of **3a-b** and **5a-b** in the presence of phosphines, further kinetic and thermodynamic studies were performed with the goal of elucidating the mechanism. These studies of the **3a** ⇌ **3b** and **5a** ⇌ **5b** exchanges are presented here and in the subsequent section (Section 2.2.5), respectively.

Variable-temperature NMR spectra of the tautomerization **3a** ⇌ **3b** were studied, and the equilibrium constants, K_{eq} = [**3b**] / [**3a**], measured between 278 and 303 K are listed in Table 2.3. A plot of ln K_{eq} vs 1/T (Figure 2.8) gave $\Delta H°$ = –1.8(0.5) kcal/mol and $\Delta S°$ = –1.5(1.7) eu.[14] The equilibrium constants (K_{eq}) range from 12.3(0.2) at 278 K to 9.37(0.12) at 303 K, indicating that the alkylidene isomer **3b** is favored. Decreasing the temperature shifts the equilibrium towards **3a**. The process **3a** ⇌ **3b** is slightly exothermic with $\Delta H°$ = –1.8(0.5) kcal/mol. It is interesting to note that the d^0 *bis*(alkylidene) complex **3b** is thermodynamically close in energy to its alkylidyne isomer **3a** [$\Delta G°_{298K}$ = –1.3(1.0) kcal/mol], although **3b** is slightly more stable. If there is an alkyl-alkylidyne scrambling process in $(Me_3SiCH_2)_3W{\equiv}CSiMe_3$ (**4a**) as in $(Bu^tCH_2)_3W{\equiv}CSiMe_3$ ⇌ $(Bu^tCH_2)_2W(CH_2SiMe_3)({\equiv}CBu^t)$, the proposed *bis*(alkylidene) intermediate "$(Me_3SiCH_2)_2W(=CHSiMe_3)_2$ (**4b**)" is much higher in energy than **4a**, and coordination with PMe_3 to give **3b** significantly lowers its energy so that **3a** ⇌ **3b** equilibrium is observed.[18,22]

In the previous study of the exchange of silyl complexes $(Bu^tCH_2)_2W({\equiv}CBu^t)(SiBu^tPh_2)$ (**2a**) ⇌ $(Bu^tCH_2)W(=CHBu^t)_2(SiBu^tPh_2)$ (**2b**), only

Table 2.3. Equilibrium (K_{eq}) and rate constants (k_1 and k_{-1}) of the **3a** ⇌ **3b** exchange [a]

T (K)	K_{eq} [b]	k_1 x 10^5 (s^{-1})[c]	k_{-1} x 10^6 (s^{-1})[c]
278 ± 1	12.3 ± 0.2	1.42 ± 0.02	1.160 ± 0.018
283 ± 1	11.52 ± 0.08	2.47 ± 0.13	2.14 ± 0.11
288 ± 1	10.941 ± 0.012	4.16 ± 0.04	3.80 ± 0.04
293 ± 1	10.43 ± 0.07	7.6 ± 0.3	7.3 ± 0.3
298 ± 1	9.80 ± 0.05	10.55 ± 0.10	10.71 ± 0.10
303 ± 1	9.37 ± 0.12	17.5 ± 0.5	18.6 ± 0.6

[a] Solvent: toluene-d_8

[b] The largest random uncertainty is $\sigma K_{eq(ran)}/K_{eq}$ = 0.2/12.3 = 1.6%. The total uncertainty $\sigma K_{eq}/K_{eq}$ of 5.2% was calculated from $\sigma K_{eq(ran)}/K_{eq}$ = 1.6% and the estimated systematic uncertainty $\sigma K_{eq(sys)}/K_{eq}$ = 5% by $\sigma K_{eq}/K_{eq} = [(\sigma K_{eq(ran)}/K_{eq})^2 + (\sigma K_{eq(sys)}/K_{eq})^2]^{1/2}$.

[c] The largest random uncertainties are $\delta k_{1(ran)}/k_1$ = 0.13/2.47 = 5.3% and $\delta k_{-1(ran)}/k_{-1}$ = 0.11/2.14 = 5.1%. The total uncertainties $\delta k_1/k_1$ = 0.0726 and $\delta k_{-1}/k_{-1}$ = 0.0717 were calculated from $\delta k_{(ran)}/k$ and the estimated systematic uncertainty $\delta k_{(sys)}/k$ = 5% by $\delta k/k = [(\delta k_{(ran)}/k)^2 + (\delta k_{(sys)}/k)^2]^{1/2}$.

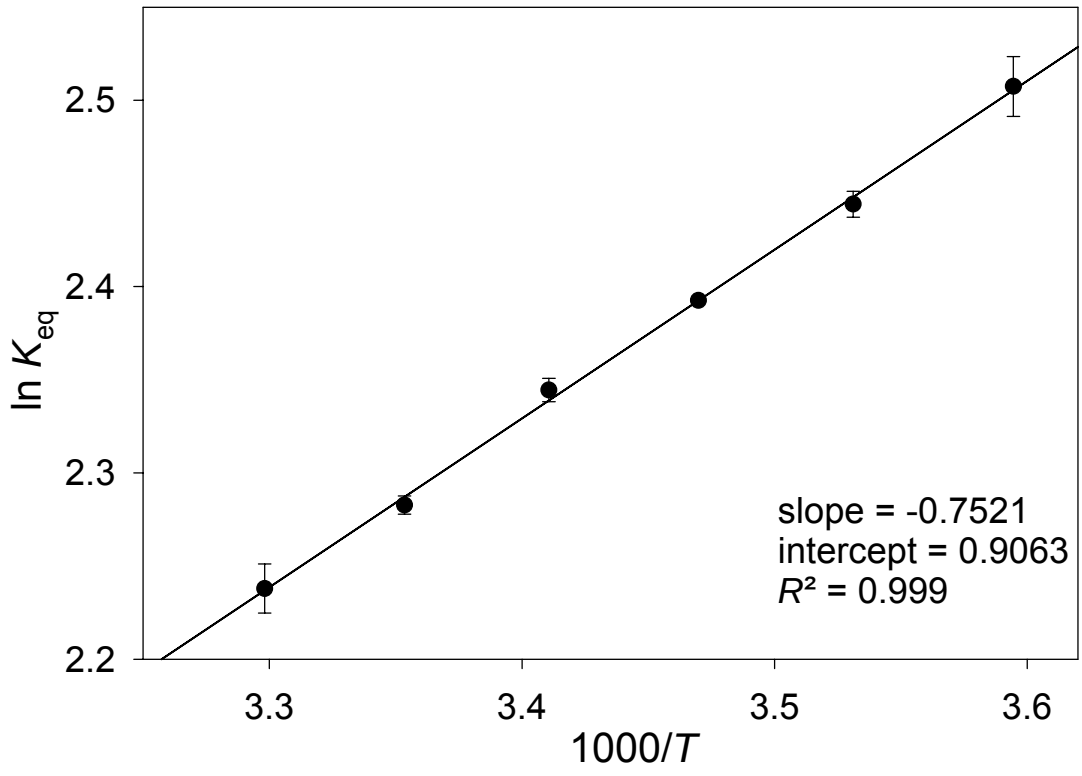

Figure 2.8. A plot of ln K_{eq} vs 1/T of the equilibrium **3a** ⇌ **3b**.

the thermodynamic properties were reported. We have conducted kinetic studies of the unusual alkyl alkylidyne and *bis*(alkylidene) exchange between **3a** and **3b**.

Variable-temperature ^{1}H NMR experiments for the **3a** ⇌ **3b** exchange between 278 and 303 K show that the α-hydrogen migrations between **3a** and **3b** follow first-order reversible kinetics (Eqs. 2.3 and 2.4),[26]

$$\ln\left[\frac{\left(I_{\mathbf{3b}-\mathrm{e}}-I_{\mathbf{3b}-\mathrm{t}}\right)}{\left(I_{\mathbf{3b}-\mathrm{e}}-I_{\mathbf{3b}-0}\right)}\right]=-\left(k_1+k_{-1}\right)t \qquad \text{(Eq. 2.3)}$$

$$K_{\mathrm{eq}}=\frac{k_1}{k_{-1}}=\frac{[\mathbf{3b}]}{[\mathbf{3a}]} \qquad \text{(Eq. 2.4)}$$

where $I_{\mathbf{3b}\text{-}0}$, $I_{\mathbf{3b}\text{-t}}$ and $I_{\mathbf{3b}\text{-e}}$ are the integrations of **3b** at time t = 0, t = t, and equilibrium, respectively; k_1 and k_{-1} are the rate constants for the forward and reverse reactions, respectively. The kinetic plots for the exchange are shown in Figure 2.9, and the rate constants from Eq. 2.3 are given in Table 2.3. Eyring plots (Figure 2.10) lead to the activation parameters of the exchange: $\Delta H_1^{\neq}$ = 16.2(1.2) kcal/mol, $\Delta S_1^{\neq}$ = –22(4) eu for the forward reaction **3a** → **3b**, and $\Delta H_2^{\neq}$ = 18.0(1.3) kcal/mol, $\Delta S_2^{\neq}$ = –21(4) eu for the reverse **3b** → **3a** reaction.

The **3a** ⇌ **3b** exchange is significantly slower than the $(Bu^tCH_2)_2W(\equiv CBu^t)(SiBu^tPh_2)$ (**2a**) ⇌ $(Bu^tCH_2)W(=CHBu^t)_2(SiBu^tPh_2)$ (**2b**) exchange; The latter was observed in the 2D-NOESY spectra (t_{mix} = 3 s) at 23 °C.[22a] The **3a** ⇌ **3b** exchange is, however, much faster than the alkyl-alkylidene scrambling in $(Bu^tCH_2)_3W\equiv CSiMe_3$ which was observed at >70 °C.[18a] The

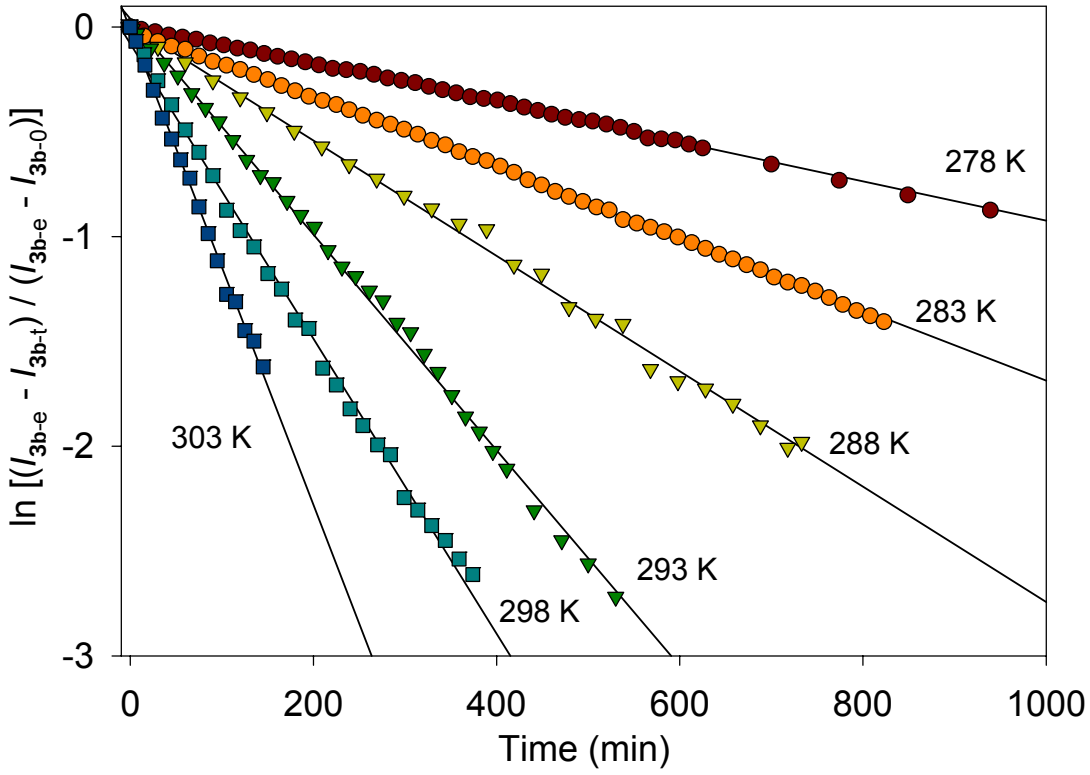

Figure 2.9. Kinetic plots of the reversible reactions **3a** ⇌ **3b**.

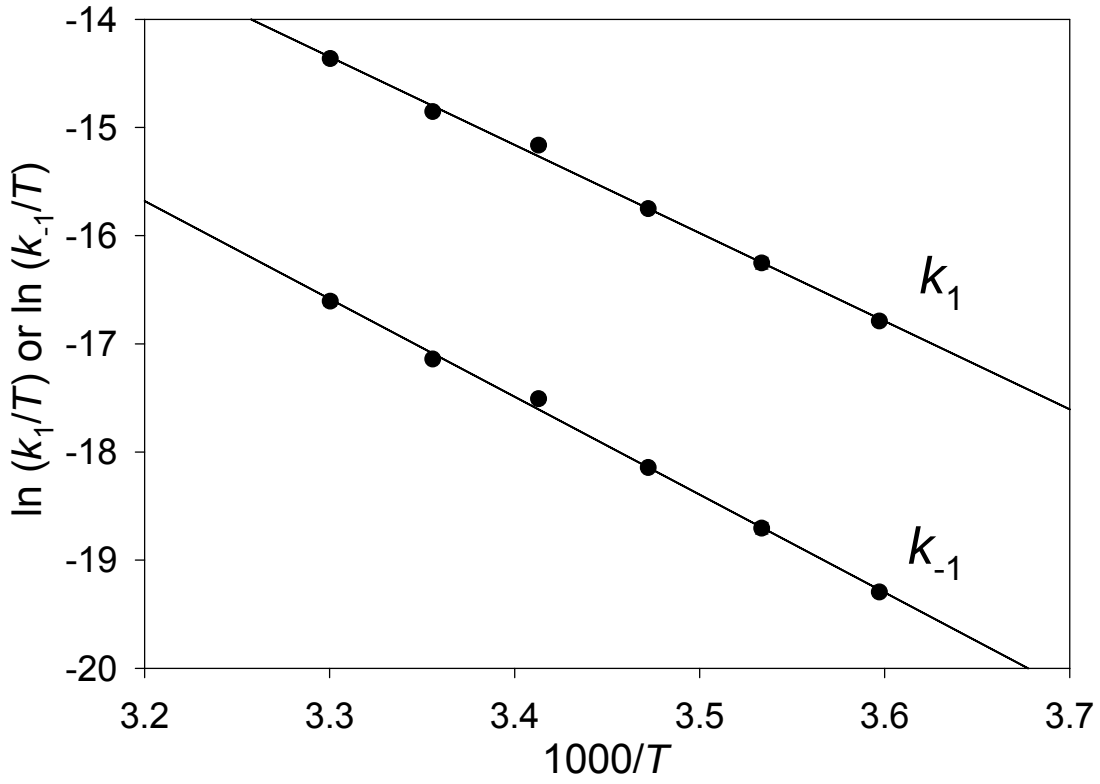

Figure 2.10. Eyring plots for the reversible reactions **3a** ⇌ **3b**.

activation free energy $\Delta G_1^{\neq}{}_{298K}$ of 23(2) kcal/mol for the forward reaction **3a** → **3b** is 28.1(1.1) kcal/mol lower than that for the alkyl-alkylidene scrambling in $(Bu^tCH_2)_3W{\equiv}CSiMe_3$.[18a]

It is interesting to note that $(Bu^tCH_2)_3W{\equiv}C^tBu$ (**1**) reacts with neat PMe_3 in a sealed tube at 100 °C, giving $(Bu^tCH_2)W({\equiv}C^tBu)(=CH^tBu)(PMe_3)_2$ (**6**) through α-hydrogen abstraction and CMe_4 elimination, as Schrock and Clark have reported (and discussed in Chapter 3).[15a] When ca. 1 equiv of PMe_3 was added to *a solution* of **1** in benzene-d_6 *at room temperature*, a similar reaction giving **6** and CMe_4 occurred. No adduct between **1** and PMe_3 was observed. The studies here reveal the differences in the reactivities of $(Me_3SiCH_2)_3W{\equiv}CSiMe_3$ (**4a**) and its analog $(Bu^tCH_2)_3W{\equiv}CBu^t$ (**1**) toward PMe_3. The role of PMe_3 in the **3a** ⇌ **3b** exchange has been studied by density functional theory calculations and will be discussed in Section 2.2.6.

2.2.5. *Thermodynamic and Kinetic Studies of the 5a ⇌ 5b Exchange. A Comparison of PMe_3 and PMe_2Ph*

PMe_2Ph is bulkier than PMe_3, and the phenyl group often acts as an electron withdrawing group. Both yielded alkylidyne adducts in their reactions with **4a**: $(Me_3SiCH_2)_3W({\equiv}CSiMe_3)(PMe_3)$ (**3a**) and $(Me_3SiCH_2)_3W({\equiv}CSiMe_3)(PMe_2Ph)$ (**5a**). The thermodynamic and kinetic studies were conducted for the $(Me_3SiCH_2)_3W({\equiv}CSiMe_3)(PMe_2Ph)$ (**5a**) ⇌ $(Me_3SiCH_2)_2W(=CHSiMe_3)_2(PMe_2Ph)$ (**5b**) exchange at 303 K. The **5a** ⇌ **5b**

equilibrium [K_{eq}' = 4.65(0.11) at 303 K] is shifted more to the left (**5a**) than the **3a** ⇌ **3b** equilibrium [K_{eq} = 9.37(0.12) at 303 K]. Our theoretical studies presented in the next section (Section 2.2.6) indicate that PMe_3 ligands prefer to bind to the *bis*(alkylidene) tautomers, and this coordination plays a critical role in the stabilization of the *bis*(alkylidene) tautomers. Perhaps the bulkier PMe_2Ph ligands with an electron-withdrawing phenyl group donate less electron density to the metal centers in **5a** and **5b**, shifting the equilibrium to alkyl alkylidyne **5a**.

Kinetic studies using a kinetic equation similar to Eq. 2.3 give k_1' = (1.0 ± 0.1) x 10^{-4} s^{-1} and k_{-1}' = (2.2 ± 0.2) x 10^{-5} s^{-1} for the **5a** → **5b** and the reverse **5b** → **5a** conversions at 303 K, respectively (Figure 2.11). In comparison, the rates for the **3a** ⇌ **3b** exchanges in the PMe_3 complexes are k_1 = (1.75 ± 0.05) x 10^{-4} s^{-1} and k_{-1} = (1.86 ± 0.06) x 10^{-5} s^{-1}. The forward **5a** → **5b** conversion in the PMe_2Ph complexes is slower than the **3a** → **3b** conversion, whereas the reverse **5b** → **5a** conversion is slightly faster than the **3b** → **3a** conversion. The **3a** ⇌ **3b** equilibrium is more shifted to **3b** [K_{eq} = 9.37(0.12)] than in the **5a** ⇌ **5b** equilibrium [K_{eq}' = 4.65(0.11)], resulting in a higher kinetic barrier for the reverse **3b** → **3a** conversion. It is not clear what leads to the higher kinetic barrier.

2.2.6. *Theoretical Studies of the 3a ⇌ 3b Exchange*

To understand the effect of the phosphine ligand on the relative stabilities of the tautomers, DFT calculations were carried out by Professors Zhen Yang Lin

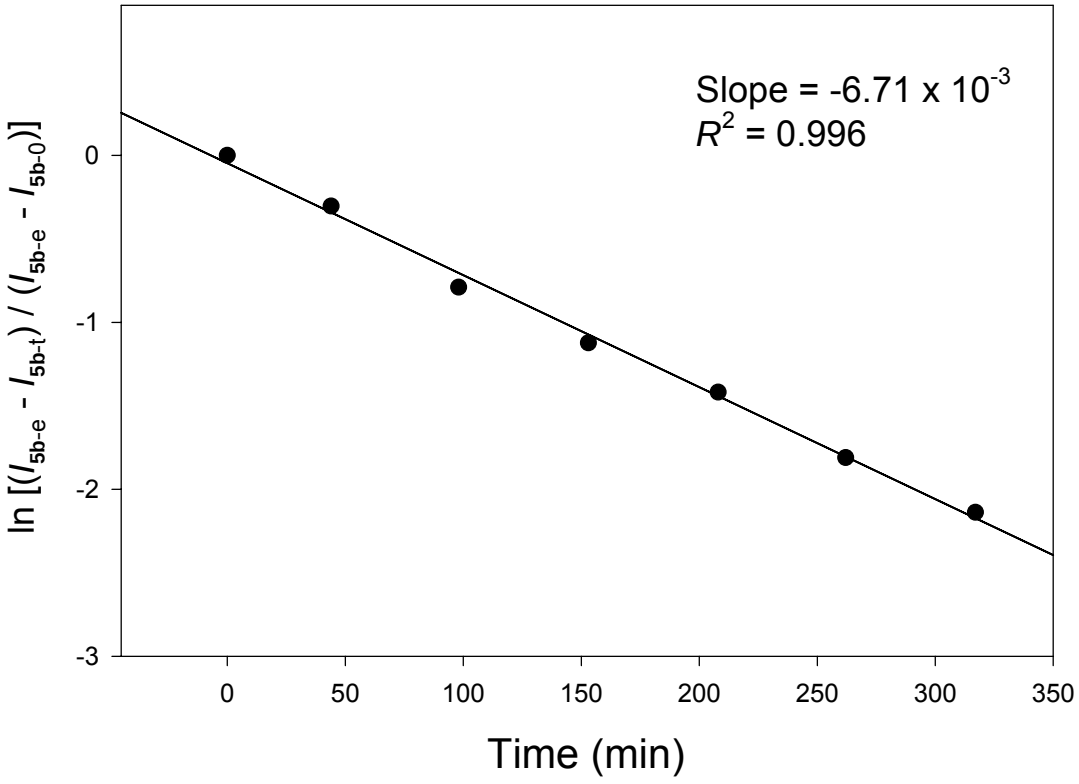

Figure 2.11. Kinetic plot of the formation of **5b** from **5a** at 303 K. $I_{\mathbf{5b}\text{-}0}$, $I_{\mathbf{5b}\text{-}t}$ and $I_{\mathbf{5b}\text{-}e}$ are the integrations of **5b** at the $t = 0$, $t = t$, and equilibrium, respectively.

and Yun-Dong Wu's research groups at the Hong Kong University of Science and Technology. The results of the DFT calculations on the corresponding model complexes are given in Scheme 2.2. The results show that PMe_3 promotes the conversion of the alkylidyne complex to the *bis*(alkilidene) tautomer. **3b'** is calculated to be more stable than **3a'** by 2.1 kcal/mol, consistent with the experimentally measured $\Delta H°$ (–1.8 kcal/mol) for the **3a** $\rightarrow$ **3b** conversion.

The relative energies shown in Scheme 2.2 suggest that PMe_3 binds with the *bis*(alkylidene) tautomer relatively more strongly than with the alkylidyne tautomer, reversing the relative stability in the two adduct isomers. To understand how PMe_3 coordinates to **4a'** and **4b'**, their lowest unoccupied orbitals (LUMOs), which are responsible for interaction with PMe_3, were examined in the frontier region. The structures of **3a'** and **3b'** together with the relative binding ability of **4a'** and **4b'** are closely related to the orbital feature and orbital energies of the LUMOs. Figure 2.12 shows the plots of the relevant LUMOs for both **4a'** and **4b'**. The maximum amplitudes of the LUMOs determine the coordination sites for the PMe_3 ligand. In both structures, the vacant sites are in the axial positions (pointing to the bottom). In the case of **4a'**, the maximum amplitudes of the LUMO are in the equatorial positions and approximately 90° to the alkylidyne ligand. In **4b'**, the maximum amplitude of one lobe in the LUMO is in the vacant site and is also approximately 90° to the two alkylidene ligands. Thus, in both **4a'** and **4b'**, PMe_3 prefers to occupy the

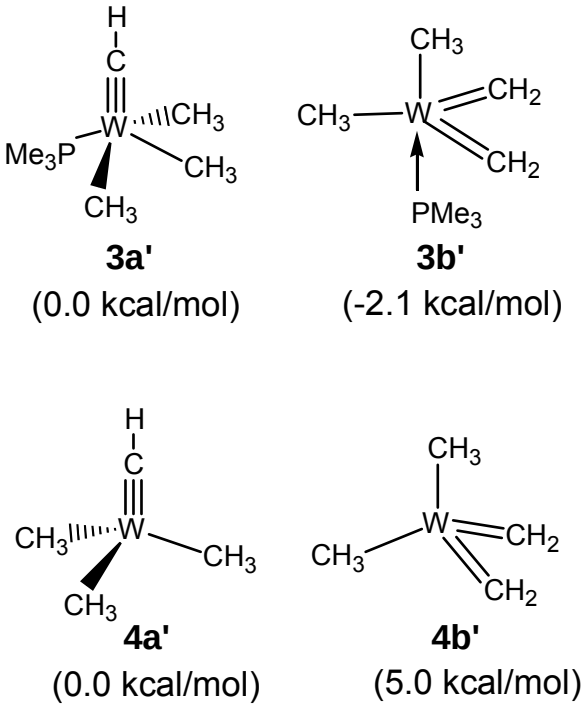

Scheme 2.2. Calculated relative energies for model complexes **3a'**, **3b'**, **4a'** and **4b'**.

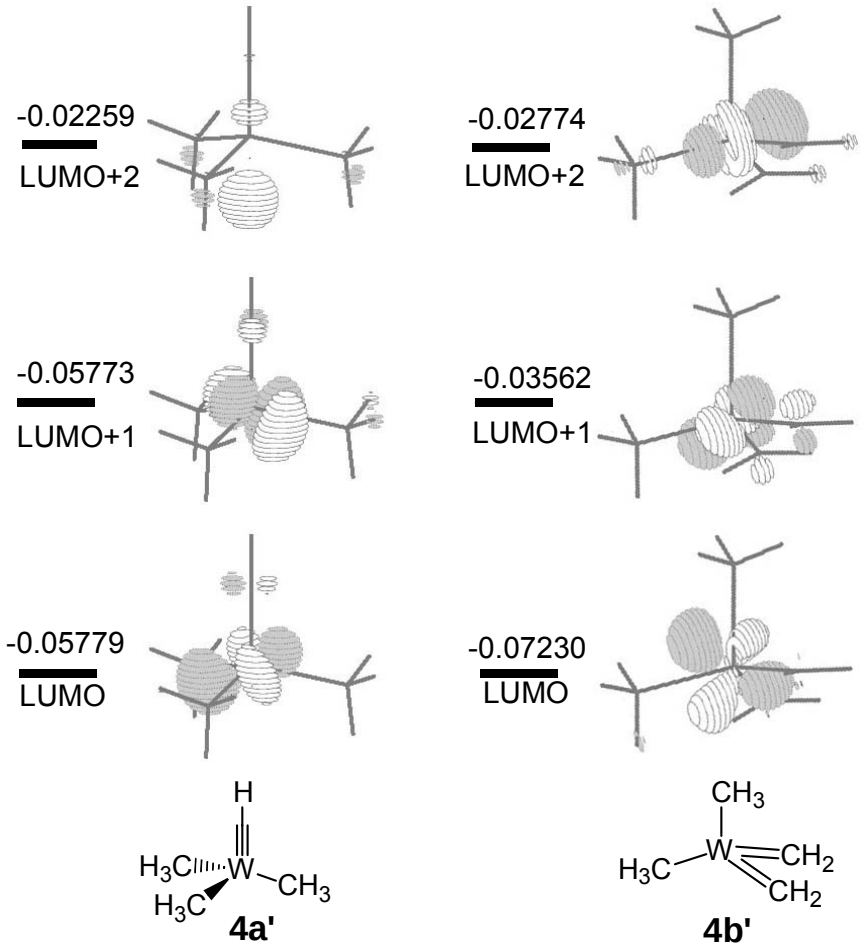

Figure 2.12. Spatial plots of three LUMOs for alkylidyne and *bis*(alkylidene) tautomers with orbital energies (au). The results were obtained from B3LYP/BSII calculations.

coordination sites *trans* to W-CH_3 instead of W=CH_2 or W≡CH, reflecting the stronger *trans* influence properties of the W=CH_2 and W≡CH bonds. The LUMO of **4b'** is much lower in energy than that of **4a'** (Figure 2.12), giving greater ligand binding energy with PMe_3. Therefore, **3b'** is more stable than **3a'**. Clearly, the PMe_3 coordination affects the thermal stabilities of the tautomers significantly.

2.3. Concluding Remarks

In this chapter, an adduct between PMe_3 and alkyl alkylidyne $(Me_3SiCH_2)_3W{\equiv}CSiMe_3$ (**4a**), $(Me_3SiCH_2)_3W(\equiv CSiMe_3)(PMe_3)$ (**3a**), was found to undergo a rare exchange with its *bis*(alkylidene) tautomer $(Me_3SiCH_2)_2W(=CHSiMe_3)_2(PMe_3)$ (**3b**). Thermodynamic studies show that the *bis*(alkylidene) tautomer **3b** is favored in the **3a** ⇌ **3b** equilibrium. The α-hydrogen exchange between **3a** and **3b** follows first-order reversible kinetics. *Bis(*alkylidene) complexes are believed to be intermediates in alkyl-alkylidyne scrambling through α-hydrogen transfer in alkylidyne complexes. The role of PMe_3 in the **3a** ⇌ **3b** exchange has been studied by density functional theory calculations. The current system provides a rare direct observation of an α-hydrogen migration product **3b** and thermodynamic, kinetic, and theoretical study of its formation. Synthesis and characterization of complexes **5a** and **5b** containing PMe_2Ph ligands was also studied. Their exchange was found to be shifted to **5a** and slower than that of the **3a** ⇌ **3b** exchange.

2.4. Experimental Section

2.4.1. *General Procedures*

All manipulations were performed under a dry nitrogen atmosphere with the use of either a dry box or standard Schlenk techniques. Solvents were purified by distillation from potassium/benzophenone ketyl. Benzene-d_6 and toluene-d_8 were dried over activated molecular sieves and stored under N_2. WCl_6 was freshly sublimed under vacuum. $(Me_3SiCH_2)_3W{\equiv}CSiMe_3$ (**4a**)[15g] was prepared from $W(OMe)_3Cl_3$ and six equiv of Me_3SiCH_2MgCl by a procedure similar to that used in the preparation of $(Me_3CCH_2)_3W{\equiv}CCMe_3$ (**1**).[15h] ^1H and ^{13}C NMR spectra were recorded on a Bruker AC-250 or AMX-400 spectrometer and referenced to solvent (residual protons in the ^1H spectra). ^{31}P, ^{29}Si, and HMQC (Heteronuclear Multiple Quantum Coherence) and ^1H-gated-decoupled-^{13}C spectra were recorded on a Bruker AMX-400 spectrometer. Elemental analysis was performed by Complete Analysis Laboratories Inc., Parsippany, New Jersey.

For the thermodynamic studies, the equilibrium constants K_{eq} were obtained from at least two separate experiments at a given temperature, and their averages are listed in Table 2.3. The *maximum* random uncertainty in the equilibrium constants was combined with the estimated systematic uncertainty of ca. 5%. The total uncertainties in the equilibrium constants were used in the ln K_{eq} vs. $1/T$ plot in Figure 2.8 and error propagation calculations. The estimated uncertainty in the temperature measurements for an NMR probe was 1 K. The enthalpy ($\Delta H°$) and entropy ($\Delta S°$) changes were calculated from an

unweighted nonlinear least-squares procedure contained in the SigmaPlot Scientific Graph System. The uncertainties in $\Delta H°$ and $\Delta S°$ were computed from the following error propagation formulas which were derived from $-RT \ln K_{eq} = \Delta H° - T\Delta S°$.[27]

$$(\sigma\Delta H°)^2 = \frac{R^2\left(T_{max}^2 T_{min}^4 + T_{min}^2 T_{max}^4\right)}{(T_{max} - T_{min})^4}\left[\ln\left(\frac{K_{eq(max)}}{K_{eq(min)}}\right)\right]^2\left(\frac{\sigma T}{T}\right)^2 + \frac{2R^2 T_{max}^2 T_{min}^2}{(T_{max} - T_{min})^2}\left(\frac{\sigma K_{eq}}{K_{eq}}\right)^2 \quad \text{(Eq. 2.4)}$$

$$(\sigma\Delta S°)^2 = \frac{2R^2 T_{min}^2 T_{max}^2}{(T_{max} - T_{min})^4}\left[\ln\left(\frac{K_{eq(max)}}{K_{eq(min)}}\right)\right]^2\left(\frac{\sigma T}{T}\right)^2 + \frac{R^2(T_{max}^2 + T_{min}^2)}{(T_{max} - T_{min})^2}\left(\frac{\sigma K_{eq}}{K_{eq}}\right)^2 \quad \text{(Eq. 2.5)}$$

T_{min} and T_{max} are the minimum and maximum temperatures in the current studies; T is the mean temperature in the current studies. $K_{eq(min)}$ and $K_{eq(max)}$ are the minimum and maximum equilibrium constants, respectively. $\sigma K_{eq}/K_{eq}$ is given in Table 2.3. For the kinetic studies, the rate constants k_1 and k_{-1} were obtained from at least two separate experiments at a given temperature, and their averages are listed. The estimated uncertainty (σT) in the temperature measurements for an NMR probe was 1 K. The enthalpy ($\Delta H^{\neq}$) and entropy ($\Delta S^{\neq}$) were calculated from an unweighted nonlinear least-squares procedure contained in the SigmaPlot Scientific Graph System. The uncertainties in $\Delta H^{\neq}$

and $\Delta S^{\neq}$ were computed from the following error propagation formulas (Eqs. 2.7 and 2.8)[27] which were derived from the Eyring Equation (Eq. 2.6) below.

$$\ln\left(\frac{k}{T}\right) = -\frac{\Delta H^{\neq}}{RT} + \left[\frac{\Delta S^{\neq}}{R} - \ln\left(\frac{h}{k_b}\right)\right] \qquad \text{(Eq. 2.6)}$$

$$(\sigma\Delta H^{\neq})^2 = \frac{R^2 T_{\max}^2 T_{\min}^2}{\Delta T^2} \times \left\{\left(\frac{\sigma T}{T}\right)^2\left[\left(1 + T_{\min}\frac{\Delta L}{\Delta T}\right)^2 + \left(1 + T_{\max}\frac{\Delta L}{\Delta T}\right)^2\right] + 2\left(\frac{\sigma k}{k}\right)^2\right\} \qquad \text{(Eq. 2.7)}$$

$$(\sigma\Delta S^{\neq})^2 = \frac{R^2}{\Delta T^2} \times \left\{\left(\frac{\sigma T}{T}\right)^2\left[T_{\max}^2\left(1 + T_{\min}\frac{\Delta L}{\Delta T}\right)^2 + T_{\min}^2\left(1 + T_{\max}\frac{\Delta L}{\Delta T}\right)^2\right] + \left(\frac{\sigma k}{k}\right)^2 (T_{\max}^2 + T_{\min}^2)\right\} \qquad \text{(Eq. 2.8)}$$

$$\Delta L = \ln\left(\frac{k_{\max}}{T_{\max}}\right) - \ln\left(\frac{k_{\min}}{T_{\min}}\right)$$

$$\Delta T = T_{\max} - T_{\min}$$

k_b and h are the Boltzman and Plank constants, respectively. The values of $\sigma k/k$ are given in Table 2.3.

2.4.2. *NMR Experiments*

Complete and unambiguous assignments of all proton and carbons resonances were achieved on the basis of chemical shift considerations, as well as NMR experiments, namely HMQC and ^{1}H-gated-decoupled-^{13}C experiments. HMQC (Heternuclear Multiple Quantum Coherence), the simplest form of an inverse H,X correlation technique,[28a,c] was used to assign diastereotopic protons in complexes **3** and **5**. ^{1}H-gated-decoupled-^{13}C experiments were utilized to determine the number of hydrogen atoms that are bonded to an α-carbon atom and to calculate the $^{1}J_{C\text{-}H}$ coupling constants.[28b,c]

2.4.3. *Preparation of $(Me_3SiCH_2)_3W(\equiv CSiMe_3)(PMe_3)$ (3a)*

3a was prepared by the vacuum transfer of PMe_3 (25 mmHg, 0.104 mmol) to a J. R. Youngs NMR tube containing **4a** (48 mg, 0.0904 mmol) in toluene-d_8. The reaction mixture is kept frozen in liquid nitrogen until placed in the pre-cooled NMR probe at –50 °C. **3a**: ^{1}H NMR (toluene-d_8, 400.11 MHz, –50 °C, J in Hz) δ 0.904 (d, 9H, P*Me*$_3$, $^{2}J_{P\text{-}H}$ = 7.2), 0.751 (dd, 2H, *eq*-C*H*$_a$H$_b$-SiMe$_3$, $^{2}J_{H\text{-}H}$ = $^{3}J_{P\text{-}H}$ = 14.4), 0.503 (s, 9H, ≡CSi*Me*$_3$), 0.487 (d, 2H, *ax*-C*H*$_2$SiMe$_3$, $^{3}J_{P\text{-}H}$ = 10.7), 0.329 (s, 9H, *ax*-CH$_2$Si*Me*$_3$), 0.316 (s, 18H, *eq*-CH$_2$Si*Me*$_3$), 0.213 (dd, 2H, *eq*-CH$_a$*H*$_b$-SiMe$_3$, $^{3}J_{P\text{-}H}$ = 28.2, $^{2}J_{H\text{-}H}$ = 14.1); ^{13}C{^{1}H} NMR (toluene-d_8, 100.63 MHz, –50 °C, J in Hz) δ 358.81 (d, ≡*C*SiMe$_3$, $^{2}J_{P\text{-}C}$ = 14.5, $^{1}J_{W\text{-}C}$ = 159.1), 81.69 (d, *ax*-*C*H$_2$SiMe$_3$, $^{2}J_{P\text{-}C}$ = 36.5, $^{1}J_{W\text{-}C}$ = 117.9), 49.45 (d, *eq*-*C*H$_2$SiMe$_3$, $^{1}J_{H\text{-}C}$ = 111.6, $^{2}J_{P\text{-}C}$ = 7.2, $^{1}J_{W\text{-}C}$ = 59.9), 17.84 (d, P*Me*$_3$, $^{1}J_{H\text{-}C}$ = 128.2, $^{1}J_{P\text{-}C}$ = 22.8), 4.23 (s,

≡CSi*Me*$_3$, $^1J_{H\text{-}C}$ = 117.8, $^3J_{W\text{-}C}$ = 50.1), 3.55 (s, *ax*-CH_2Si*Me*$_3$, $^1J_{H\text{-}C}$ = 117.1, $^3J_{W\text{-}C}$ = 33.2), 3.48 (s, *eq*-CH_2Si*Me*$_3$, $^1J_{H\text{-}C}$ = 117.1, $^3J_{W\text{-}C}$ = 25.0); $^{31}P\{^1H\}$ (toluene-d_8, 161.97 MHz, –50 °C, *J* in Hz) δ –5.64 (s, $^1J_{W\text{-}P}$ = 28.9); $^{29}Si\{^1H\}$ (toluene-d_8, 79.49 MHz, –50 °C, *J* in Hz) δ –0.269 (d, *ax*-CH_2*Si*Me_3, $^3J_{P\text{-}Si}$ = 2.0), –2.482 (d, *eq*-CH_2*Si*Me_3, $^3J_{P\text{-}Si}$ = 4.9, $^2J_{W\text{-}Si}$ = 50.2), –21.129 (d, ≡C*Si*Me_3, $^3J_{P\text{-}Si}$ = 2.3, $^2J_{W\text{-}Si}$ = 52.3). The assignments of the ^1H and ^{13}C NMR were confirmed by low-temperature HMQC experiments.

2.4.4. *Preparation of $(Me_3SiCH_2)_2W(=CHSiMe_3)_2(PMe_3)$ (3b)*

A solution of $(Me_3SiCH_2)_3W{\equiv}CSiMe_3$ (**4a**, 95 mg, 0.179 mmol) in pentane was frozen by liquid nitrogen in a 125-ml Schlenk flask. The flask headspace was evacuated. PMe_3 (100 mmHg, 0.358 mmol) was then vacuum transferred to the flask submerged in liquid nitrogen. The PMe_3 was then condensed in the flask, and the flask was warmed to room temperature. The flask was then added nitrogen, and stirred overnight at room temperature. Cooling the solution at –30 °C overnight gave crystals of **3b** (87 mg, 0.143 mmol, 80% yield). ^1H NMR (toluene-d_8, 400.11 MHz, –20 °C, *J* in Hz) δ 7.985 (d, 1H, =C*H*$SiMe_3$, $^3J_{P\text{-}H}$ = 5.6), 7.192 (d, 1H, =C*H*$SiMe_3$, $^3J_{P\text{-}H}$ = 4.0), 1.024 (d, 9H, P*Me*$_3$, $^2J_{P\text{-}H}$ = 7.8), 0.917 (dd, 1H, *eq*-C*H*$_a$H$_b$-$SiMe_3$, $^3J_{P\text{-}H}$ = 17.7, $^2J_{H\text{-}H}$ = 11.3), 0.876 (dd, 1H, *eq*-CH_a*H*$_b$-$SiMe_3$, $^3J_{P\text{-}H}$ = 32.2, $^2J_{H\text{-}H}$ = 11.3; overlapped with *eq*-C*H*$_a$H$_b$-$SiMe_3$ peak), 0.388 (s, 9H, *ax*-CH_2Si*Me*$_3$, $^2J_{Si\text{-}H}$= 6.0), 0.388 (d, 2H, *ax*-C*H*$_2$$SiMe_3$, $^3J_{P\text{-}H}$ = 11.4; overlapped with *ax*-CH_2Si*Me*$_3$ peak), 0.342 (s, 9H, *eq*-CH_2Si*Me*$_3$), 0.280 (s, 9H, =CHSi*Me*$_3$),

0.128 (s, 9H, =CHSi*Me*$_3$); ^{13}C{^{1}H} (toluene-d_8, 100.63 MHz, –40 °C, *J* in Hz) δ 256.43 (d, =*C*HSiMe$_3$, $^1J_{H\text{-}C}$ = 123.5, $^2J_{P\text{-}C}$ = 11.8), 254.71 (d, =*C*HSiMe$_3$, $^1J_{H\text{-}C}$ = 102.6, $^2J_{P\text{-}C}$ = 12.6), 50.71 (s, *eq*-*C*H$_2$SiMe$_3$, $^1J_{H\text{-}C}$ = 105.3, $^1J_{W\text{-}C}$= 43.0), 38.01 (d, *ax*-*C*H$_2$SiMe$_3$, $^1J_{H\text{-}C}$ = 111.0, $^2J_{P\text{-}C}$ = 32.3), 18.80 (d, P*Me*$_3$, $^1J_{H\text{-}C}$ = 126.4, $^1J_{P\text{-}C}$ = 26.4), 4.82 (s, *ax*-CH$_2$Si*Me*$_3$, $^1J_{H\text{-}C}$ = 118.1), 3.08 (s, *eq*-CH$_2$Si*Me*$_3$, $^1J_{H\text{-}C}$ = 118.8), 1.76 (s, =CHSi*Me*$_3$, $^1J_{H\text{-}C}$ = 117.3), 1.64 (s, =CHSi*Me*$_3$, $^1J_{H\text{-}C}$ = 117.3); ^{31}P{^{1}H} (toluene-d_8, 161.97 MHz, –50 °C, *J* in Hz) δ 0.61 (s, $^1J_{W\text{-}P}$ = 115.5); ^{29}Si{^{1}H} (toluene-d_8, 79.49 MHz, –50 °C, *J* in Hz) δ –0.73 (d, *ax*-CH$_2$*Si*Me$_3$, $^3J_{P\text{-}Si}$ = 19.2), –1.96 (d, *eq*-CH$_2$*Si*Me$_3$, $^3J_{P\text{-}Si}$ = 4.1), –8.63 (d, =CH*Si*Me$_3$, $^3J_{P\text{-}Si}$ = 2.9), –9.89 (d, =CH*Si*Me$_3$, $^3J_{P\text{-}Si}$ = 4.8). ^{1}H and ^{13}C assignments were confirmed by low-temperature HMQC experiments. Anal. Calcd. C, 37.61, H, 8.47. Found C, 37.43, H, 8.66.

2.4.5. *Preparation of (Me$_3$SiCH$_2$)$_3$W(≡CSiMe$_3$)(PMe$_2$Ph) (5a)*

A solution of (Me$_3$SiCH$_2$)$_3$W≡CSiMe$_3$ (**4a**, 50 mg, 0.094 mmol) in toluene-d_8 was added ca. 10-fold excess PMe$_2$Ph *via* cannula transfer to a J. R. Youngs NMR tube. An immediate color change from yellow to orange-red was observed signifying the formation of **5a**. At –50 °C the solution of **5a** was stable. **5a**: ^{1}H NMR (toluene-d_8, 399.97 MHz, –50 °C, *J* in Hz) δ 7.4-7.0 (m, 5H, PMe$_2$*Ph*), 1.30 (d, 6H, P*Me*$_2$Ph, $^2J_{P\text{-}H}$ = 6.0), 0.750 (dd, 2H, *eq*-C*H*$_a$H$_b$-SiMe$_3$, $^2J_{H\text{-}H}$ = $^3J_{P\text{-}H}$ = 14.8), 0.506 (s, 9H, ≡CSi*Me*$_3$), 0.599 (broad singlet, 2H, *ax*-C*H*$_2$SiMe$_3$), 0.363 (s, 9H, *ax*-CH$_2$Si*Me*$_3$), 0.243 (s, 18H, *eq*-CH$_2$Si*Me*$_3$), 0.530 (broad, 2H, *eq*-CH$_a$*H*$_b$-

$SiMe_3$); $^{13}C\{^1H\}$ NMR (toluene-d_8, 100.59 MHz, –60 °C, *J* in Hz) δ 358.91 (d, ≡*C*$SiMe_3$, $^2J_{P\text{-}C}$ = 14.1), 83.86 (d, *ax*-*C*H_2SiMe_3, $^2J_{P\text{-}C}$ = 34.2), 50.38 (d, *eq*-*C*H_2SiMe_3, $^2J_{P\text{-}C}$ = 7.0, 16.74 (d, P*Me*$_2$Ph, $^1J_{P\text{-}C}$ = 22.1), 3.59 (s, ≡CSi*Me*$_3$, $^3J_{W\text{-}C}$ = 51.3), 2.97(s, *ax*-CH_2Si*Me*$_3$), 2.82 (s, *eq*-CH_2Si*Me*$_3$); $^{31}P\{^1H\}$ (toluene-d_8, 161.92 MHz, –60 °C, *J* in Hz) δ 6.57 (s); $^{29}Si\{^1H\}$ (toluene-d_8, 79.46 MHz, –60 °C, *J* in Hz) δ 0.677 (d, *ax*-CH_2*Si*Me_3, $^3J_{P\text{-}Si}$ = 1.0), –1.22 (d, *eq*-CH_2*Si*Me_3, $^3J_{P\text{-}Si}$ = 4.8), –19.28 (d, ≡C*Si*Me_3, $^3J_{P\text{-}Si}$ = 1.9, $^2J_{W\text{-}Si}$ = 51.0).

2.4.6. Preparation of $(Me_3SiCH_2)_2W(=CHSiMe_3)_2(PMe_2Ph)$ (5b)

Upon warming a solution of **5a** to room temperature it was converted to **5b**. **5b** was stable for several days in solution at room temperature. Attempts to obtain pure crystals of **5** yielded a dark brown oil, which was thermally unstable.[25] **5b**: ^1H NMR (toluene-d_8, 399.97 MHz, –20 °C, *J* in Hz) δ 8.22 (d, 1H, =C*H*$SiMe_3$, $^3J_{P\text{-}H}$ = 5.3), 7.62 (d, 1H, =C*H*$SiMe_3$, $^3J_{P\text{-}H}$ = 3.6), 7.5-7.0 (m, PMe_2*Ph*), 1.38 (d, 6H, P*Me*$_2$Ph, $^2J_{P\text{-}H}$ = 7.6), 0.728 (dd, 1H, *eq*-C*H*$_a$H$_b$-$SiMe_3$, $^3J_{P\text{-}H}$ = 18.6, $^2J_{H\text{-}H}$ = 11.2), 1.01 (dd, 1H, *eq*-CH_a*H*$_b$-$SiMe_3$, $^3J_{P\text{-}H}$ = 33.0, $^2J_{H\text{-}H}$ = 11.2), 0.331 (s, 9H, *ax*-CH_2Si*Me*$_3$), 0.372 (d, 2H, *ax*-C*H*$_2$$SiMe_3$, $^3J_{P\text{-}H}$ =9.2), 0.326 (s, 9H, *eq*-CH_2Si*Me*$_3$), 0.137 (s, 9H, =CHSi*Me*$_3$), 0.056 (s, 9H, =CHSi*Me*$_3$); $^{13}C\{^1H\}$ (toluene-d_8, 100.59 MHz, –20 °C, *J* in Hz) δ 257.8 (d, =*C*H$SiMe_3$, $^2J_{P\text{-}C}$ = 12.1), 256.0 (d, =*C*H$SiMe_3$, $^2J_{P\text{-}C}$ = 11.1), 53.5 (s, *eq*-*C*H_2SiMe_3), 37.4 (d, *ax*-*C*H_2SiMe_3, $^2J_{P\text{-}C}$ = 32.2), 15.5 (d, P*Me*$_2$Ph, $^1J_{P\text{-}C}$ = 26.2), 4.25 (s, *ax*-CH_2Si*Me*$_3$), 2.90 (s, *eq*-CH_2Si*Me*$_3$), 1.86 (s, =CHSi*Me*$_3$), 1.67 (s, =CHSi*Me*$_3$); $^{31}P\{^1H\}$ (toluene-d_8, 161.92 MHz, –60 °C, *J* in

Hz) δ 13.9 (s, $^{1}J_{W\text{-}P}$ = 97.1); ^{29}Si{^{1}H} (toluene-d_8, 79.46 MHz, –20 °C, J in Hz) δ 1.09 (s, *ax*-CH_2SiMe$_3$), –1.75 (d, *eq*-CH_2SiMe$_3$, $^{3}J_{P\text{-}Si}$ = 5.6), –7.85 (d, =CHSiMe$_3$, $^{3}J_{P\text{-}Si}$ = 2.9), –9.16 (d, =CHSiMe$_3$, $^{3}J_{P\text{-}Si}$ = 4.0).

2.4.7. *Kinetic Study of the Conversion of $(Me_3SiCH_2)_3W(\equiv CSiMe_3)(PMe_3)$ (3a) to 3b*

At least two experiments for each temperature were conducted. A mixture of $(Me_3SiCH_2)_3W\equiv CSiMe_3$ (**4a**), 4,4'-dimethylbiphenyl (an internal standard), and toluene-d_8 in J. R. Youngs NMR tubes in liquid nitrogen were added ca. 2-21 equiv of PMe_3 through vacuum transfer. The samples were kept below –78 °C before insertion into the NMR probe. The NMR probe was pre-cooled or pre-heated to the set temperature. After the NMR tubes were inserted into the probe, the ^{1}H NMR spectra were taken after the temperature was stabilized, and the integrations of **3b**, relative to those of the internal standard, were used as $I_{\mathbf{3b}\text{-}0}$ at t = 0. Once the equilibrium between **3a** and **3b** was reached, the integration of **3b** was used as $I_{\mathbf{3b}\text{-}e}$.

2.4.8. *Thermodynamic Study of the Equilibrium between 3a and 3b*

Three samples of **3a-b** were prepared with at least 10 equiv of PMe_3, and kept at room temperature for over 24 hours to ensure equilibrium was established. The samples were then placed in a circulation bath at 278.0(0.1), 283.0(0.1), 288.0(0.1), 293.0(0.1), 298.0(0.1), or 303.0(0.1) K for at least 6 hours.

^{31}P NMR spectra were taken at −50 °C with a relaxation delay of 10 s. K_{eq} = [**3b**] / [**3a**] = I_{3b} / I_{3a} were calculated from the integrations of the two tautomers.

2.4.9. *Kinetic and Thermodynamic Studies of the Conversion of $(Me_3SiCH_2)_3W(\equiv CSiMe_3)(PMe_2Ph)$ (5a) to 5b at 303 K*

A mixture of $(Me_3SiCH_2)_3W\equiv CSiMe_3$ (**4a**, 35 mg, 0.066 mmol), 4,4'-dimethylbiphenyl (an internal standard), and toluene-d_8 in J. R. Youngs NMR tubes were added ca. 10-fold excess PMe_2Ph *via* cannula transfer. Kinetic measurements were taken in duplicate on a Bruker 400 MHz NMR at 303 K. Integration of the ^{1}H PMe_2– peak of **5b** was used in the kinetic plot. For thermodynamic measurements, two samples of **5a-b** were prepared with at least 10 equiv of PMe_2Ph, and kept at room temperature for over 24 hours to ensure that equilibrium was established. The samples were placed in a circulation bath at 303.0(0.1) K for at least 6 hours. ^{31}P NMR spectra were taken at −50 °C with a relaxation delay of 10 s. K_{eq} = [**5b**] / [**5a**] = I_{5b} / I_{5a} were calculated from the integrations of the two tautomers.

2.4.10. *Reaction of $(Bu^tCH_2)_3W\equiv CBu^t$ (1) with PMe_3 at Room Temperature in Benzene-d_6*

This experiment was conducted by Ruitao Wang, a post-doctoral researcher in our group, as part of the current project.

Schrock and Clark have reported that the reaction of **1** with *neat* PMe_3 in a sealed tube at 100 °C gave $(Bu^tCH_2)W(\equiv C^tBu)(=CH^tBu)(PMe_3)_2$ (**6**).[15a] The current studies were conducted at room temperature *in a solution* to see if an adduct formed between **1** and PMe_3. **1** (100 mg, 0.214 mmol) in benzene-d_6 in a J. R. Youngs NMR tube in liquid nitrogen was added ca. 1 equiv of PMe_3 through vacuum transfer. A slow reaction at room temperature occurred to give **6**. After 3 days at 23 °C, a mixture of unreacted **1** (and PMe_3) and **6** in ca. 1 : 2 ratio was observed. No adduct between **1** and PMe_3 in the mixture was observed.

2.4.11. *Determination of the X-ray Crystal Structure of 3b*

The crystal structure was determined on a Bruker AXS Smart 1000 X-ray diffractometer equipped with a CCD area detector, and fitted with an upgraded Nicolet LT-2 low temperature device. Suitable crystals were coated with Paratone oil and mounted under a stream of nitrogen at −100 °C. Intensity data were measured with graphite-monochromated Mo K_α radiation (λ = 0.71073 Å). Background counts were measured at the beginning and the end of each scan with the crystal and counter kept stationary. The structure was solved by direct method, and then a 2-fold twinning law (TWIN 0 1 0 1 0 0 0 0 –1, and BASF 0.45126) was used to solve the twinning by merohdry. All non-hydrogen atoms but four C's in both axial ligands were refined with anisotropic displacement coefficients. All hydrogen atoms were placed in calculated positions and introduced into the refinement as fixed contributors with an isotropic U value of 0.008 $Å^2$.

2.4.12. *Computational Details*

These calculations were performed by the research groups of Professors Zhenyang Lin and Yun-Dong Wu at the Hong Kong University of Science and Technology through collaboration with our research group.

All calculations were performed using the Gaussian 03 package[29a] with density functional theory at the B3LYP level. Full geometry optimizations were carried out with basis set I (BSI): LanL2DZ with f polarization functions for W[29b] and 6-31G* for the rest of elements. Single point energies were calculated with basis set II (BSII): SDDAll for W[29c] and 6-311++G** for other elements. Vibration frequency calculations were performed for all the structures with the BSI. The calculated relative energies shown in the text have been corrected with zero-point-energy (ZPE).

CHAPTER 3

Synthesis of Unusual Tungsten Alkyl Alkylidene Alkylidyne Complexes and Kinetic Studies of Their Formation

3.1. Introduction

Tungsten and molybdenum alkylidene and alkylidyne complexes have been extensively studied in part for their potential applications in olefin metathesis. $(Me_3CCH_2)_3W{\equiv}CCMe_3$ (**1**), one of the first alkyl alkylidyne complexes, was originally prepared in ca. 25% yield from WCl_6 and six equiv of $LiCH_2CMe_3$.[32a] It is now prepared from $W(OMe)_3Cl_3$ and six equiv of Me_3CCH_2MgCl in ca. 50% yield.[32b] This method to prepare trialkyl alkylidyne complexes is probably limited to those containing bulky alkyls free of β-hydrogen atoms, as these are unlikely to undergo β-hydrogen elimination. Other trialkyl alkylidyne complexes include $(Me_3SiCH_2)_3M{\equiv}CSiMe_3$ [M = Mo, W (**4a**)] and $(Me_3CCH_2)_3W{\equiv}CSiMe_3$.[15g,18a] The reactivity of $(Me_3SiCH_2)_3W{\equiv}CSiMe_3$ (**4a**) has been extensively studied throughout this dissertation.

High-oxidation-state alkylidyne complexes such as $(Me_3SiCH_2)_3W{\equiv}CSiMe_3$ (**4a**) contain unoccupied low-lying metal d orbitals, and, as a result, they are generally stabilized by the presence of σ-donor ligands (e.g., PMe_3). The first complex containing alkyl, alkylidene, and alkylidyne ligands was reported by Schrock and Clark in 1978.[15a] Upon heating a solution of $(Me_3CCH_2)_3W{\equiv}CCMe_3$ (**1**) in liquid PMe_3 at 100 °C, the transition metal complex undergoes α-hydrogen

abstraction to yield $(Me_3CCH_2)(Me_3CCH=)(Me_3CC\equiv)W(PMe_3)_2$ (**6**) (Scheme 3.1). An analogous complex, $(Me_3CCH_2)(Me_3CCH=)(Me_3CC\equiv)W(dmpe)$ (**7**), which contained the chelating phosphine dmpe ($Me_2PCH_2CH_2PMe_2$), was also reported by Schrock and Clark.[15a] The crystal structure of this complex was later reported by Churchill and Youngs in 1979.[24] Complex **7**, unlike the bis-PMe_3 complex **6**, exhibited *cis* coordination of the chelating phosphine and the alkylidyne ligand occupied the axial site (Scheme 3.1). It is hypothesized that the phosphine ligands in complex **6** are coordinated *trans* to one another, and the other ligands occupy the equatorial sites to form a trigonal bipyramidal configuration. d^0 Alkyl alkylidene alkylidyne complexes $Re(CH_2CMe_3)_2(=CHCMe_3)(\equiv CCMe_3)$, $(Me_3CCH_2)(Me_3CCH=)(Me_3CC\equiv)Re(py)_2(OTf)$, and their derivatives have also been reported (Scheme 3.1b-c).[19]

We reported earlier unusual reactions of d^0 tantalum *bis*(alklyidene) complexes such as $(Me_3SiCH_2)Ta(=CHSiMe_3)_2(PMe_3)_2$ with silanes.[23d,e] The reactivities of the d^0 tungsten complexes containing $Me_3SiCH=$ and $Me_3SiC\equiv$ ligands toward silanes were of interest to us. We have recently prepared $(Me_3SiCH_2)(Me_3SiCH=)(Me_3SiC\equiv)W(PMe_3)_2$ (**8a-b**) and $(Me_3SiCH_2)(Me_3SiCH=)(Me_3SiC\equiv)W(PMe_2Ph)_2$ (**9a-b**) through heating the **3a** ⇌ **3b** and **5a** ⇌ **5b** equilibrium mixtures in the presence of excess phosphine, PMe_3 and PMe_2Ph, respectively (Scheme 3.2).

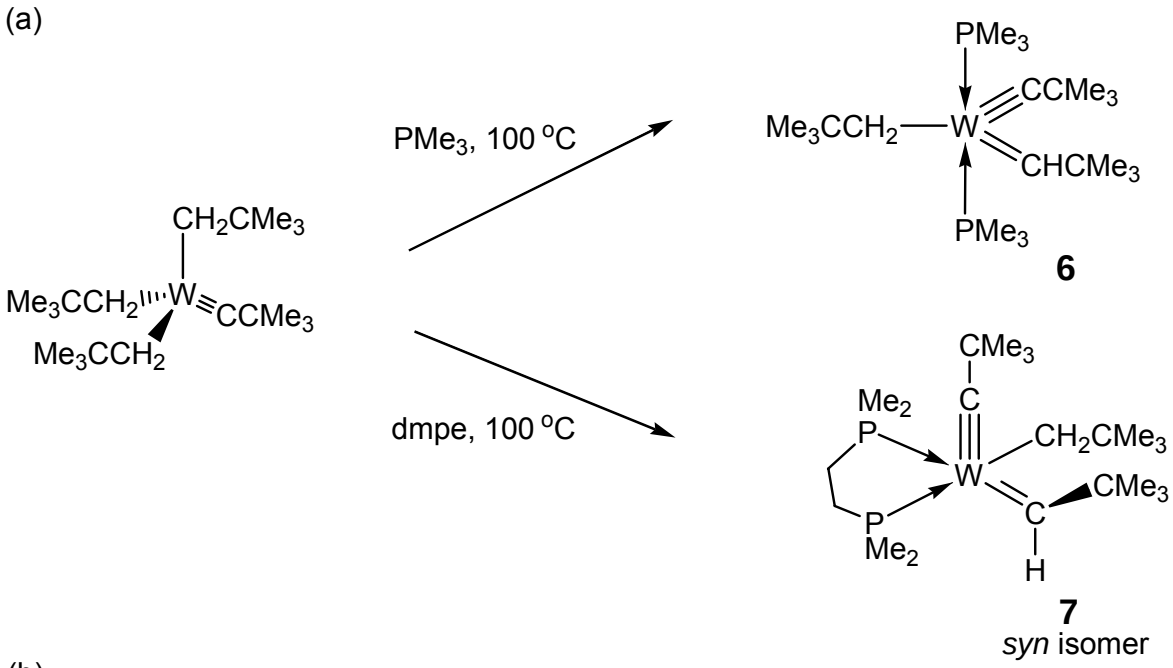

Scheme 3.1. Some reported d^0 complexes containing metal-carbon single, double, and triple bonds.[15a,19]

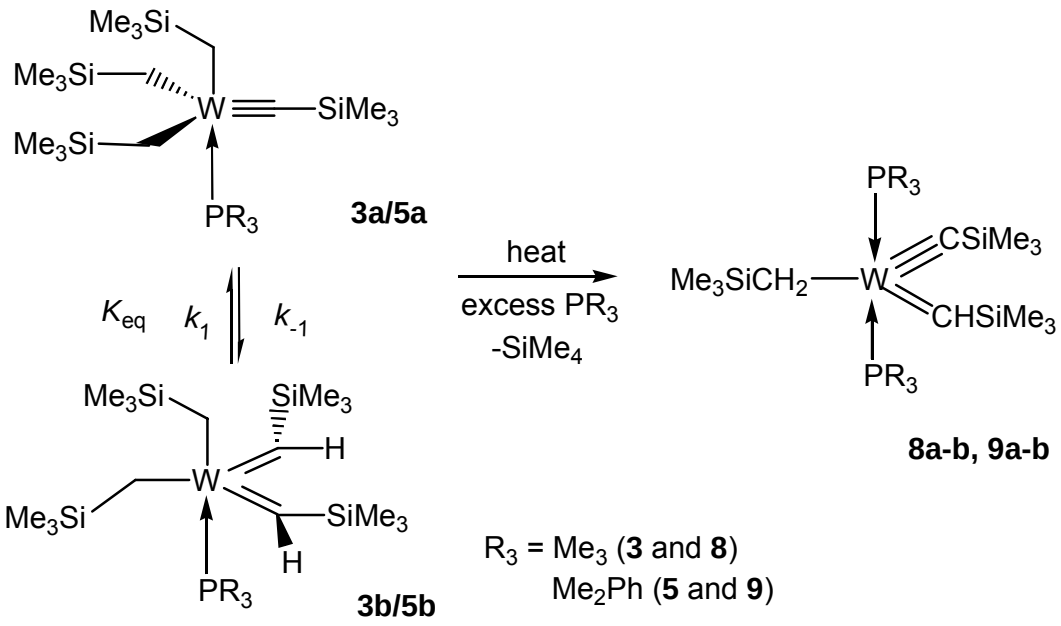

Scheme 3.2. Formation of complexes **8a-b** and **9a-b** from the equilibrium mixtures of **3a-b** and **5a-b**.

Both complexes **8** and **9** exist as mixtures of two isomers, **8a-b** and **9a-b**, as observed by NMR spectroscopy. Our preparation and characterization of **8a-b** and **9a-b** as well as kinetic studies of their formation are reported here.

3.2. Results and Discussion

3.2.1. *Synthesis and Characterization of* $(Me_3SiCH_2)W(\equiv CSiMe_3)(=CHSiMe_3)(PMe_3)_2$ *(8a-b)*

We reported in Chapter 2 the synthesis of complexes $(Me_3SiCH_2)_3W(\equiv CSiMe_3)(PMe_3)$ (**3a**) and $(Me_3SiCH_2)_2W(=CHSiMe_3)_2(PMe_3)$ (**3b**),[14] as well as $(Me_3SiCH_2)_3W(\equiv CSiMe_3)(PMe_2Ph)$ (**5a**) and $(Me_3SiCH_2)_2W(=CHSiMe_3)_2(PMe_2Ph)$ (**5b**), which undergo α-hydrogen migrations to establish the exchange equilibria, **3a** $\rightleftharpoons$ **3b**, and **5a** $\rightleftharpoons$ **5b**. Upon heating these equilibrium systems in the presence of excess PMe_3 or PMe_2Ph, respectively, the mixtures were found to yield alkyl alkylidene alkylidyne complexes $(Me_3SiCH_2)W(\equiv CSiMe_3)(=CHSiMe_3)(PMe_3)_2$ (**8a-b**) and $(Me_3SiCH_2)W(\equiv CSiMe_3)(=CHSiMe_3)(PMe_2Ph)_2$ (**9a-b**) through α-hydrogen abstraction and elimination of $SiMe_4$.

The ^1H, ^{13}C, and ^{31}P NMR spectral analysis of complex **8** revealed two distinct isomers, **8a** and **8b**, in solution (Figures 3.1 and 3.2). The ratio of the two isomers (**8a** : **8b**) is 7 : 1 based on ^1H NMR integration. NMR spectroscopic characterization (^1H, ^{13}C, ^{31}P, ^{29}Si, ^1H-gated-decoupled ^{13}C and HMQC) of the

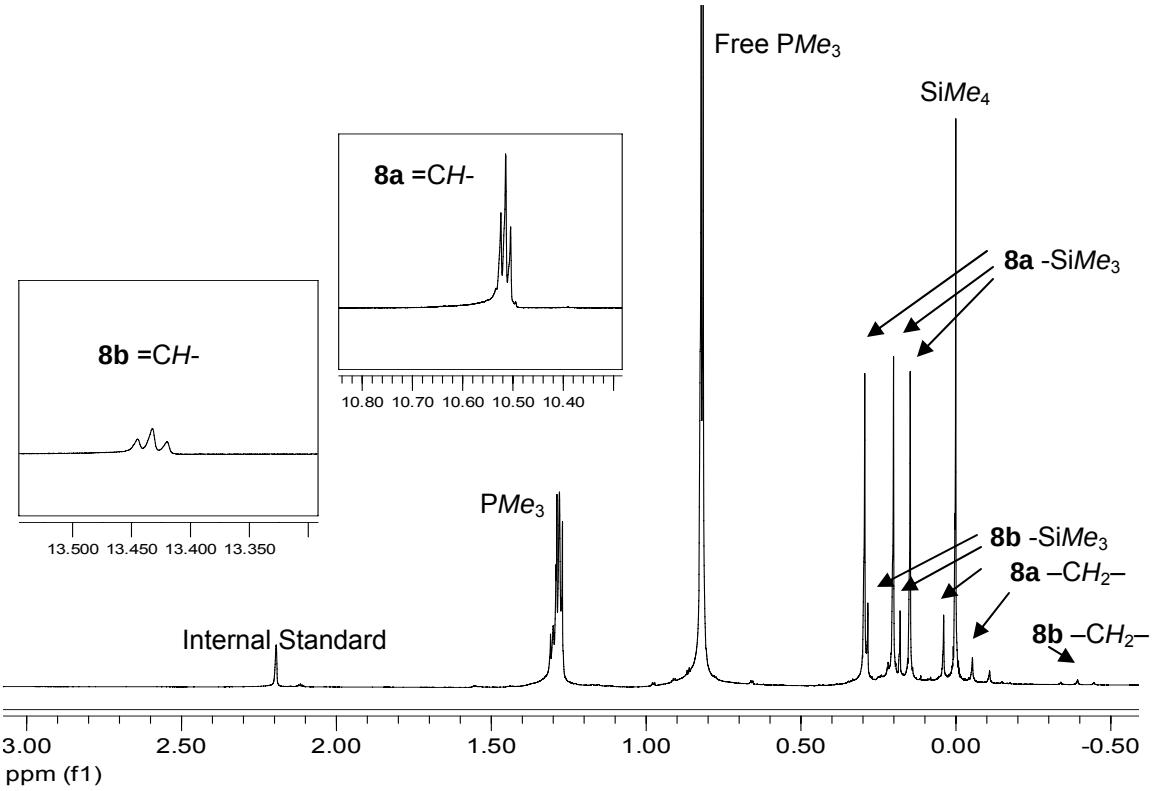

Figure 3.1. ^{1}H NMR spectrum of a mixture of **8a** and **8b** (toluene-d_8).

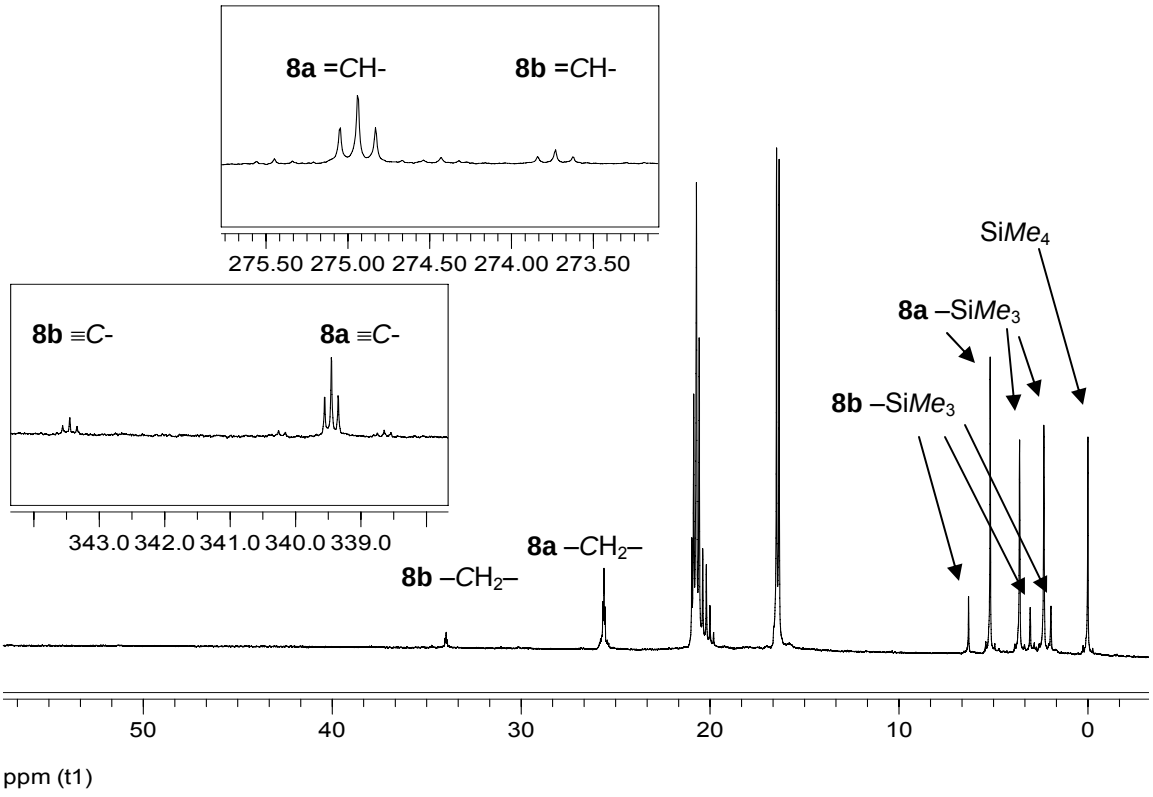

Figure 3.2. ^{13}C NMR spectrum of a mixture of **8a** and **8b** (toluene-d_8).

more abundant **8a** suggests that the PMe_3 ligands coordinate *trans* to one another. One resonance in the ^{31}P NMR spectrum for **8a** was observed at −2.21 ppm ($^1J_{P\text{-}W}$ = 124.7 Hz). The two *trans*-PMe_3 ligands exhibit virtual coupling and appear as a pseudo-triplet in the ^1H and ^{13}C NMR spectra at 1.26 and 20.74 ppm, respectively.[4b] Three singlet resonances of $-SiMe_3$ groups were observed in the ^1H, ^{13}C and ^{29}Si NMR spectra of **8a**; their chemical shifts are listed in Table 3.1. The ^1H resonances of the α-hydrogen atoms in $-CH_2SiMe_3$ appear as a triplet at −0.036 ppm with a large $^2J_{P\text{-}H}$ = 22.4 Hz. In the Ta *bis*(alkylidene)-*bis*(phosphine) complex, $(Me_3SiCH_2)Ta(=CHSiMe_3)_2(PMe_3)_2$, where the phosphines are *trans* to one another, a large coupling constant ($^2J_{P\text{-}H}$ = 19.8 Hz) was observed as well.[31] The resonance of the alkylidyne C atom in **8a** appears at 339.0 ppm as a triplet ($^2J_{P\text{-}C}$ = 11.1 Hz; $^1J_{W\text{-}C}$ = 161.8 Hz) due to its coupling with two equivalent P atoms, and is shifted up-field from that of $(Me_3SiCH_2)_3W{\equiv}CSiMe_3$ (**4a**) at 343.27 ppm.[20h] The alkylidene C and alkyl α-C atoms appear as triplets as well at 275.0 ppm ($^2J_{P\text{-}C}$ = 11.1 Hz; $^1J_{W\text{-}C}$ = 101.5 Hz) and 25.63 ppm ($^2J_{P\text{-}C}$ = 6.2 Hz; $^1J_{W\text{-}C}$ = 36.3 Hz), respectively. Most of the ^1H, ^{13}C, and ^{31}P resonances of complex **8b** are only slightly shifted from those of **8a**, and their chemical shifts are given in Table 3.1. One exception in the ^1H NMR spectrum, the alkylidene proton, $W{=}CHSiMe_3$, is significantly shifted in **8b** to 13.46 ppm, from 10.54 ppm for **8a**. Likewise, the $W{-}CH_2SiMe_3$ resonance in the ^{13}C NMR spectrum at 34.0 ppm is shifted in **8b** from 25.6 ppm in **8a**.

Table 3.1. NMR resonances of **8a** and **8b** (ppm)

Ligand	8a	8b
^{1}H resonances		
$-CH_xSiMe_3$, x = 0, 1, 2	0.331, 0.231, 0.185	0.323, 0.217, 0.060
$=CHSiMe_3$	10.54	13.46
$-CH_2SiMe_3$	−0.036	−0.373
PMe_3	1.26	1.29
^{13}C resonances		
$-CH_xSiMe_3$, x = 0, 1, 2	5.2, 3.7, 2.4	6.4, 3.1, 2.0
$=CHSiMe_3$	275.0	273.8
$\equiv CSiMe_3$	339.0	343.5
$-CH_2SiMe_3$	25.6	34.0
PMe_3	20.74	20.7
^{31}P resonances		
PMe_3	−2.21	−2.40
^{29}Si resonances		
$=CHSiMe_3$	−4.66	n/a* (not available)
$\equiv CSiMe_3$	−23.08	n/a
$-CH_2SiMe_3$	−2.06	n/a

Attempts to isolate pure crystals of **8a-b** for elemental analysis or X-ray diffraction were unsuccessful. **8a-b** are unstable without excess PMe_3. Once excess PMe_3 and other volatiles were removed, **8a-b** was found to decompose. The ^1H NMR spectrum of the solid, dissolved in toluene-d_8, reveals unknown decomposed products. Numerous attempts to isolate **8a-b** failed in the presence of PMe_3. Phosphine ligands are believed to be labile in **8a-b** and dissociate readily from the complexes, leading to the decomposition of **8a-b**.

The two isomers **8a** and **8b** are likely *syn*- and *anti*- rotamers (Figure 3.3).[19b,32] In the former, the $-SiMe_3$ group on the alkylidene ligand points toward the alkylidyne ligand. Such rotameric mixtures were also observed in alkylidene alkylidyne complexes $Re(=CHCMe_3)(\equiv CCMe_3)(OR)_2$.[32a] In the dmpe complex $(Me_3CCH_2)(Me_3CCH=)(Me_3CC\equiv)W(dmpe)$ (**7**), the only isomer observed in the X-ray crystal structure is the *syn* isomer (Scheme 3.1a). Only one isomer of $(Me_3CCH_2)(Me_3CCH=)(Me_3CC\equiv)Re(py)_2(OTf)$ in an octahedral environment was observed, and it was believed to be the *syn* isomer (Scheme 3.1c).[19b] **8a-b**, while in a trigonal bipyramidal environment, are sterically hindered. It is likely that the *syn* **8a** is the major rotamer (Figure 3.3).

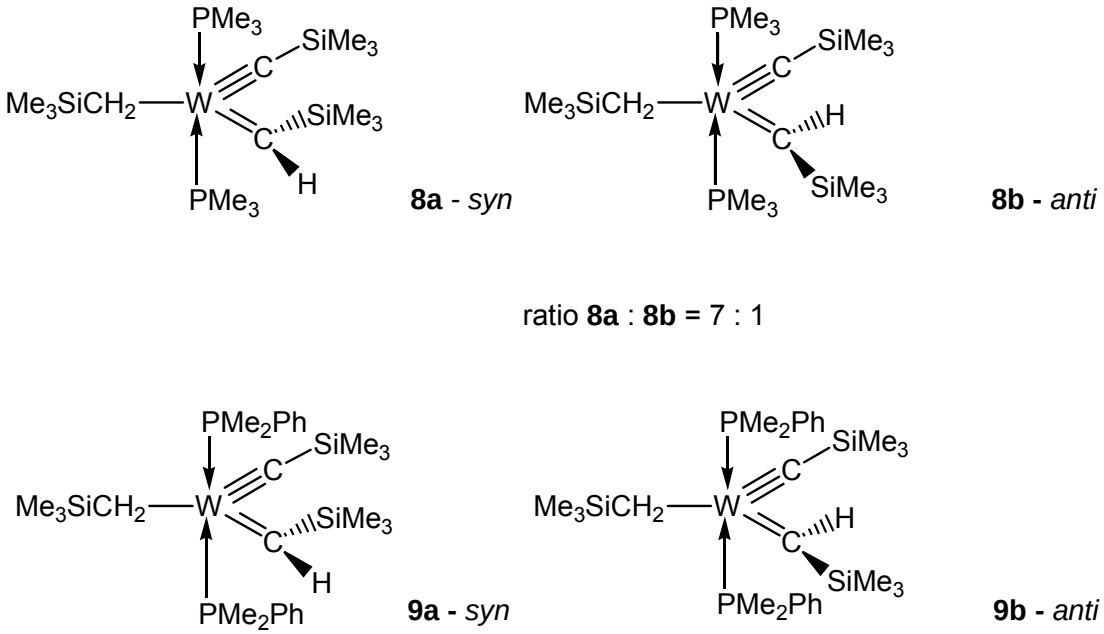

Figure 3.3. Spatial drawings of complexes **8a**, **8b**, **9a**, and **9b** showing stereochemistry around the W=C bond.

3.2.2. *Synthesis and Characterization of* *$(Me_3SiCH_2)W(\equiv CSiMe_3)(=CHSiMe_3)(PMe_2Ph)_2$ (9a-b)*

$(Me_3SiCH_2)W(\equiv CSiMe_3)(=CHSiMe_3)(PMe_2Ph)_2$ (**9a-b**) was prepared by heating the **5a** ⇌ **5b** mixture in the presence of excess PMe_2Ph where it undergoes an α-hydrogen abstraction reaction to form **9a-b**. Complex **9** also exists as two isomers in solution, **9a** ⇌ **9b**, in a ratio of **9a** : **9b** = 27 : 1 based on their ^1H NMR spectra. The ^1H and ^{31}P NMR resonances of **9a** and **9b**, and ^{13}C NMR resonances for **9a** are presented in Table 3.2. The ^1H and ^{31}P NMR spectra of complexes **9a** and **9b** are given in Figures 3.4 and 3.5. Attempts to obtain ^{13}C and ^{29}Si NMR spectra of the minor isomer **9b** failed due to its very low concentration in solution. ^{13}C NMR spectra of a mixture of **9a** and **9b** (prepared from **5a-b**), after 48 hours of data acquisition at 23 °C on a Bruker AMX-400 spectrometer, revealed only the resonances of the major isomer **9a**. Repeated attempts to grow crystals in the presence of excess PMe_2Ph were unsuccessful, as were the attempts to grow crystals of **8a-b**. Without excess PMe_2Ph, **9a-b** was found to be unstable and decompose, as in the case of **8a-b**.

The methyl groups on the PMe_2Ph ligand in complex **9a-b** are diastereotopic. Figure 3.6 shows the Newman projection of **9a** down a W–P bond. The methyl groups of **9a** thus appear as two pseudo triplets in the ^1H and ^{13}C NMR spectra. The ^1H NMR resonance of one of the methyl groups on **9b** overlaps with those of **9a**.

Table 3.2. NMR resonances of **9a** and **9b** (ppm)

Ligand	9a	9b
^{1}H resonances		
$-CH_xSi\mathit{Me}_3$, x = 0, 1, 2	0.487, 0.307, −0.266	0.323, 0.217, −0.060
$=C\mathit{H}SiMe_3$	10.89	13.73
$-C\mathit{H}_2SiMe_3$	−0.025	−0.134
$P\mathit{Me}_a\mathit{Me}_bPh$	1.687, 1.659	1.614, 1.640
^{13}C resonances		
$-CH_xSi\mathit{Me}_3$, x = 0, 1, 2	3.76, 3.20, 2.45	n/a* (not available)
$=\mathit{C}HSiMe_3$	277.02	n/a
$\equiv\mathit{C}SiMe_3$	340.72	n/a
$-\mathit{C}H_2SiMe_3$	27.71	n/a
$P\mathit{Me}_a\mathit{Me}_bPh$	22.44, 20.01	n/a
^{31}P resonances		
$\mathit{P}Me_aMe_bPh$	12.58	10.85
^{29}Si resonances		
$=CH\mathit{Si}Me_3$	−3.79	n/a* (not available)
$\equiv C\mathit{Si}Me_3$	−22.10	n/a
$-CH_2\mathit{Si}Me_3$	−2.82	n/a

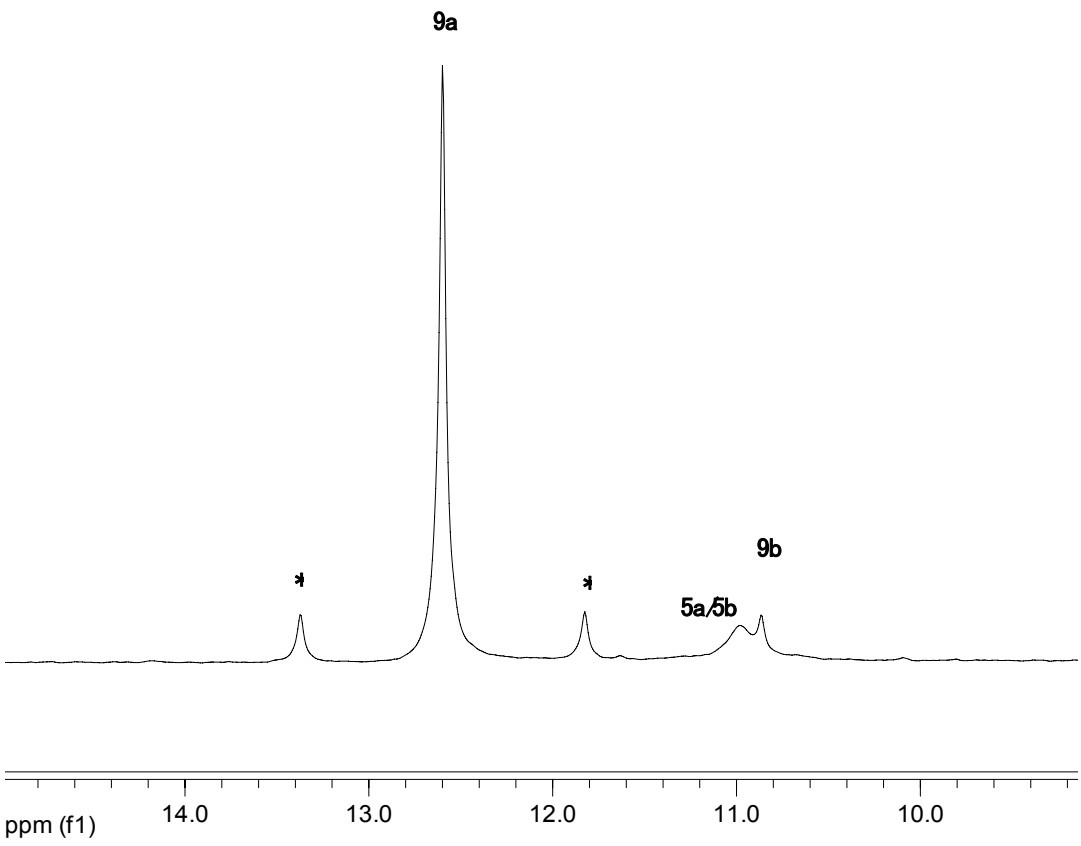

Figure 3.4. ^{31}P NMR spectrum of **9a** and **9b**. A small amount of **5a-b** is present in solution as a broad peak overlapping with **9b**. (* indicates ^{183}W satellites)

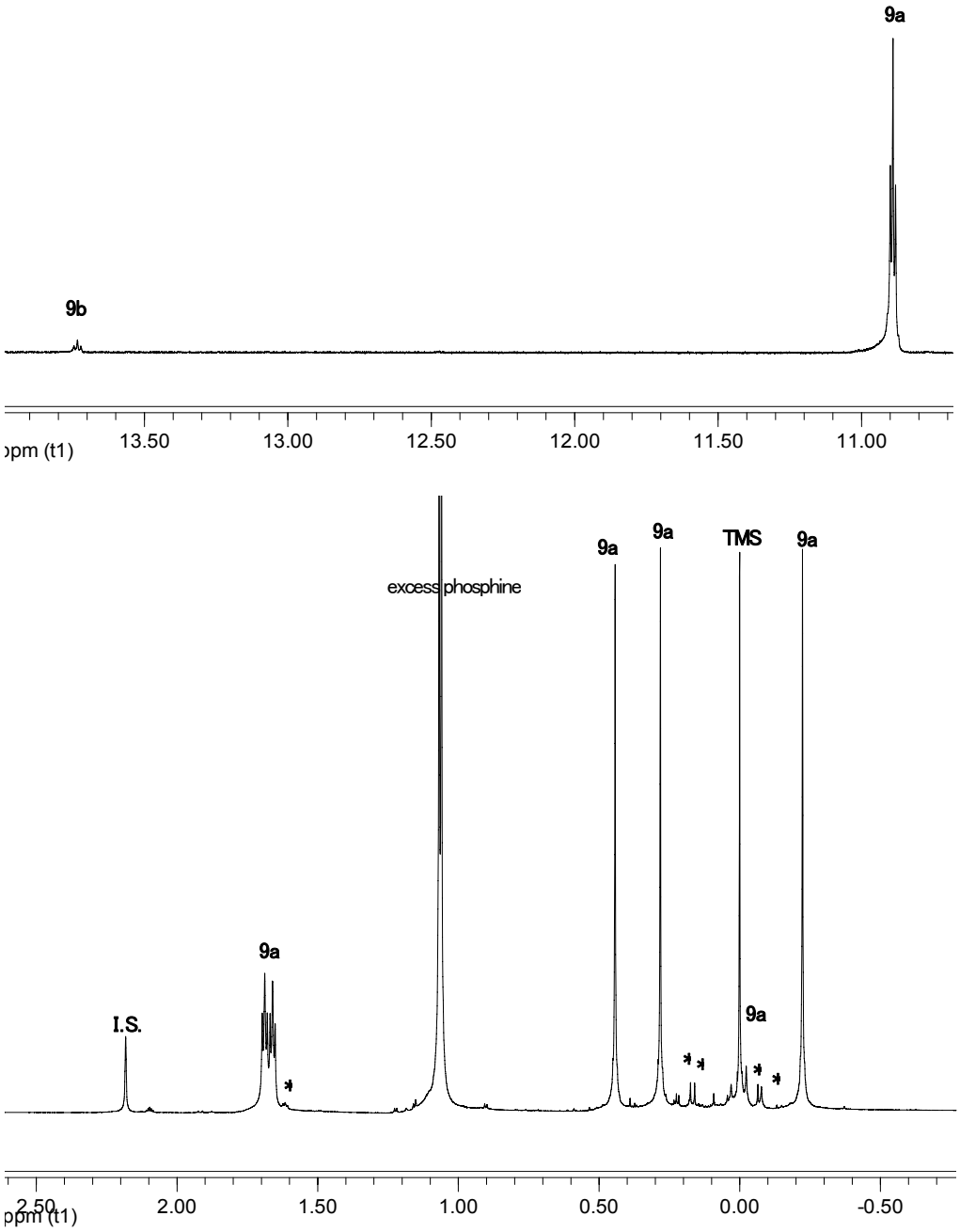

Figure 3.5. ^{1}H NMR spectrum of **9a-b**. (Top) Alkylidene W=C*H*SiMe$_3$ region for **9a** and **9b**. (Bottom) Alkyl and phosphine region. **9b** is marked by (*). (I.S. = internal standard 4,4'-dimethylbiphenyl)

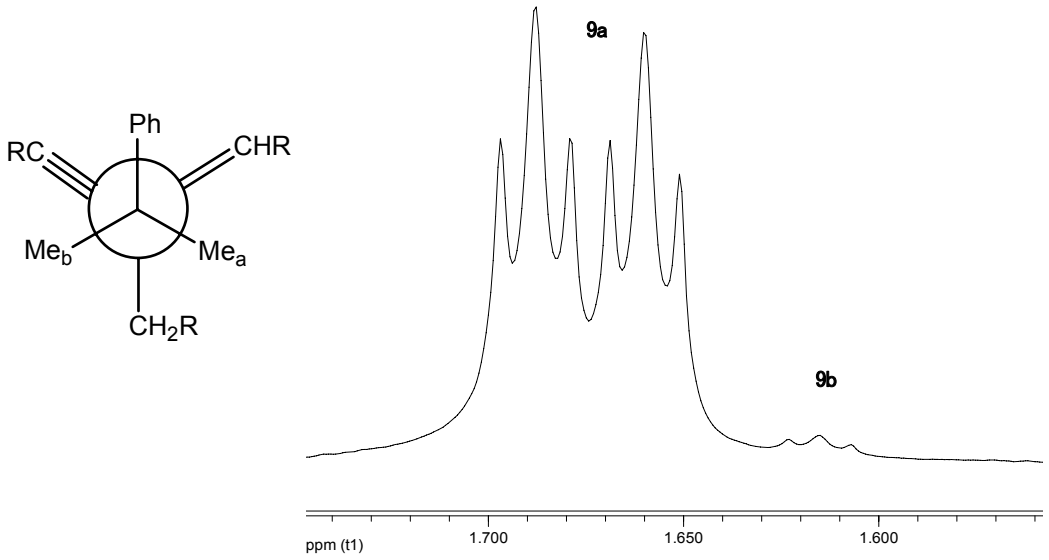

Figure 3.6. The Newman projection of **9a-b** and the ^{1}H NMR spectrum showing the two methyl resonances in PMe_2Ph with virtual ^{31}P-^{1}H coupling.

3.2.3. *Kinetic Study of the Conversion of the 3a ⇌ 3b Mixture to 8a-b*

In the previous chapter, we reported the exchange between $(Me_3SiCH_2)_3W(\equiv CSiMe_3)(PR_3)$ (**3a** and **5a**) and $(Me_3SiCH_2)_2W(=CHSiMe_3)_2(PR_3)$ (**3b** and **5b**, R = Me_3 or Me_2Ph). In the presence of excess phosphine, kinetic studies were conducted to study the α-hydrogen abstraction reactions to yield alkyl alkylidene alkylidyne complexes **8a-b** and **9a-b**, as discussed in the current chapter.

The α-hydrogen abstraction reaction to give **8a-b** follows second-order kinetics. In the presence of excess PMe_3, the α-hydrogen abstraction reaction of **3a-b** to give **8a-b** was found to follow pseudo first-order kinetics (Eqs. 3.1 and 3.2),[26] as the ^{1}H NMR spectra of the conversion revealed.

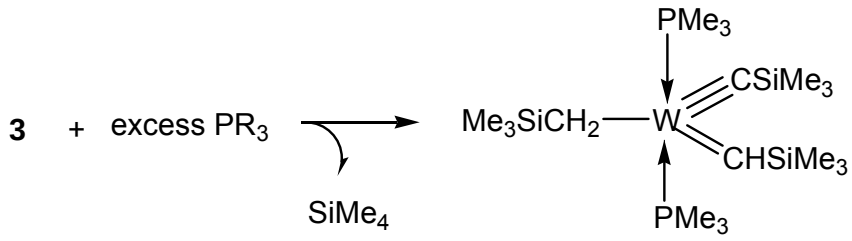

(Eq. 3.1)

$$\frac{d[\mathbf{3}]}{dt} = -k_2[PMe_3][\mathbf{3}] = -k_2'[\mathbf{3}]; \text{ when } [PMe_3] >> [\mathbf{3}],\ k_2' = k_2[PMe_3] \quad \text{(Eq. 3.2)}$$

$$\ln\left(\frac{I_{3_0} - I_{8_t}}{I_{3_0}}\right) = -k_2't \quad \text{(Eq. 3.3)}$$

where I_{3_0} and I_{8_t} are integrations of the PMe_3 ligands in **3a-b** (total) at t = 0, and in **8a-b** (total) at $t = t$ in the ^{1}H NMR spectra.

The kinetic studies for the conversion of **3** $\rightarrow$ **8** were conducted between 333.2(0.1) and 358.2(0.1) K. The kinetic plots and rate constants (k_2) are given in Figure 3.7 and Table 3.3, respectively. The Eyring plot (Figure 3.8) gives the activation parameters of the conversion: $\Delta H^{\neq}$ = 29.2(1.5) kcal/mol and $\Delta S^{\neq}$ = 4.2(1.3) eu.

It is not clear whether alkyl alkylidyne **3a**, *bis*(alkylidene) **3b** or both undergo the α-hydrogen abstraction to give **8a-b**. The process may involve a cyclometalation transition state. The activation parameters of the conversion $\Delta H^{\neq}$ = 29.2(1.5) kcal/mol and $\Delta S^{\neq}$ = 4.2(1.3) eu are similar to other reported reactions through cyclometalation transition states for complexes containing $-CH_2CMe_3$ and/or $-CH_2SiMe_3$ ligands (Table 3.4).[33,18a,16c]

3.2.4. *Kinetic Studies of the 5 $\rightarrow$ 9 Conversion and a Comparison of Its Rate with the Rate of the Formation of 8*

PMe_2Ph is bulkier than PMe_3, and the phenyl group often acts as an electron withdrawing group. In their reactions with **3** and **5**, both yielded alkyl alkylidene alkylidyne complexes: $(Me_3SiCH_2)(Me_3SiCH=)W(\equiv CSiMe_3)(PMe_3)_2$ (**8**) and $(Me_3SiCH_2)(Me_3SiCH=)W(\equiv CSiMe_3)(PMe_2Ph)_2$ (**9**). The kinetics of the formation of **9a-b** was also studied at 348.2 K (Figure 3.9) and analyzed with a kinetic equation similar to Eq. 3.3. These kinetic studies yield the rate constant k_3 = 1.5 $\times$ 10^{-5} $M^{-1}s^{-1}$ at 348.2(0.1) K. In comparison, the rate constant (k_2) for the formation of the PMe_3 analog **8a-b** at 348.2(0.1) K is 3.0(0.2) $\times$ 10^{-5} $M^{-1}s^{-1}$.

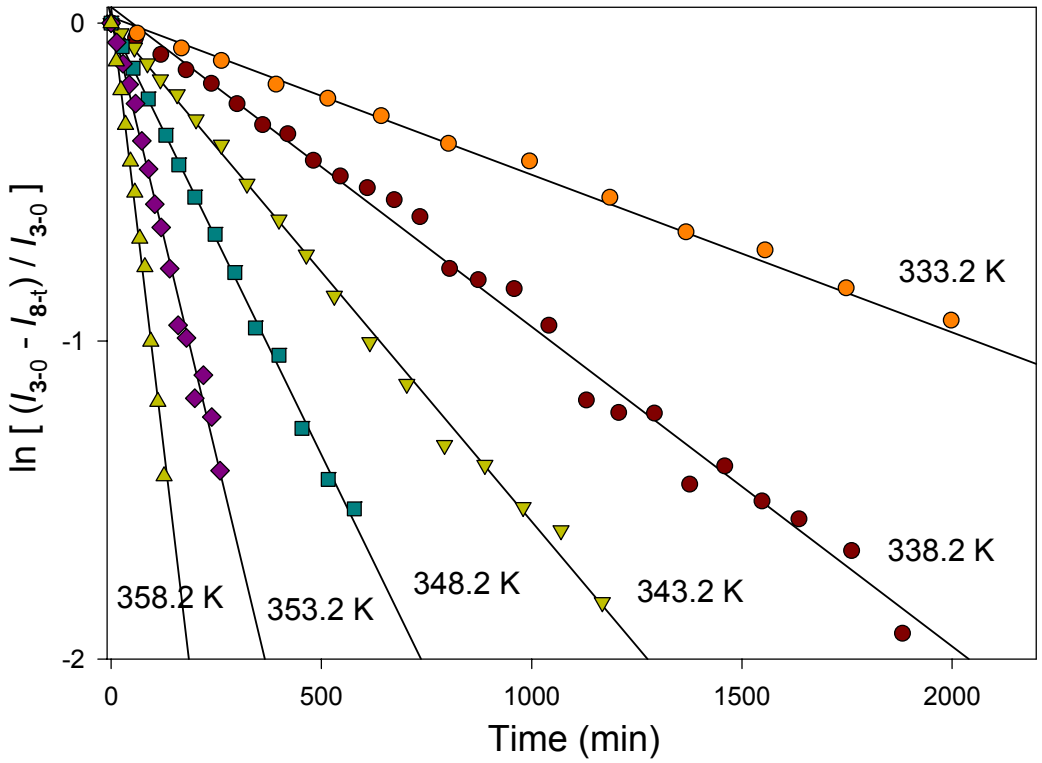

Figure 3.7. Kinetic plots for the conversion of **3a**-**b** → **8a**-**b**. $I_{3\text{-}0}$ and $I_{8\text{-}t}$ are total integrations of the P*Me*$_3$ ligands in both **3a** and **3b** at t = 0, and in both **8a** and **8b** at t = t in the ^{1}H NMR spectra.

Table 3.3. Rate constant (k_2) of the formation of **8a-b**.[a]

T (K)	k_2 x 10^5 (M^{-1} s^{-1})[b]
333.2 ± 0.1	0.35 ± 0.03
338.2 ± 0.1	0.85 ± 0.06
343.2 ± 0.1	1.53 ± 0.07
348.2 ± 0.1	3.0 ± 0.2
353.2 ± 0.1	5.1 ± 0.5
358.2 ± 0.1	8.6 ± 0.6

[a] Solvent: toluene-d_8.

[b] The largest random uncertainty is $\delta k_{2(ran)}/k_2$ = 0.5/5.1 = 9.8%. The total uncertainty $\delta k_2/k_2$ = 0.1100 was calculated from $\delta k_{2(ran)}/k_2$ and the estimated systematic uncertainty $\delta k_{2(sys)}/k_2$ = 5% by $\delta k_2/k_2 = [(\delta k_{2(ran)}/k_2)^2 + (\delta k_{2(sys)}/k_2)^2]^{1/2}$.

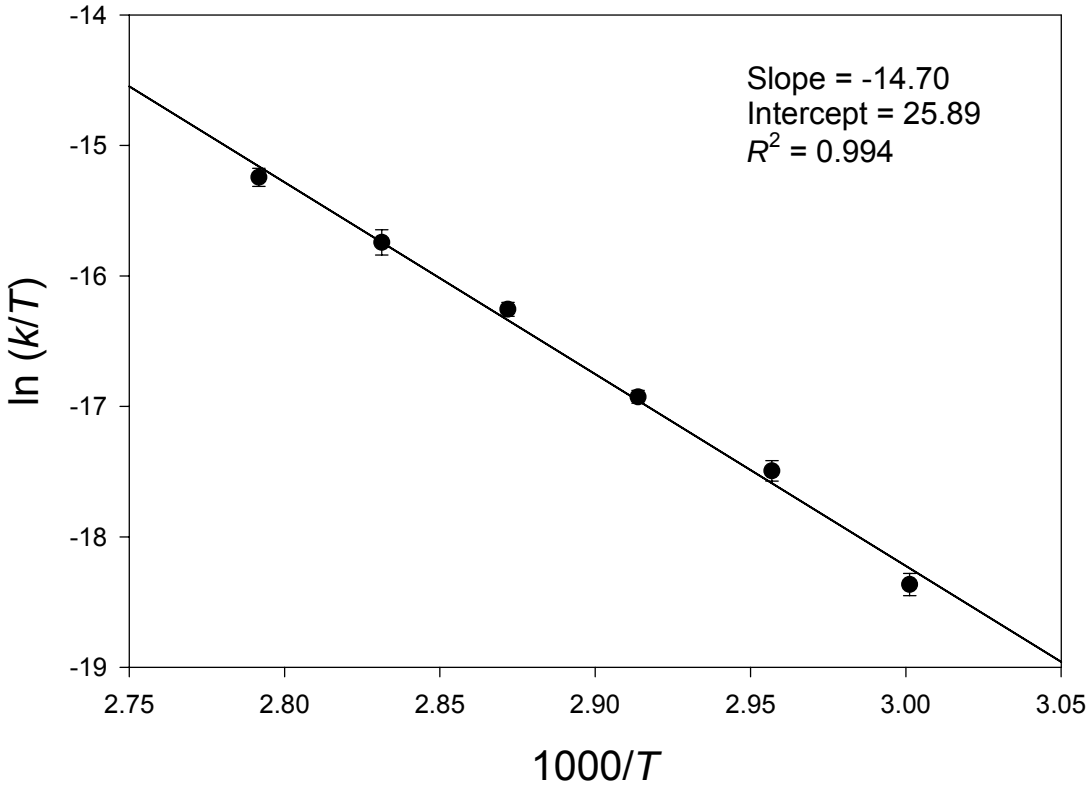

Figure 3.8. Eyring plot of the conversion **3a**-**b** → **8a**-**b**.

Table 3.4. Activation parameters in reactions through cyclometalation transition states

Reactions	$\Delta H^{\neq}$ **(kcal/mol)**	$\Delta S^{\neq}$ **(eu)**
$CpTaCl_2(CH_2CMe_3)_2 \rightarrow$ $CpTaCl_2(=CHCMe_3) + CMe_4$ [33]	21 ± 2	-4 ± 10
$(Me_3CCH_2)_3W{\equiv}CSiMe_3 \rightarrow$ $(Me_3CCH_2)_2(Me_3SiCH_2)W{\equiv}CCMe_3$ [18a]	27.5 ± 0.6	-2.0 ± 1.7
$(Me_3CCH_2)_2(Me_3SiCH_2)W{\equiv}CCMe_3 \rightarrow$ $(Me_3CCH_2)_3W{\equiv}CSiMe_3$ [18a]	25.4 ± 0.8	-9.5 ± 1.9
$(Me_3SiCH_2)_5Ta \rightarrow (Me_3SiCH_2)_3Ta{=}CHSiMe_3$ [16c]	21.6 ± 1.4	-5 ± 5

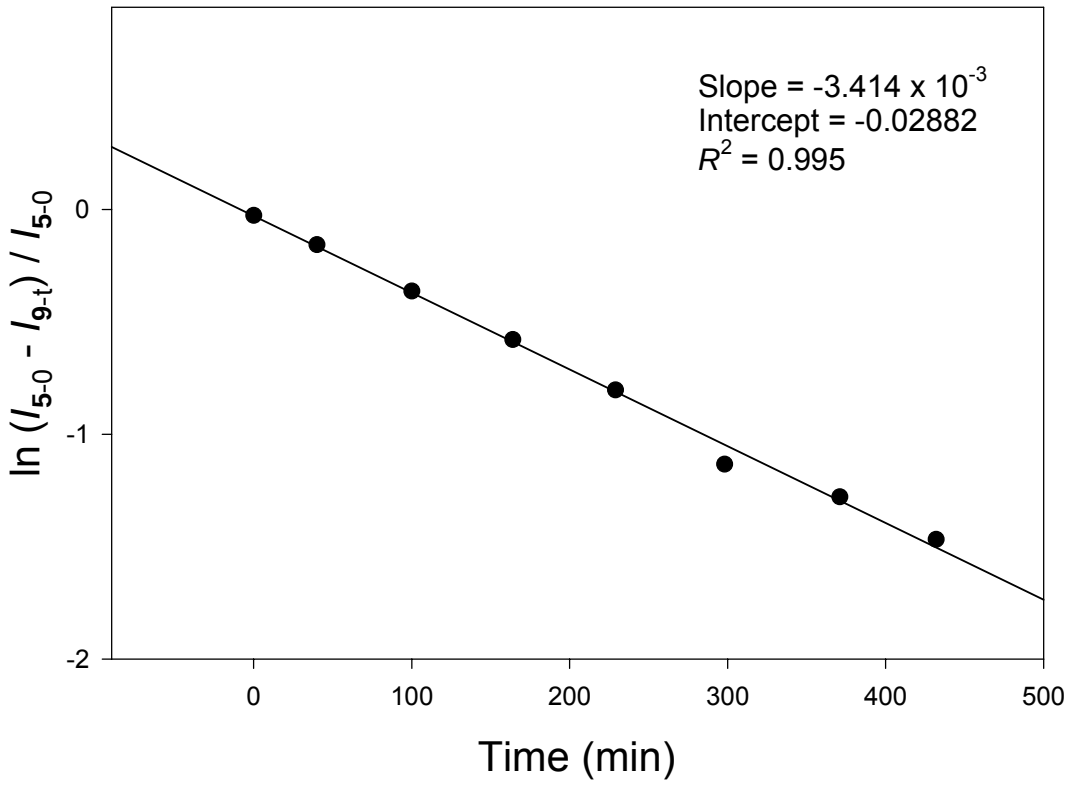

Figure 3.9. Kinetic plot for the formation of **9a-b** at 348.2 K.

In other words, the rate of the formation of the bulkier **9a-b** is about a half of the rate in the formation of the PMe_3 adduct **8a-b**. This is similar to the slower rate of the **5a** ⇌ **5b** inter-conversion reported in Chapter 2.

3.2.5. *Attempted Reactions of $(Me_3SiCH_2)_3W{\equiv}CSiMe_3$ (4a) with PCy_3 and PPh_3*

Attempts were made to prepare compounds analogous to **8a-b** and **9a-b** using phosphines other than PMe_3 and PMe_2Ph. The addition of excess PCy_3 or PPh_3 to solutions of **4a** in toluene, and heating the solutions for two days at 100 °C yielded no products. No complexation was observed between PPh_3 or PCy_3 and **4a**. It is not clear why these two phosphines do not form alkyl alkylidene alkylidyne complexes.

3.3. Concluding Remarks

In this chapter, equilibrium mixtures $(Me_3SiCH_2)_3W(\equiv CSiMe_3)(PR_3)$ (**3a/5a**) ⇌ $(Me_3SiCH_2)_2W(=CHSiMe_3)_2(PR_3)$ (**3b/5b**), were shown to convert to alkyl alkylidene alkylidyne complexes $(Me_3SiCH_2)W(\equiv CSiMe_3)(=CHSiMe_3)(PR_3)_2$ (**8a-b** and **9a-b**). Two isomers of complexes **8** (**8a** and **8b**) and **9** (**9a** and **9b**) were observed in solution. Kinetic studies show that the α-hydrogen abstraction reactions to form **8a-b** and **9a-b** follow second-order kinetics. The presence of excess phosphine (PMe_3 or PMe_2Ph) in solution has been proven necessary for the stability of both **8a-b** and **9a-b**.

It is interesting to note the difference in the reactivities of $(Me_3SiCH_2)_3W{\equiv}CSiMe_3$ (**4a**) and its analog $(Me_3CCH_2)_3W{\equiv}CCMe_3$ (**1**) toward PMe_3. $(Me_3CCH_2)_3W{\equiv}CCMe_3$ (**1**) reacts with neat PMe_3 in a sealed tube at 100 °C, giving alkyl alkylidene alkylidyne complex $(Me_3CCH_2)W(\equiv CCMe_3)(=CHCMe_3)(PMe_3)_2$ (**6**) through α-hydrogen abstraction and CMe_4 elimination, as Schrock and Clark have reported.[15a] When a *solution* of **1** in benzene-d_6 was added ca. 1 equiv of PMe_3 *at room temperature*, a similar reaction giving **6** and CMe_4 occurred (Chapter 2, Section 2.4.10). *No* adduct between alkylidyne $(Me_3CCH_2)_3W{\equiv}CCMe_3$ (**1**) and PMe_3 was observed. In comparison, PR_3 coordinates readily to $(Me_3SiCH_2)_3W{\equiv}CSiMe_3$ (**4a**), an analog of **1**, to give the phosphine alkylidyne adducts $(Me_3SiCH_2)_3W(\equiv CSiMe_3)(PR_3)$ (**3a** and **5a**). These phosphine alkylidyne adducts then undergo α-hydrogen migration to give the *bis*(alkylidene) tautomers $(Me_3SiCH_2)_2W(=CHSiMe_3)_2(PR_3)$ (**3b** and **5b**). Coordination of the second phosphine ligands to the tautomeric mixtures leads to α-hydrogen abstraction to give the alkyl alkylidene alkylidyne complexes **8a-b** and **9a-b** reported in the current chapter. In other words, in the current case involving the $-CH_2SiMe_3$ and $\equiv CSiMe_3$ ligands, there are intermediates [alkyl alkylidyne-PR_3 $\rightleftharpoons$ *bis*(alkylidene)-PR_3 tautomeric mixtures] before the formation of two alkyl alkylidene alkylidyne complexes. The current work exemplifies the differences in $-CH_2CMe_3$ and $-CH_2SiMe_3$ ligand systems.

3.4. Experimental Section

3.4.1. *General Procedures*

All manipulations were performed under a dry nitrogen atmosphere with the use of either a glovebox or standard Schlenk techniques. Solvents were purified by distillation from potassium benzophenone ketyl. NMR solvents were dried and stored over 5 Å molecular sieves. ^{1}H and $^{13}C\{^{1}H\}$ NMR spectra were recorded on a Bruker AC-250 or AMX-400 spectrometer and referenced to solvent (residual protons in the ^{1}H spectra). ^{31}P, ^{29}Si, and HMQC (Heteronuclear Multiple Quantum Coherence) spectra were recorded on a Bruker AMX-400 spectrometer. ^{29}Si chemical shifts were referenced to $SiMe_4$. **3** and **5** were prepared by procedures in Chapter 2.

3.4.2. *Preparation of $(Me_3SiCH_2)W(\equiv CSiMe_3)(=CHSiMe_3)(PMe_3)_2$ (8a-b)*

8a-b was prepared by heating an equilibrium mixture of **3a** ⇌ **3b** with excess PMe_3. A sample was prepared by vacuum transferring at least a 10-fold excess of PMe_3 to a J.R. Youngs tube containing **4a** (50.0 mg, 0.0942 mmol) and toluene-d_8 (0.5 mL). The mixture was kept at 23 °C overnight and then heated at 75 °C overnight. The formation of the **8a** ⇌ **8b** mixture is 100% based on ^{1}H NMR studies. When the volatiles ($SiMe_4$, PMe_3, and solvent) from the reaction were removed, **8a** and **8b** were found to quickly decompose to unknown species. Repeated attempts to grow crystals of **8a-b** in the presence of excess PMe_3 failed. **8a** was thus characterized by ^{1}H, ^{31}P, ^{29}Si, ^{13}C, DEPT, HMQC, and ^{1}H-

gated-decoupled-^{13}C NMR. **8a**: ^{1}H NMR (toluene-d_8, 399.97 MHz, 23 °C, *J* in Hz) δ 10.54 (t, 1H, =C*H*SiMe$_3$, $^{3}J_{P\text{-}H}$ = 4.2), 1.26 (m, 9H, P*Me*$_3$), 0.331 (s, 9H, -Si*Me*$_3$), 0.231 (s, 9H, -Si*Me*$_3$), 0.185 (s, 9H, -Si*Me*$_3$), –0.036 (t, 2H, C*H*$_2$-SiMe$_3$, $^{3}J_{P\text{-}H}$ = 22.4); ^{13}C{^{1}H} NMR (toluene-d_8, 100.59 MHz, 23 °C, *J* in Hz) δ 339.0 (t, ≡*C*SiMe$_3$, $^{2}J_{P\text{-}C}$ = 11.1, $^{1}J_{W\text{-}C}$ = 161.8), 275.0 (t, =*C*HSiMe$_3$, $^{2}J_{P\text{-}C}$ = 11.1, $^{1}J_{W\text{-}C}$ = 101.5), 25.63 (t, *C*H$_2$SiMe$_3$, $^{2}J_{P\text{-}C}$ = 6.2, $^{1}J_{W\text{-}C}$ = 36.3), 20.74 (m, P*Me*$_3$), 5.21 (s, -Si*Me*$_3$), 3.66 (s, -Si*Me*$_3$), 2.38 (s, -Si*Me*$_3$); ^{31}P{^{1}H} NMR (toluene-d_8, 161.92 MHz, 23 °C, *J* in Hz) δ –2.21 (s, $^{1}J_{W\text{-}P}$ = 124.7); ^{29}Si{^{1}H} NMR (toluene-d_8, MHz, °C, *J* in Hz) δ –2.06 (s, -CH$_2$*Si*Me$_3$), –4.66 (s, =CH*Si*Me$_3$), –23.08 (s, ≡C*Si*Me$_3$). ^{1}H and ^{13}C assignments were confirmed by HMQC experiments. **8b**: ^{1}H NMR (toluene-d_8, 399.97 MHz, 23 °C, *J* in Hz) δ 13.46 (t, 1H, =C*H*SiMe$_3$, $^{3}J_{P\text{-}H}$ = 5.6), 1.29 (m, 9H, P*Me*$_3$), 0.323 (s, 9H, -Si*Me*$_3$), 0.217 (s, 9H, -Si*Me*$_3$), 0.060 (s, 9H, -Si*Me*$_3$), –0.373 (t, 2H, C*H*$_2$-SiMe$_3$, $^{3}J_{P\text{-}H}$ = 21.4); ^{13}C{^{1}H} NMR (toluene-d_8, 100.59 MHz, 23 °C, *J* in Hz) δ 343.5 (t, ≡*C*SiMe$_3$, $^{2}J_{P\text{-}C}$ = 10.5), 273.8 (t, =*C*HSiMe$_3$, $^{2}J_{P\text{-}C}$ = 11.1) 34.0 (t, *C*H$_2$SiMe$_3$, $^{2}J_{P\text{-}C}$ = 6.2), 20.7 (m, overlapping with **8a** and toluene-d_8 peaks, P*Me*$_3$), 6.4 (s, -Si*Me*$_3$), 3.1 (s, -Si*Me*$_3$), 2.0 (s, -Si*Me*$_3$); ^{31}P{^{1}H} NMR (toluene-d_8, 161.92 MHz, 23 °C, *J* in Hz) δ –2.4 (s).

3.4.3. *Preparation of (Me$_3$SiCH$_2$)W(≡CSiMe$_3$)(=CHSiMe$_3$)(PMe$_2$Ph)$_2$ (9a-b)*

9a-b were prepared by a procedure similar to that used to prepare **8**, by heating an equilibrium mixture of **5a** ⇌ **5b** with excess PMe$_2$Ph. PMe$_2$Ph (ca. 10-fold excess) was added *via* cannula transfer to a J.R. Youngs tube containing **4a**

and toluene-d_8. The solution was kept for 24 hours at room temperature to establish the **5a** ⇌ **5b** equilibrium. The solution was then heated at 75 °C for 24 hours to give the **9a** ⇌ **9b** mixture in 100% yield based on ^{1}H NMR. **9a** was characterized by ^{1}H, ^{31}P, ^{29}Si, ^{13}C, and HMQC NMR. Upon removal of excess PMe_2Ph, **9a-b** were found to decompose to unknown species. The ratio of **9a** : **9b** in solution was 27 : 1. Repeated attempts to grow crystals of **9a-b** in the presence of PMe_2Ph were unsuccessful. **9a**: ^{1}H NMR (toluene-d_8, 399.97 MHz, –20 °C, *J* in Hz) δ 10.89 (t, 1H, =C*H*SiMe$_3$, $^3J_{P\text{-}H}$ = 3.7), 7.4-7.0 (m, 5H, PMe$_2$*Ph*), 1.640 (m, 3H, P*Me*$_a$Me$_b$Ph), 1.622 (m, 3H, PMe$_a$*Me*$_b$Ph), 0.441 (s, 9H, -Si*Me*$_3$), 0.279 (s, 9H, -Si*Me*$_3$), –0.226 (s, 9H, -Si*Me*$_3$), –0.025 (t, 2H, C*H*$_2$-SiMe$_3$, $^3J_{P\text{-}H}$ = 21.6); ^{13}C{^{1}H} NMR (toluene-d_8, 100.59 MHz, –20 °C, *J* in Hz) δ 340.72 (t, ≡*C*SiMe$_3$, $^2J_{P\text{-}C}$ = 9.9), 277.02 (t, =*C*HSiMe$_3$, $^2J_{P\text{-}C}$ = 11.7), 130-124 (m, PMe$_2$*Ph*), 27.71 (s, *C*H$_2$SiMe$_3$, $^2J_{P\text{-}C}$ = 5.6), 22.44 (m, P*Me*$_a$Me$_b$), 20.01 (m, PMe$_a$*Me*$_b$), 3.76 (s, -Si*Me*$_3$), 3.20 (s, -Si*Me*$_3$), 2.45 (s, -Si*Me*$_3$); ^{31}P{^{1}H} NMR (toluene-d_8, 161.92 MHz, 23 °C, *J* in Hz) δ 12.58 (s, $^1J_{W\text{-}P}$ = 126.4); ^{29}Si{^{1}H} NMR (toluene-d_8, 79.46 MHz, –20 °C, *J* in Hz) δ –2.82 (s, -CH$_2$*Si*Me$_3$), –3.79 (s, =CH*Si*Me$_3$), –22.10 (s, ≡C*Si*Me$_3$). ^{1}H and ^{13}C assignments were confirmed by HMQC experiments. **9b**: ^{1}H NMR (toluene-d_8, 399.97 MHz, –20 °C, *J* in Hz) δ 13.73 (t, 1H, =C*H*SiMe$_3$, $^3J_{P\text{-}H}$ = 4.9), 1.61 (m, 3H, P*Me*$_a$Me$_b$Ph), 1.64 (m, 3H, PMe$_a$*Me*$_b$Ph, overlapping with **9a**), 0.175 (s, 9H, -Si*Me*$_3$), 0.159 (s, 9H, -Si*Me*$_3$), –0.066 (s, 9H, -Si*Me*$_3$), –0.134 (t, 2H, C*H*$_2$-SiMe$_3$, overlapping with **9a**); ^{31}P{^{1}H} NMR (toluene-d_8, 161.92 MHz, 23 °C, *J* in Hz) δ 10.85 (s, $^1J_{W\text{-}P}$ = 125.4).

3.4.4. *Kinetic Studies of the Formation of 8a-b and 9a-b*

In the kinetic studies of the formation of **3a-b**, a mixture of $(Me_3SiCH_2)_3W{\equiv}CSiMe_3$ (29.8-37.8 mg, 0.0562-0.0712 mmol) 4,4'-dimethylbiphenyl (an internal standard), and toluene-d_8 in J. R. Young's NMR tubes were added at least a 10-fold excess PMe_3 ([PMe_3]: 1.42-2.31 M) *via* vacuum transfer. The sample was kept at 23 °C overnight to establish the **3a** ⇌ **3b** equilibrium. The sample was then placed in a circulation bath between 60 °C (333.2 K) and 85 °C (358.2 K). After a measured period of time, the experiment was quenched by placing the sample in a dry ice/ethanol bath at −78 °C, and ^{1}H NMR was acquired at room temperature. Integration of the ^{1}H –P*Me*$_3$ resonances at 1.26-1.29 ppm for **8a-b** versus an internal standard was used to give the kinetic plots in Figure 3.7. Both isomers were integrated together since the peaks overlap in the ^{1}H NMR spectra. The average slope of two experiments was used to calculate k_2. The enthalpy ($\Delta H^{\neq}$) and entropy ($\Delta S^{\neq}$) were calculated from an unweighted nonlinear least-squares procedure contained in the SigmaPlot Scientific Graph System. The uncertainties in $\Delta H^{\neq}$ and $\Delta S^{\neq}$ were computed from the error propagation formulas, Eqs. 2.7 and 2.8,[27] which were presented in Chapter 2.

Similar to **8a-b**, the kinetics of the conversion of **5a-b** to **9a-b** was monitored by ^{1}H NMR. A mixture of $(Me_3SiCH_2)_3W{\equiv}CSiMe_3$ (33.2 mg), PMe_2Ph ([PMe_2Ph] = 3.79 M), and 4,4'-dimethylbiphenyl (an internal standard) in toluene-d_8 in J. R. Young's NMR tube was heated in a circulation bath at 75.0 °C (348.2

K) for a measured amount of time, and the reaction was then quenched in dry ice/ethanol bath at −78 °C. ^{1}H NMR was acquired at room temperature, and the integration of the ^{1}H –P*Me*$_2$Ph resonances at 1.61-1.64 ppm for **9a-b** versus an internal standard was used to give the kinetic plot in Figure 3.9.

3.4.5. *Attempted Synthesis of the Adducts between PCy_3 or PPh_3 and 4a*

Two separate experiments were conducted with 50 mg of $(Me_3SiCH_2)_3W{\equiv}CSiMe_3$ (**4a**), 4,4'-dimethylbiphenyl (an internal standard), and toluene-d_8 in J. R. Youngs NMR tubes. PCy_3 or PPh_3, respectively, was added in at least a 10-fold excess. The solution was heated for two days at 100 °C. No reaction or adducts were observed in ^{1}H NMR spectroscopy.

CHAPTER 4

Synthesis of $(Me_3SiCH_2)_3(Me_3SiC\equiv)W\leftarrow O=PMe_3$ (11) and Studies of Its Reaction with Dioxygen

4.1. Introduction

Reactions of dioxygen with transition metal complexes have been extensively investigated in part because they are essential steps in some biological and catalytic processes.[1,34] Such studies have focused mainly on d^n ($n \neq 0$) transition metal complexes, and oxidation of the metals by dioxygen are often involved in these reactions. In comparison, there are relatively fewer studies of reactions of d^0 transition metal complexes with dioxygen.[10,11] Schwartz,[10a,b] Gibson,[10c] and coworkers reported oxygen-atom insertion into the Zr-R bond in the reaction of Cp_2ZrRCl with dioxygen. Similar reactions between Cp_2ZrR_2 and dioxygen were shown to give $Cp_2Zr(OR)_2$.[10d] Bercaw and coworkers studied the conversion of $Cp^*_2Hf(R)(O\text{-}OBu^t)$ to $Cp^*_2Hf(OR)(OBu^t)$.[10e,f] Tilley reported oxygen-atom insertion into the Zr-Si bond in the reaction of $Cp_2ZrClSiMe_3$ with dioxygen to give $Cp_2MCl(OSiMe_3)$.[10g] In Cp-free complexes, Wolczanski, Rothwell, Gibson and their coworkers reported reactions of dioxygen with $(RO)_2TiMe_2$,[11a,b] $(ArO)_2TaMe_3$,[11c] and $(ArN=)_2MoMe_2$[11d] to yield $(RO)_2Ti(OMe)_2$, $(ArO)_2Ta(OMe)_3$, and $[(ArN=)_2Mo(Me)(\mu\text{-}OMe)]_2$, respectively (Scheme 4.1). Autoxidation of $M(CH_2R)_4$ by dioxygen was found to be rapid.[11e] Reactions of dioxygen with diamides (N~N)TiMeX (X = Me, Cl; N~N = silacyclo-

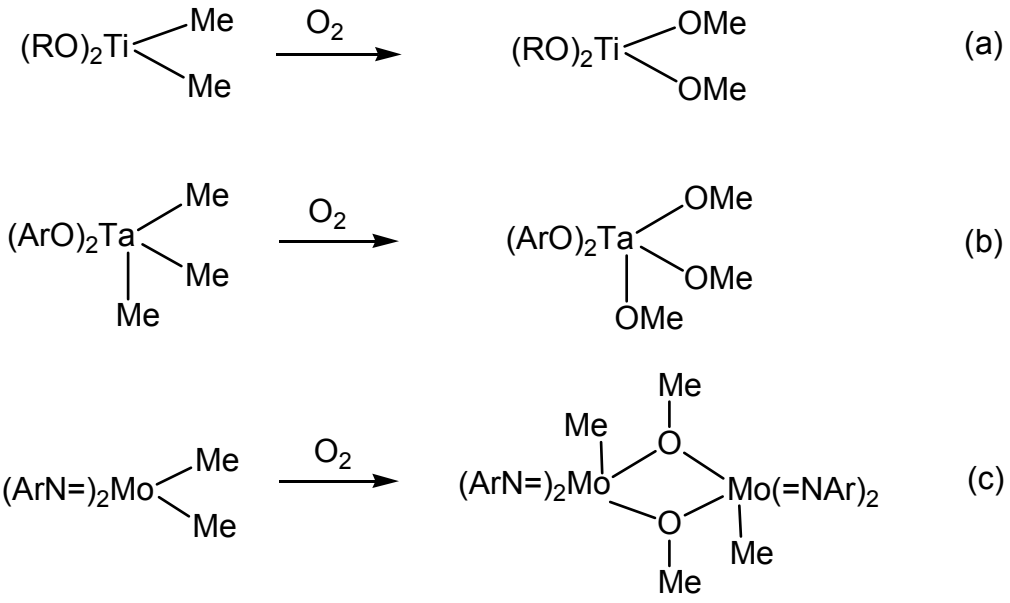

Scheme 4.1. Formation of metal alkoxide complexes from oxygen insertion reactions.[11a,b,c,d]

alkane or -alkene bridge) gave $[(N\sim N)Ti(X)(\mu\text{-}OMe)]_2$.[11f] In contrast, the reaction of alkyl-free $(N\sim N)TiCl_2$ with O_2 led to diamide ligand oxidation. $LY(\mu\text{-}Me)_2AlMe_2$ (L = porphyrin) was found to activate O_2 to give $LY(\mu\text{-}OMe)_2AlMe_2$.[11g,h] In recent years, reactions of O_2 with d^0 complexes such as $Ta(NR_2)_5$ and $(Et_2N)_3Ta{=}NBu^t$ have been of intense interest in the preparation of microelectronic metal oxide thin films.[12] The mechanistic pathways in these chemical vapor deposition reactions are, however, not clear.

We have been intrigued by our recent observations of (a) the formation of an oxo alkylidene $(Bu^tCH_2)_2W(=O)[=CR(SiPh_2Bu^t)]$ (**10**) in the reaction of dioxygen with d^0 silyl alkylidyne $(Bu^tCH_2)_2W(\equiv CBu^t)(SiPh_2Bu^t)$ (**2a**);[22a] (b) O insertion into Ta-Si and Ta-N bonds in the reaction of O_2 with d^0 $(Me_2N)_4Ta\text{-}Si(SiMe_3)_3$ (Scheme 4.2);[22b] and (c) the formation of rare trinuclear oxo aminoxide complexes $M_3(NMe_2)_6(\mu\text{-}NMe_2)_3(\mu_3\text{-}O)(\mu_3\text{-}ONMe_2)$ (M = Zr, Hf) from the reactions of d^0 amides $M(NMe_2)_4$ (M = Zr, Hf) with O_2.[22c,d] In particular, the formation of the oxo alkylidene **10** was the result of an unusual silyl to alkylidyne migration promoted by the reaction with O_2.[22a] We have prepared $(Me_3SiCH_2)_3(Me_3SiC{\equiv})W{\leftarrow}O{=}PMe_3$ (**11**), an adduct between d^0 alkyl alkylidyne $(Me_3SiCH_2)_3W{\equiv}CSiMe_3$ (**4a**) and trimethylphosphine oxide ($O{=}PMe_3$). As part of our studies of metal silyl complexes and similarities/differences between M-Si (silyl) and M-C (alkyl) bonds, we have investigated the reaction of **11** with O_2, and were surprised to find that this reaction gave an oxo siloxy complex $O{=}W(OSiMe_3)(CH_2SiMe_3)_3$ (**12**) which was isolated as an adduct (**13**) with $(Me_3SiCH_2)_3W{\equiv}CSiMe_3$ (**4a**, Scheme 4.3). The $-SiMe_3$ group in the $\equiv CSiMe_3$

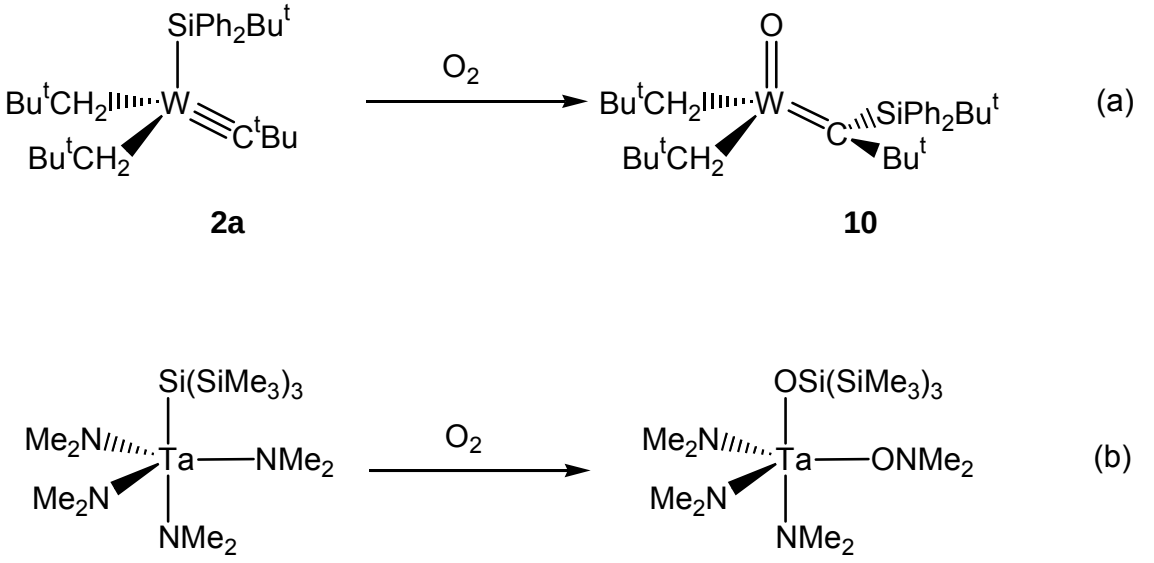

Scheme 4.2. Oxygen reactions with d^0 complexes.[23]

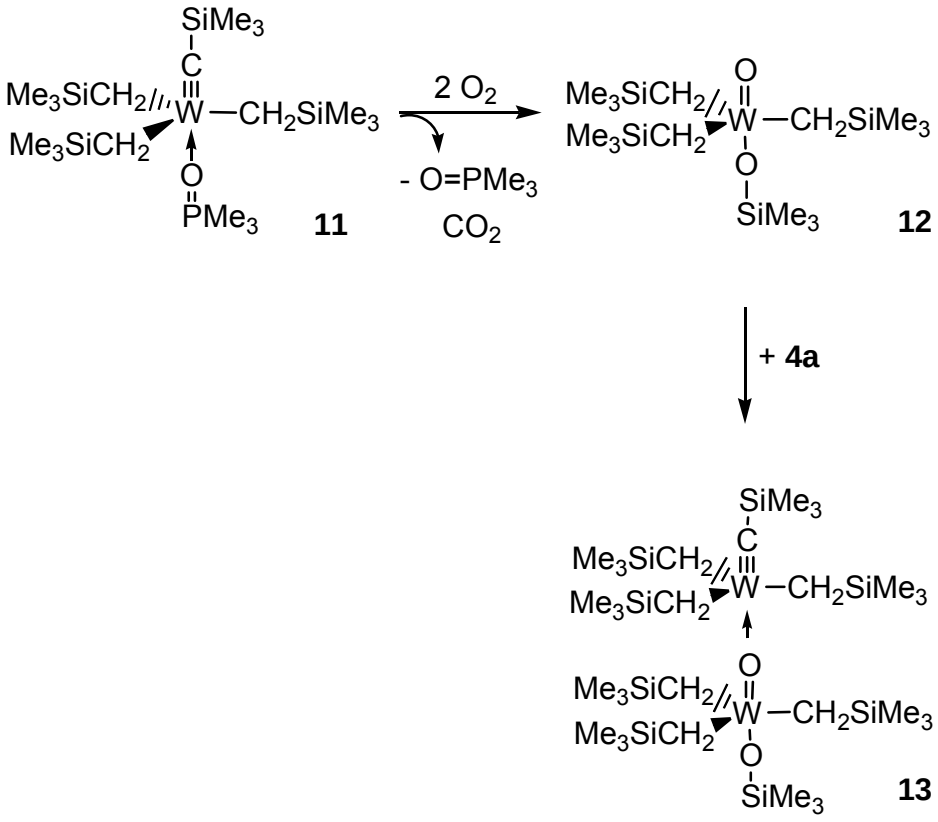

Scheme 4.3. Preparation of complexes **12** and **13**.

ligand in **11** underwent an unusual migration to give the -$OSiMe_3$ ligand in **12**.[5b,15c,20a] The preparation of **11** and **12** and our studies of their formation are reported in this chapter.

4.2. Results and Discussion

4.2.1. *Synthesis and Characterization of $(Me_3SiCH_2)_3(Me_3SiC{\equiv})W{\leftarrow}O{=}PMe_3$ (11)*

$(Me_3SiCH_2)_3W{\equiv}CSiMe_3$ (**4a**)[15g] was found to readily form the adduct $(Me_3SiCH_2)_3(Me_3SiC{\equiv})W{\leftarrow}O{=}PMe_3$ (**11**, Eq. 4.1) with $O{=}PMe_3$. Mixing the two compounds in Et_2O, and cooling the solution to –30 °C yielded pale yellow crystals of $(Me_3SiCH_2)_3(Me_3SiC{\equiv})W{\leftarrow}O{=}PMe_3$ (**11**) in 57.9% yield.

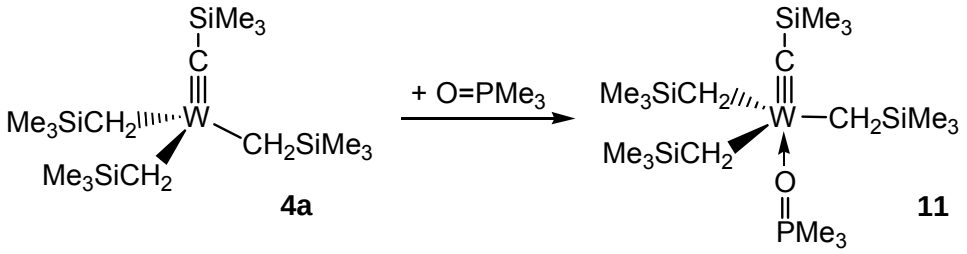

(Eq. 4.1)

11 was characterized by ^1H, ^{13}C, ^{29}Si, and ^{31}P NMR and X-ray diffraction. The ^1H NMR resonance of the α-H atoms (1.30 ppm, benzene-d_6) in the –CH_2SiMe$_3$ ligands in **11** is down-field shifted from that (0.710 ppm) in its parent complex $(Me_3SiCH_2)_3W{\equiv}CSiMe_3$ (**4a**). The ^{13}C resonances of the α-C atoms (the alkylidyne ≡*C*SiMe$_3$ and alkyl -*C*H_2SiMe$_3$ ligands) in **11** at 327.39 and 69.56 ppm, respectively, in benzene-d_6, are both up-field shifted from those (343.67 and

75.85 ppm) in $(Me_3SiCH_2)_3W{\equiv}CSiMe_3$ (**4a**). The NMR shift differences of both α-H and α-C atoms are perhaps a reflection of increased electron densities in 14e $(Me_3SiCH_2)_3(Me_3SiC{\equiv})W{\leftarrow}O{=}PMe_3$ (**11**), as a result of $O{=}PMe_3$ coordination to 12e $(Me_3SiCH_2)_3W{\equiv}CSiMe_3$ (**4a**).

The ^{1}H NMR resonances of the γ-H atoms in the $-CH_2Si\mathit{Me}_3$ and $\equiv CSi\mathit{Me}_3$ ligands in **11** at 0.533 and 0.303 ppm, respectively, are shifted down-field from those (0.427 and 0.162 ppm) in **4a**. The ^{13}C resonances of the γ-C atoms at 3.26 and 2.19 ppm for $-CH_2Si\mathit{Me}_3$ and $\equiv CSi\mathit{Me}_3$ ligands in **11**, respectively, are both down-field shifted from those (2.32 and 2.15 ppm) in $(Me_3SiCH_2)_3W{\equiv}CSiMe_3$ (**4a**), although the resonances of the $\equiv CSi\mathit{Me}_3$ ligands in both complexes are close. It is not clear why these resonances are down-field shifted.

The ^{31}P NMR resonance of **11** at 41.95 ppm for the $O{=}\mathit{P}Me_3$ ligand in **11** is down-field shifted from that (31.68 ppm) of $O{=}\mathit{P}Me_3$. The ^{1}H and ^{13}C NMR resonances of γ-H and γ-C atoms of the $O{=}PMe_3$ ligands in **11** at 0.842 and 17.28 ppm, respectively, are both slightly up-field shifted from those (0.87 and 18.03 ppm) in $O{=}P\mathit{Me}_3$. The ^{29}Si NMR resonances of the β-Si atoms at –3.42 and –23.17 ppm for the $-CH_2\mathit{Si}Me_3$ and $\equiv C\mathit{Si}Me_3$ ligands in 14e **11**, respectively, are both up-field shifted from those (–0.837 and –17.57 ppm) in phosphine oxide-free, 12e $(Me_3SiCH_2)_3W{\equiv}CSiMe_3$ (**4a**).

$(Me_3SiCH_2)_3(Me_3SiC{\equiv})W{\leftarrow}O{=}PMe_3$ (**11**) yielded crystals that were suitable for X-ray diffraction studies. A representation of the molecular structure, crystallographic refinement data, and selected bond distances and angles of **11**

are given in Figure 4.1, and Tables 4.1 and 4.2, respectively. $(Me_3SiCH_2)_3(Me_3SiC\equiv)W\leftarrow O{=}PMe_3$ (**11**) adopts the pseudo trigonal bipyramidal structure (Figure 4.1). The $O{=}PMe_3$ ligand and the alkylidyne $\equiv CSiMe_3$ ligand are in the axial positions with the C(4)-W(1)-O(1) angle of 179.5(3)°. The P(1)-O(1)-W(1)-C(4)-Si(4) linkage is nearly linear. The W(4)≡C(4) bond distance of 1.763(8) Å is slightly longer than that [1.739(8) Å] in $(Me_3CCD_2)_3W\equiv CSiMe_3$,[18] which will be discussed later. As expected, the C(4)-W(1)-C(n) (n = 1, 2, 3) angles of 96.4(3)-97.3(4)° in the trigonal bipyramidal **11** are significantly smaller than that [106.59(13)°] in the tetra-coordinated $(Me_3CCD_2)_3W\equiv CSiMe_3$.[18] The W(1)-C(n) (n = 1, 2, 3) bond distances of 2.097(7)-2.115(1) Å are similar to those [2.096(5) Å] in $(Me_3CCD_2)_3W\equiv CSiMe_3$.[18]

It is interesting to note that the current reaction of d^0 $(Me_3SiCH_2)_3W\equiv CSiMe_3$ (**4a**) with $O{=}PMe_3$ yields the adduct **11**. In comparison, Wolczanski and coworkers recently found that, in the reaction of a d^2 metal complex with $O{=}PR_3$, the oxygen atom transfers from the P atom to the metal complex and oxidizes the metal (Eq. 4.2).[35]

$$M(OSiBu^t)_3 + O{=}PR'_3 \longrightarrow \overset{O}{\underset{||}{M}}(OSiBu^t)_3 + PR'_3 \qquad \text{(Eq. 4.2)}$$

M = Ta, V; R' = Me, Ph

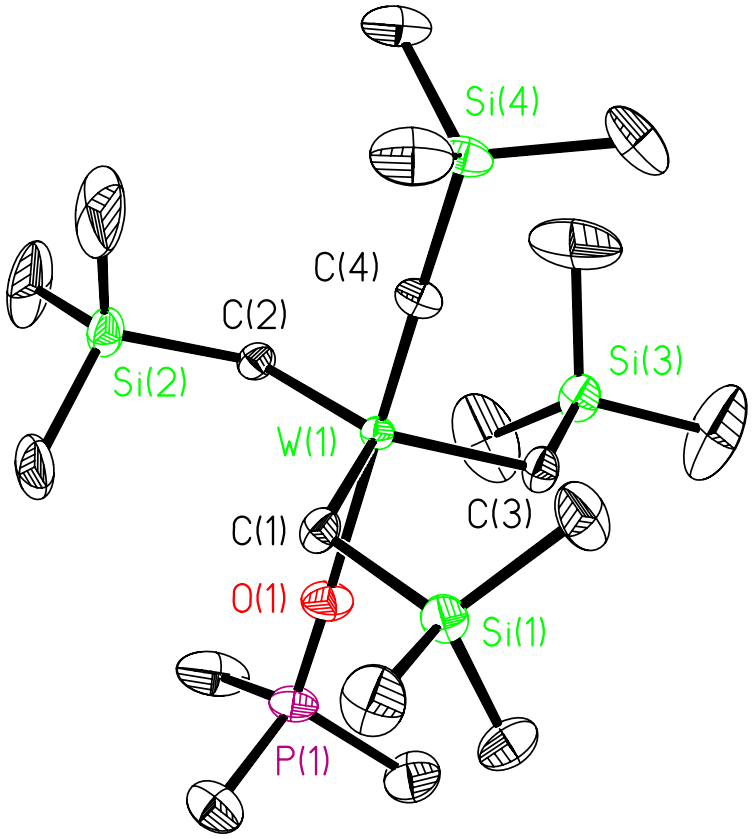

Figure 4.1. An ORTEP view of complex **11**.

Table 4.1. Crystal data and structure refinement for $(Me_3SiCH_2)_3(Me_3SiC{\equiv})W{\leftarrow}O{=}PMe_3$ (**11**).

Compound No.	**11**
Empirical formula (Formula weight)	$C_{19}H_{51}O_1P_1Si_4W_1$ (622.78)
Temperature	−100(2) °C
Wavelength	0.71073 Å
Crystal system	Orthorhombic
Space group	*P*nma
Unit cell dimensions	*a* = 17.903(4) Å α = 90°
	b = 10.516(2) Å β = 90°
	c = 17.191(4) Å γ = 90°
Volume	3236.6(12) Å^3
Z	4
Density (calculated)	1.278 g/cm^3
Absorption coefficient	3.773 mm^{-1}
F(000)	1272
Crystal size	0.30 × 0.30 × 0.20 mm^3
θ range for data collection	2.25 to 28.34°
Index ranges	$-23 \le h \le 23$, $-13 \le k \le 13$, $-22 \le l \le 22$
Reflections collected	32436
Independent reflections	7734 [R_{int} = 0.0526]
Completeness to θ = 28.34°	97.9%
Max. and min. transmission	0.5191 and 0.3973

Table 4.1. Continued

Compound No.	**11**
Refinement method	Full-matrix least-squares on F^2
Data / restraints / parameters	7734 / 1 / 250
Goodness-of-fit on F^2	0.973
Final R indices [$I > 2\sigma(I)$]	$R1$ = 0.0373, w$R2$ = 0.0746
R indices (all data)	$R1$ = 0.0669, w$R2$ = 0.0866
Absolute structure parameter	0.023(11)
Largest diff. peak and hole	1.845 and −0.761 eÅ^{-3}

[a] $R1 = \Sigma||F_o| - |F_c|| / \Sigma|F_o|$; $wR2 = [\Sigma\, w(F_o^2 - F_c^2)^2 / \Sigma\, w(F_o^2)^2]^{1/2}$;
$w = 1/[\sigma^2(F_o) + (aP)^2 + bP]$; $P = [2F_c^2 + \mathrm{Max}(F_o^2, 0)]/3$

Table 4.2. Selected bond distances (Å) and angles (°) for **11**

Distances			
C(1)-W(1)	2.115(11)	O(1)-P(1)	1.479(8)
C(2)-W(1)	2.097(7)	C(1)-Si(1)	1.873(10)
C(3)-W(1)	2.102(7)	C(2)-Si(2)	1.860(8)
C(4)-W(1)	1.763(8)	C(3)-Si(3)	1.856(7)
O(1)-W(1)	2.307(8)	C(4)-Si(4)	1.842(8)

Angles			
W(1)-C(4)-Si(4)	175.7(5)	Si(3)-C(3)-W(1)	119.8(4)
C(4)-W(1)-O(1)	179.5(3)	P(1)-O(1)-W(1)	178.7(6)
C(4)-W(1)-C(1)	97.3(4)	C(2)-W(1)-C(3)	118.1(3)
C(2)-W(1)-C(1)	119.5(3)	C(4)-W(1)-C(1)	97.3(4)
Si(1)-C(1)-W(1)	116.7(5)	C(2)-W(1)-O(1)	84.0(3)
Si(2)-C(2)-W(1)	120.4(4)		

4.2.2. *Reaction of 11 with O_2. Synthesis and Characterization of the Tungsten Oxo Siloxy Complex $O{=}W(OSiMe_3)(CH_2SiMe_3)_3$ (12)*

When $(Me_3SiCH_2)_3(Me_3SiC{\equiv})W{\leftarrow}O{=}PMe_3$ (**11**) was exposed to O_2, **11** was found to convert to $O{=}W(OSiMe_3)(CH_2SiMe_3)_3$ (**12**) containing a siloxy ($-OSiMe_3$) and an oxo ligand. A mass spectrometric (MS) analysis of the gaseous products revealed the formation of CO_2 in the reaction (Scheme 4.3), which is discussed below. When $(Me_3SiCH_2)_3W{\equiv}CSiMe_3$ (**4a**) was exposed to O_2 in the absence of $O{=}PMe_3$, in comparison, decomposition of **4a** was observed, giving unknown species.

Addition of $(Me_3SiCH_2)_3W{\equiv}CSiMe_3$ (**4a**) to the reaction mixture and crystallization at –30 °C gave crystals of $(Me_3SiCH_2)_3(Me_3SiC{\equiv})W{\leftarrow}O{=}W(OSiMe_3)(CH_2SiMe_3)_3$ (**13**) that were suitable for X-ray diffraction studies. A representation of the molecular structure of **13**, a 1 : 1 adduct between **12** and electron deficient **4a**, is shown in Figure 4.2. Crystallographic refinement data and selected bond distances and angles are listed in Tables 4.3 and 4.4, respectively. ^{1}H, ^{13}C and ^{29}Si NMR spectra of **13** showed the resonances of the $-OSiMe_3$ ligand at 0.283, 1.99, and 10.74 ppm, respectively. The ^{29}Si NMR resonance of $-O-SiMe_3$ at 10.74 ppm is down-field shifted from those of $-C{\equiv}W-CH_2SiMe_3$ at –1.50 ppm, $O{=}W-CH_2SiMe_3$ at –2.97 ppm, and $\equiv CSiMe_3$ at –19.76 ppm in **13**. The NMR resonances of $(Me_3SiCH_2)_3(Me_3SiC{\equiv})W$ moiety in **13** were found to be slightly shifted from those of $(Me_3SiCH_2)_3W{\equiv}CSiMe_3$ (**4a**).

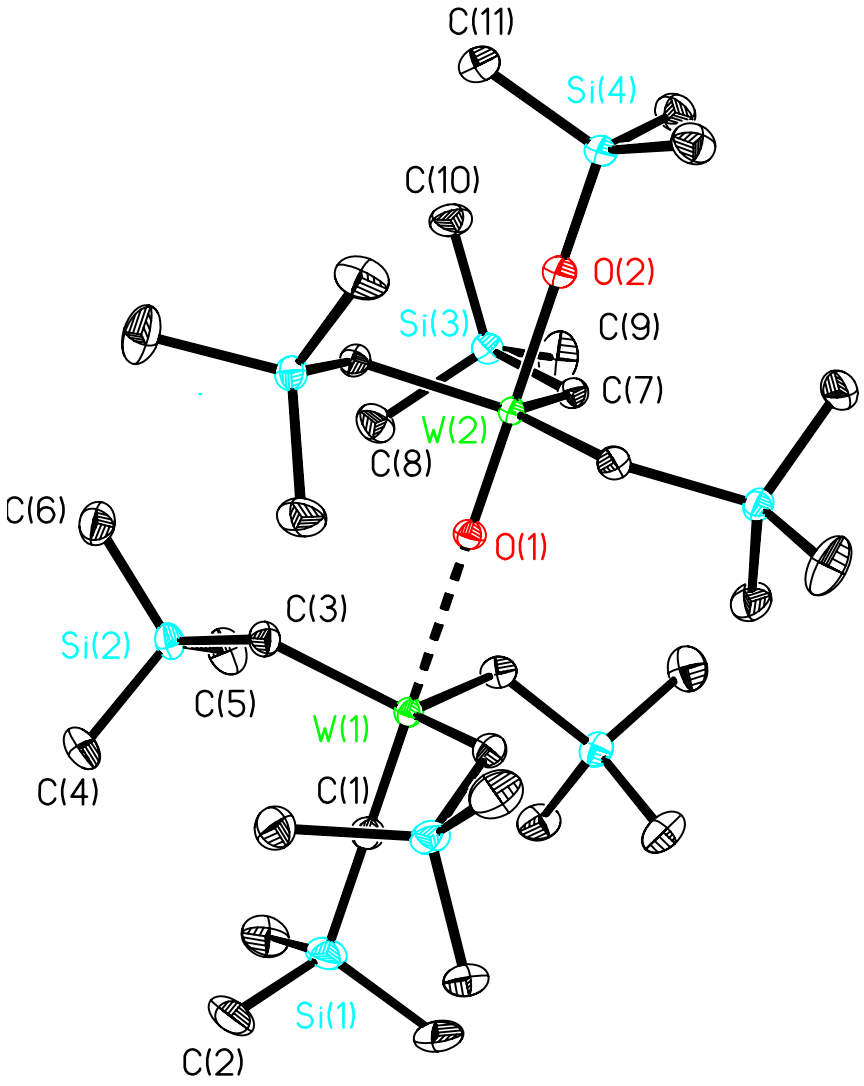

Figure 4.2. An ORTEP view of complex **13**.

Table 4.3. Crystal data and structure refinement for **13**.

Compound No.	**13**
Empirical formula (Formula weight)	$C_{31}H_{84}O_2Si_8W_2$ (1081.40)
Temperature	−100(2) °C
Wavelength	0.71073 Å
Crystal system	Hexagonal
Space group	*R*-3
Unit cell dimensions	*a* = 16.1077(7) Å α = 90°
	b = 16.1077(7) Å β = 90°
	C = 68.397(4) Å γ = 120°
Volume	15368.5(13) Å^3
Z	12
Density (calculated)	1.402 Mg/m^3
Absorption coefficient	4.697 mm^{-1}
F(000)	6552
Crystal size	0.29 × 0.25 × 0.15 mm^3
θ range for data collection	1.58 to 22.50°
Index ranges	$-17 \le h \le 17$, $-17 \le k \le 17$, $-73 \le l \le 73$
Reflections collected	30361
Independent reflections	4488 [*R*(int) = 0.0392]
Completeness to θ = 22.50°	99.9%

Table 4.3. Continued

Compound No.	**13**
Max. and min transmission	0.5393 and 0.3428
Refinement method	Full-matrix least-squares on F^2
Data / restraints / parameters	4488 / 0 / 275
Goodness-of-fit on F^2	0.889
Final R indices [$I > 2\sigma(I)$]	$R1$ = 0.0228, w$R2$ = 0.0559
R indices (all data)	$R1$ = 0.0396, w$R2$ = 0.0706
Largest diff. peak and hole	1.533 and −0.458 eÅ^{-3}

[a] $R1 = \Sigma||F_o| - |F_c|| / \Sigma|F_o|$; $wR2 = [\Sigma\, w(F_o^2 - F_c^2)^2 / \Sigma\, w(F_o^2)^2]^{1/2}$;
$w = 1/[\sigma^2(F_o) + (aP)^2 + bP]$; $P = [2F_c^2 + \mathrm{Max}(F_o^2, 0)]/3$

Table 4.4. Selected bond distances (Å) and angles (°) for **13**

Distances			
C(1)-W(1)	1.775(11)	O(1)-W(1)	2.578(6)
C(3)-W(1)	2.100(5)	O(2)-W(2)	1.924(6)
C(7)-W(2)	2.098(5)	O(1)-W(2)	1.735(6)
O(2)-Si(4)	1.630(6)	C(3)-Si(2)	1.872(6)
C(7)-Si(3)	1.895(5)	C(1)-Si(1)	1.846(11)
C(2)-Si(1)	1.871(6)	C(5)-Si(2)	1.852(6)
C(11)-Si(4)	1.851(6)	C(10)-Si(3)	1.866(6)
Angles			
W(1)-C(1)-Si(1)	180.0	Si(3)-C(7)-W(2)	119.0(3)
W(2)-O(1)-W(1)	180.0	Si(2)-C(3)-W(1)	123.7(3)
Si(4)-O(2)-W(2)	180.0	C(1)-W(1)-O(1)	180.000(1)
O(2)-W(2)-C(7)	87.67(14)	O(1)-W(2)-O(2)	180.000(1)
C(1)-W(1)-C(3)	100.45(15)		

In the reaction of O_2 with d^0 *silyl* alkylidyne $(Bu^tCH_2)_2W(\equiv CBu^t)(SiPh_2Bu^t)$ (**2a**), the silyl ligand migrates to the alkylidyne ligand to give an oxo alkylidene $(Bu^tCH_2)_2W(=O)[=CR(SiPh_2Bu^t)]$ (**10**).[22a] In contrast, in the reaction of O_2 with d^0 *alkyl* alkylidyne **11**, the silyl moiety in the $Me_3SiC\equiv W$ ligand migrates to the newly formed oxo ligand. These are two rare examples of the reactions of d^0 alkylidynes with O_2,[1,10,11,34] and they demonstrate rich chemistry in the reactions of d^0 complexes with O_2. Silicon is known to be oxophilic, and this perhaps drives the unusual silyl migration in the reaction of **11** with O_2. Theoretical calculations, performed by Professor Yun-Dong Wu's research group at the Hong Kong University of Science and Technology, indicate that $O=PMe_3$ mediates and significantly lowers the activation of the migration.

The X-ray structure of **13** reveals a crystallographically imposed C_3 symmetry through the C≡W←O=W-O-Si bonds, giving thus a linear W(2)-O(2)-Si(4) linkage. **4a** and **11** are bonded through a W=O→W dative bond [2.578(6) Å]. The W≡C bond distance of 1.775(11) Å in **13** is longer than those in $(Me_3CCD_2)_3W\equiv CSiMe_3$ [1.739(8) Å][18] and **11** [1.763(8) Å] (Table 4.5). In the structures of both **11** and **13**, the $\equiv CSiMe_3$ ligands are *trans* to oxygen atoms that use their lone pair electrons to form dative bonds to the W atoms in (W←O). The longer W≡C bond distances in **11** and **13** may reflect *trans* influence of the O ligands.[4] The C(1)-W(1)-C(3) bond angle of 100.45(15)° in **13** is smaller than that [106.59(13)°] in $(Me_3CCD_2)_3W\equiv CSiMe_3$,[18] as a result of the coordination of

Table 4.5. Bond distance comparison.[18]

Complex	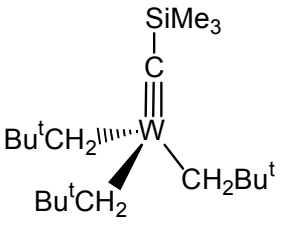	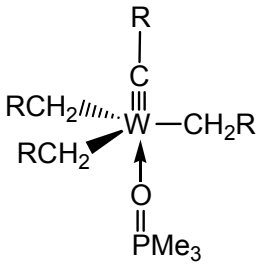 **11**	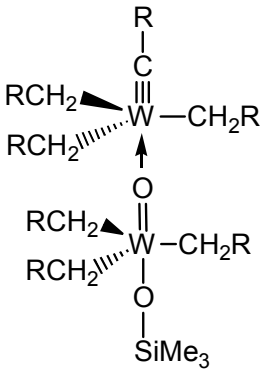 **13**
Bond	**Bond Distance (Å)**		
W≡C	1.739(8)	1.763(8)	1.796(8)
W-C	2.096(5)	2.104(8) (avg)	2.100(5)
O→W		2.307(8)	2.572(5)

12 to $(Me_3SiCH_2)_3W{\equiv}CSiMe_3$ (**4a**). The W=O bond distance of 1.735(6) Å in **13** is similar to those in other W oxo complexes.[5b,36]

4.2.3. *HRMS Study of CO_2 Produced from the Reaction of 11 with O_2 and Determination of Its Yield by $^{13}CO_2$ Analysis*

We devised a method to quantitatively determine the molar amount of CO_2 produced during the reaction of **11** with O_2. An HRMS analysis of the gaseous products using $^{13}CO_2$ as the calibration revealed the formation of CO_2 (CO_2 : **12** ≈ 0.91 : 1). Given the yield of **12**, it is not clear if CO_2 is indeed a byproduct of the formation of **12**. It is, however, reasonable to assume that, in the oxidation of **11** to give **12**, the alkylidyne C atom in $(Me_3SiCH_2)_3(Me_3SiC{\equiv})W{\leftarrow}O{=}PMe_3$ (**11**) was thus oxidized by 2 equiv of O_2 from the former –4[37] to +4 oxidation state, and removed as CO_2.

4.2.4. *Mass Spectrometric Studies of the Reaction of 11 with $^{18}O_2$*

Mass spectrometric studies were also carried out to determine, during the reaction with $^{18}O_2$, whether oxygen scrambling occurs between the $O{=}PMe_3$ ligand and $^{18}O_2$. MS analysis was performed to determine whether $C^{18}O^{16}O$, $C^{16}O^{16}O$ and/or $C^{18}O^{18}O$ were present in the product mixture. The mass spectra are shown in Figures 4.3 and 4.4. In the reaction of **11** with excess $^{18}O_2$, an MS analysis of the gaseous products revealed the formation of $^{16}O{=}C{=}^{18}O$ (25%) and $^{18}O{=}C{=}^{18}O$ (75%), suggesting that the O atom in the $O{=}PMe_3$ ligand in **11**

was transferred to CO_2 during the reaction. The observations of the 46 and 48 Dalton peaks in Figure 4.3 indicate that both $^{16}O=^{12}C=^{18}O$ and $^{18}O=^{12}C=^{18}O$ were products from the reaction. Using the intensities of the 40 (^{40}Ar) peaks in Figure 4.3 as reference, the ratio of the 46 ($^{16}O=^{12}C=^{18}O$) and 48 ($^{18}O=^{12}C=^{18}O$) Dalton peaks in the sample (Figure 4.3, Bottom) is 1 : 3. Because the ratios of the 40 and 44 Dalton peak intensities in both sample (Bottom) and background (Top) are similar, it is unlikely that $^{16}O=^{12}C=^{16}O$ was yielded from the reaction. The nature of the exchange(s) is not clear.

The mass spectra (30-38 Dalton region) of dioxygen isotopomers ($^{16}O=^{16}O$; $^{16}O=^{18}O$; $^{18}O=^{18}O$) in the gaseous products and background prior to the introduction of gases to the mass spectrometer are shown in Figure 4.4. These spectra suggest that there was little $^{16}O=^{16}O$ or $^{16}O=^{18}O$ in the sample that would have contributed to the formation of $^{16}O=^{12}C=^{18}O$.

4.2.5. *Reaction of O_2 with the Equilibrium Mixture of 3a ⇌ 3b*

The first synthesis of **12** occurred serendipitously through unwanted exposure to air during the reaction of **4a** with PMe_3. Complex **13** crystallized from a solution containing **3a-b**, **4a**, PMe_3, and solvent. Controlled experiments later confirmed this reaction was reproducible in approximately 10% yield based on ^1H NMR. Scheme 4.4 shows both routes to form complex **13**.

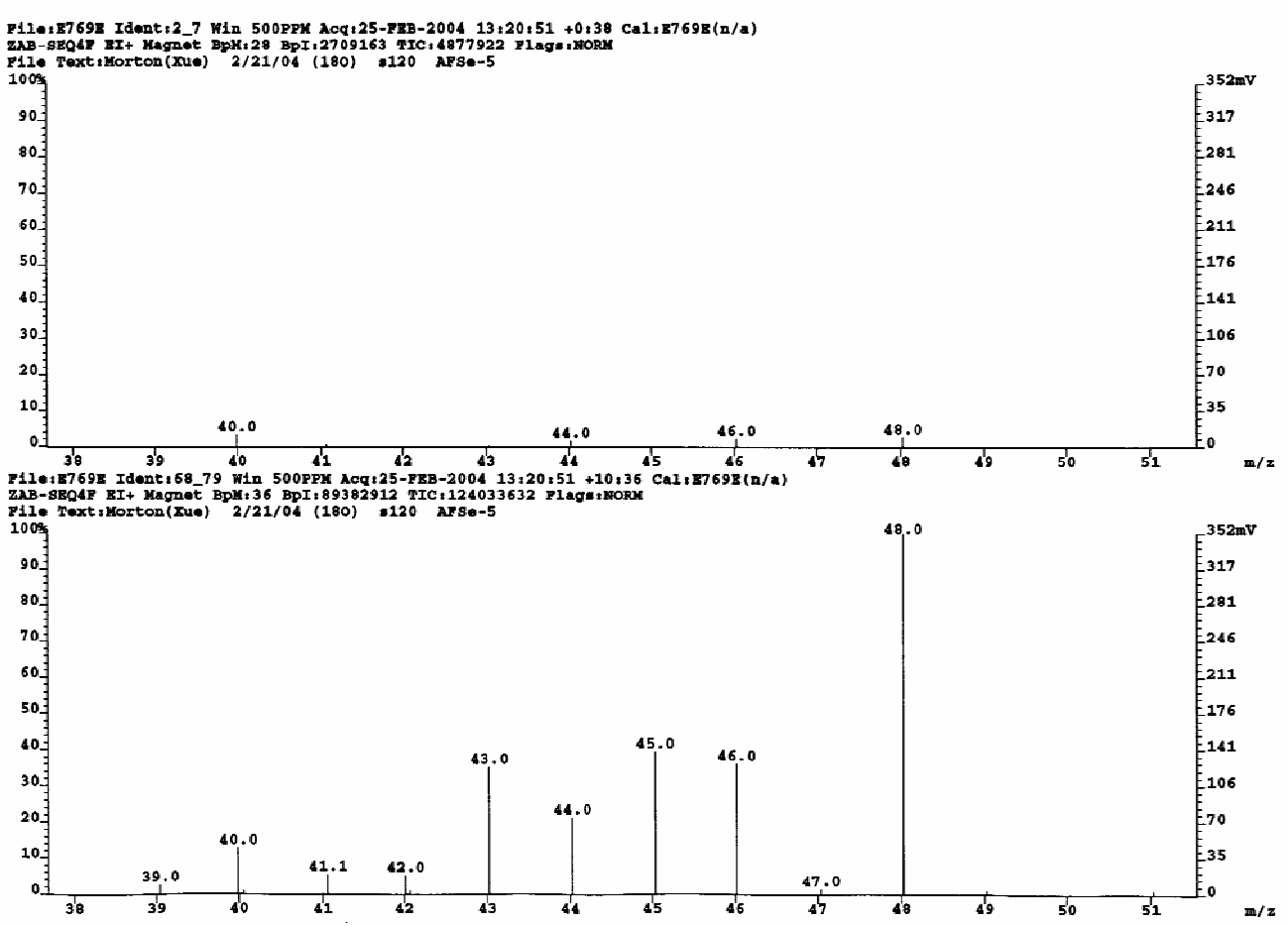

Figure 4.3. Mass spectra (38-51 Dalton region) of the isotopomers of carbon dioxide: (Top) The background prior to the introduction of the gases into the spectrometer; (Bottom) The gaseous products from the reaction of **11** with $^{18}O_2$.

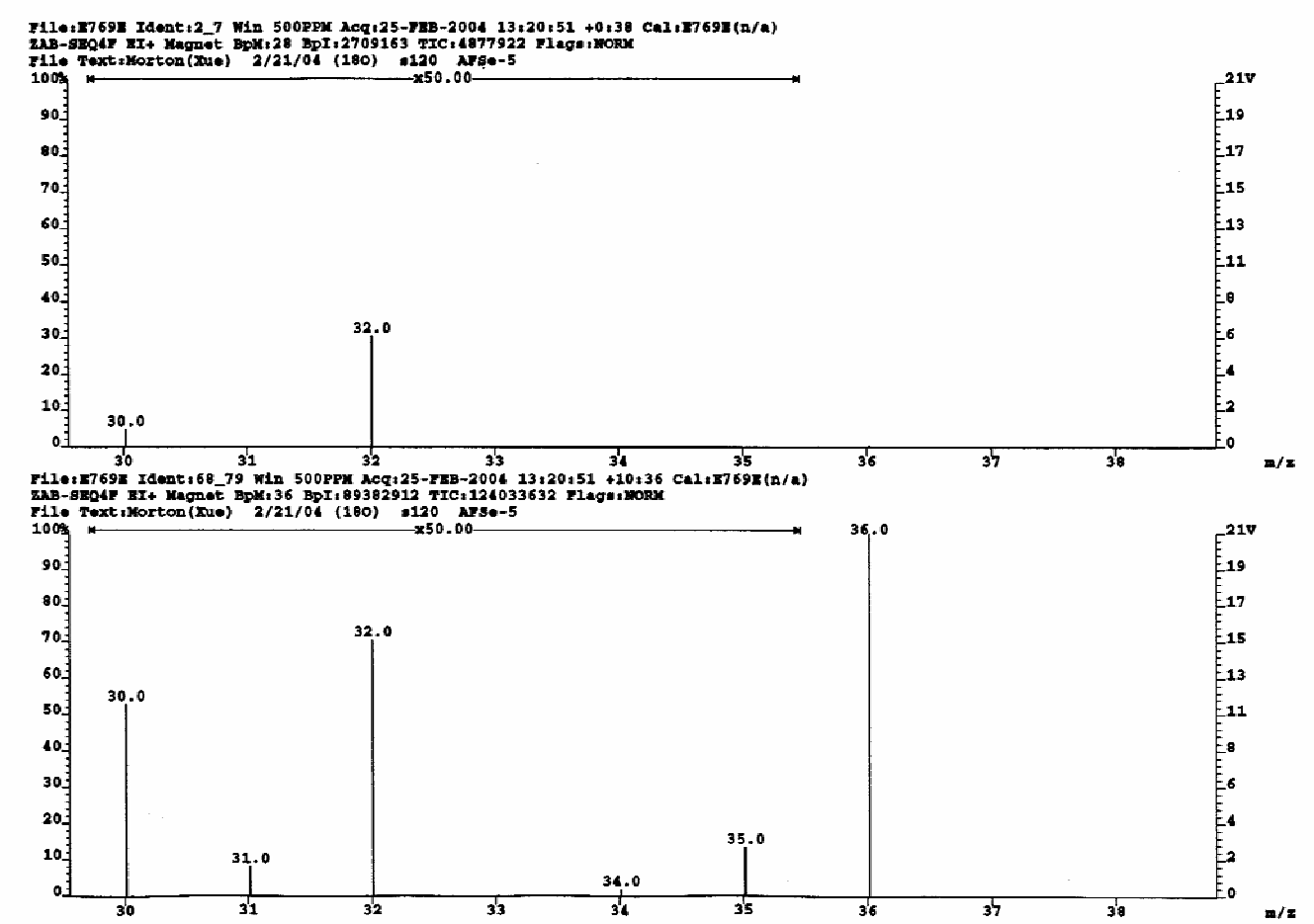

Figure 4.4. Mass spectra of dioxygen isotopomers ($^{16}O=^{16}O$; $^{16}O=^{18}O$; $^{18}O=^{18}O$): (Top) The background spectrum; (Bottom) The gaseous products from the reaction of **11** with $^{18}O_2$. The 30-35 Dalton region was enlarged by 50 times.

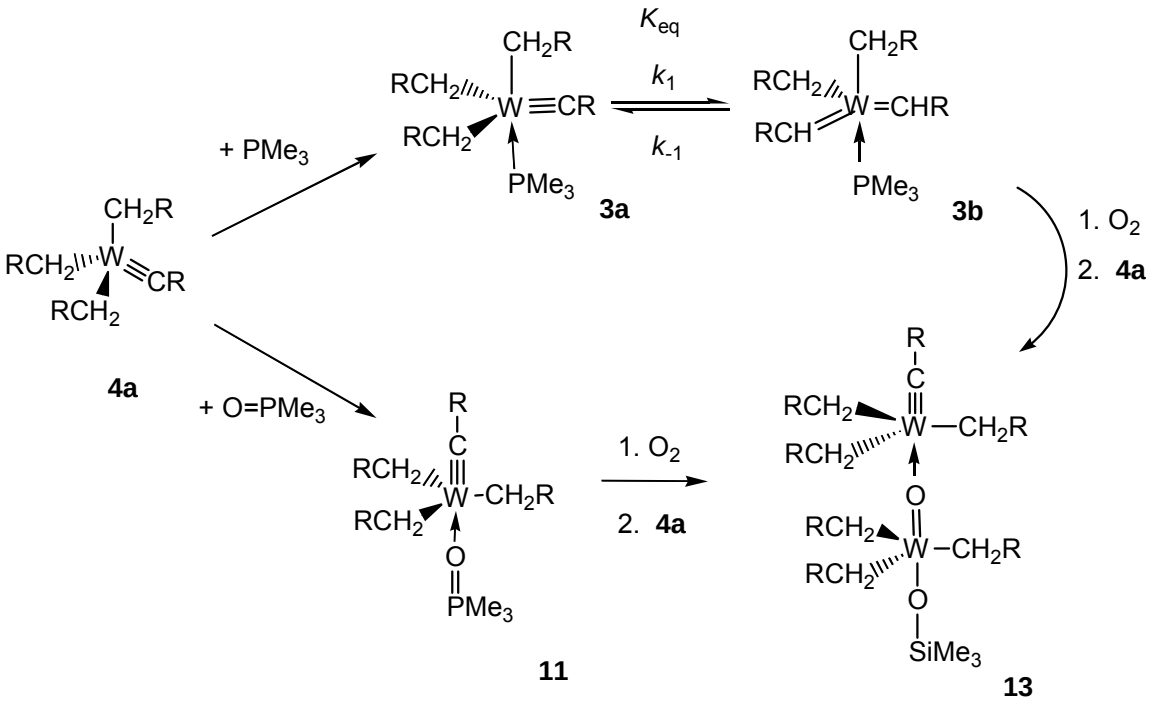

Scheme 4.4. Two pathways leading to **13**.

4.3. Concluding Remarks

$(Me_3SiCH_2)_3(Me_3SiC\equiv)W\leftarrow O{=}PMe_3$ (**11**), an adduct between $(Me_3SiCH_2)_3W\equiv CSiMe_3$ (**4a**) and $O{=}PMe_3$, was found to react with O_2 to give $O{=}W(OSiMe_3)(CH_2SiMe_3)_3$ (**3**) and CO_2. In the absence of $O{=}PMe_3$, **12** was not observed. **12** was isolated as an adduct with $(Me_3SiCH_2)_3W\equiv CSiMe_3$ (**4a**), $(Me_3SiCH_2)_3(Me_3SiC\equiv)W\leftarrow O{=}W(OSiMe_3)(CH_2SiMe_3)_3$ (**13**), which was characterized by X-ray crystallography.

4.4. Experimental Section

4.4.1. *General Procedures*

All manipulations were performed under a dry nitrogen atmosphere with the use of either a glovebox or standard Schlenk techniques. Solvents were purified by distillation from potassium benzophenone ketyl. NMR solvents were dried and stored over 5 Å molecular sieves. NMR spectra were recorded on Bruker AC-250 and AMX-400 Fourier transform spectrometers. ^1H and ^{13}C NMR spectra were referenced to solvents (residual protons in the ^1H spectra). ^{29}Si chemical shifts were referenced to $SiMe_4$. Elemental analyses were carried out by E+R Microanalytical Laboratory, Inc., Parsippany, New Jersey. $(Me_3SiCH_2)_3W\equiv CSiMe_3$ (**4a**)[15g] was prepared from $WCl_3(OMe)_3$ and $ClMgCH_2SiMe_3$ using a procedure similar to that for the preparation of $(Me_3CCH_2)_3W\equiv CCMe_3$.[15h] $O{=}PMe_3$ was purchased from Organometallics, Inc. (East Hampstead, New Hampshire) and used as received. O_2 (99.6% purity)

and $^{18}O_2$ (>99% ^{18}O, Isotec, Miamisburg, Ohio) were used as received. $^{13}CO_2$ (99% ^{13}C, <1% ^{18}O) was purchased from Cambridge Isotope Laboratories, Inc. (Andover, Massachusetts) and used as received.

4.4.2. *Preparation of $(Me_3SiCH_2)_3(Me_3SiC\equiv)W\leftarrow O=PMe_3$ (11)*

Solids of $(Me_3SiCH_2)_3W\equiv CSiMe_3$ (**4a**, 200 mg, 0.377 mmol) and $O=PMe_3$ (34.7 mg, 0.377 mmol) were placed in a Schlenk flask, and were then dissolved in Et_2O (ca. 15 mL). The mixture was stirred until all $O=PMe_3$ was dissolved in ca. 10 min. Cooling the solution at −30 °C overnight gave crystals of **11** (136 mg, 0.218 mmol, 57.9% yield). ^1H NMR (benzene-d_6, 400.04 MHz, 23 °C, J in Hz) δ 1.30 (-CH_2SiMe$_3$), 0.842 (d, O=PMe_3 $^2J_{P\text{-}H}$ = 12.7), 0.533 (≡CSiMe_3), 0.303 (-CH_2SiMe_3). $^{13}C\{^1H\}$ NMR (benzene-d_6, 100.6 MHz, 23 °C) δ 327.39 (≡CSiMe$_3$), 69.56 (CH$_2$SiMe$_3$), 17.38 (d, O=PMe_3, $^2J_{P\text{-}C}$ = 70.4), 3.26 (-CH_2SiMe_3), 2.19 (≡CSiMe_3). $^{31}P\{^1H\}$ NMR (benzene-d_6, H_3PO_4 internal standard, 161.94 MHz, 23 °C) δ 41.95. $^{29}Si\{^1H\}$ NMR (benzene-d_6) δ −23.17 (≡CSiMe$_3$), −3.42 (CH_2SiMe$_3$). Anal. Calcd. C 36.64, H 8.25. Found C 36.45, H 8.06.

4.4.3. *Preparation of $O=W(OSiMe_3)(CH_2SiMe_3)_3$ (12) and $(Me_3SiCH_2)_3W(\equiv CSiMe_3)\leftarrow O=W(OSiMe_3)(CH_2SiMe_3)_3$ (13)*

$(Me_3SiCH_2)_3(Me_3SiC\equiv)W\leftarrow O=PMe_3$ (**11**, 86.4 mg, 0.139 mmol) was dissolved in toluene-d_8 (ca. 0.5 mL) in a Youngs NMR tube. Three aliquots of 1000 mmHg (0.325 mmol) O_2 were added over a period of 4 days, and product

formation was monitored by ^{1}H NMR spectroscopy. The yield of **12** was ca. 30% as estimated by NMR. When the reaction was completed, the solution was transferred to a Schlenk flask, and all volatiles were removed *in vacuo.* The remaining solid was dissolved in pentane and filtered into a solution of $(Me_3SiCH_2)_3W{\equiv}CSiMe_3$ (**4a**) in pentane. Cooling the solution to –30 °C gave crystals of $(Me_3SiCH_2)_3(Me_3SiC{\equiv})W{\leftarrow}O{=}W(OSiMe_3)(CH_2SiMe_3)_3$ (**13**, 25.8 mg, 0.0238 mmol, 17.1%). ^{1}H NMR (toluene-d_8, 400.04 MHz, 23 °C) δ 1.640 (6H, CH_2–W=O; $^{2}J_{W\text{-}H}$ = 10.8 Hz), 0.697 (6H, CH_2–W≡C; $^{2}J_{W\text{-}H}$ = 9.8 Hz), 0.403 (9H, Me_3SiC≡), 0.283 (9H, Me_3Si-O), 0.241 (27H, Me_3SiCH_2-W=O), 0.160 (27H, Me_3SiCH_2-W≡C). ^{13}C{^{1}H} NMR (toluene-d_8, 100.6 MHz, 23 °C) δ 343.49 ($Me_3SiC{\equiv}$), 75.77 (CH_2W–), 62.90 (CH_2W=O), 2.39 ($Me_3SiCH_2W{\equiv}C$), 1.58 (Me_3SiCH_2W=O), 2.07 ($Me_3SiC{\equiv}$), 1.99 (O-SiMe_3). ^{29}Si{^{1}H} NMR (toluene-d_8, 79.49 MHz, 23 °C) δ 10.74 (Me_3Si-O), –1.50 (Me_3SiCH_2-W≡C), –2.97 (Me_3SiCH_2-W=O), –19.76 ($Me_3SiC{\equiv}$). Anal. Calcd. for $C_{31}H_{84}O_2Si_8W_2$: C 34.43, H 7.83, Si 20.78, P 0.00. Found: C 34.42, H 7.86, Si 21.03, P <0.02. The elemental analysis of phosphorus was conducted to rule out that the –OSiMe$_3$ ligand observed in the X-ray crystal structure of **13** was O=PMe$_3$.

In a separate study, $(Me_3SiCH_2)_3(Me_3SiC{\equiv})W{\leftarrow}O{=}PMe_3$ (**11**, 86.4 mg, 0.139 mmol) in toluene-d_8 (ca. 0.5 mL) in a Youngs NMR tube was added O_2. Formation of $O{=}W(OSiMe_3)(CH_2SiMe_3)_3$ (**12**) was observed, and subsequent analyses with mass spectrometry (MS) of the gaseous products were conducted.

4.4.4. *Reaction of $(Me_3SiCH_2)_3W{\equiv}CSiMe_3$ (4a) with O_2*

$(Me_3SiCH_2)_3W{\equiv}CSiMe_3$ (**4a**, 50 mg, 0.094 mmol) in benzene–d_6 (ca. 0.5 mL) in a Youngs NMR tube was frozen by liquid nitrogen and all volatiles were removed from the NMR tube. O_2 (1200 mmHg, ca. 0.1 mmol) was introduced into the Youngs tube and allowed to react at 5 °C. The reaction was monitored by ^1H NMR. Only unidentifiable decomposition products and $SiMe_4$ were observed.

4.4.5. *Reaction of O_2 with the Equilibrium Mixture of $(Me_3SiCH_2)_3W(\equiv CSiMe_3)(PMe_3)$ (3a) ⇌ $(Me_3SiCH_2)_2W(=CHSiMe_3)_2(PMe_3)$ (3b)*

O_2 (1200 mmHg, 0.1 mmol) was added to an equilibrium mixture of **3a** ⇌ **3b** prepared from 33 mg of $(Me_3SiCH_2)_3W(\equiv CSiMe_3)$ (**4a**) in excess PMe_3 (0.062 mmol) in benzene-d_6. The reaction was monitored by NMR, and the yield of $O{=}W(OSiMe_3)(CH_2SiMe_3)_3$ (**12**) estimated by NMR was 10%.

4.4.6. *Determination of X-ray Crystal Structures of 11 and 13*

The X-ray crystal structures of **11** and **13** were determined on a Bruker AXS Smart 1000 X-ray diffractometer equipped with a CCD area detector and a graphite-monochromated Mo source (K_α radiation, 0.71073 Å) and fitted with an upgraded Nicolet LT-2 low temperature device. Suitable crystals were coated with paratone oil (Exxon) and mounted on a glass fiber under a stream of nitrogen at –100(2) °C. The structures of **11** and **13** were solved by direct

method. All non-hydrogen atoms were anisotropically refined. Empirical absorption correction was performed with SADABS. Global refinements for the unit cells and data reductions were performed under the Saint program (Version 6.02). All calculations were performed using SHELXTL (Version 5.1) proprietary software package.

4.4.7. *Quantitative Determination of CO_2 Yielded from the Reaction of $(Me_3SiCH_2)_3(Me_3SiC{\equiv})W{\leftarrow}O{=}PMe_3$ (11) with O_2*

In a Youngs NMR tube, $(Me_3SiCH_2)_3W{\equiv}CSiMe_3$ (**4a**, 66 mg, 0.12 mmol), $O{=}PMe_3$ (11.2 mg, 0.12 mmol), and 4,4'-dimethylbiphenyl (5.9 mg, 0.032 mmol, internal standard) were dissolved in ca. 0.5 mL of toluene-d_8. ^{1}H NMR spectrum of the solution revealed the nearly quantitative formation of $(Me_3SiCH_2)_3(Me_3SiC{\equiv})W{\leftarrow}O{=}PMe_3$ (**11**). The Youngs tube (headspace = 2.8 mL) was then attached to a gas manifold, and the solution was frozen in liquid nitrogen, while most of the Youngs tube was immersed in liquid nitrogen. The N_2 gas in the Youngs tube was removed in vacuo. Approximately 1.3 mmol of O_2 (0.5 atm) was introduced into a gas manifold (65 mL). The valve on the Youngs NMR tube was opened for approximately 5 sec to introduce O_2 gas into the tube. Since the boiling point of O_2 (90.2 K) is high than that (77.4 K) of N_2, O_2 was condensed into the Youngs tube. An HRMS analysis of the production mixture *after* the reaction showed the presence of excess O_2.

The solution was warmed to room temperature and shaken. ^{1}H NMR spectrum revealed the formation of $O{=}W(OSiMe_3)(CH_2SiMe_3)_3$ (**12**, 0.011 mmol,

9.4% yield based on **11**). On a calibrated vacuum line with a volume of 170.7 mL, $^{13}CO_2$ (0.0145 atm, 0.101 mmol) was introduced. The Youngs tube containing the product, attached to the line previously, was opened and allowed to mix with the $^{13}CO_2$ gas in the manifold for approximately 15 min. The Youngs tube was frozen by liquid nitrogen to condense the CO_2 gas ($^{13}CO_2$ and $^{12}CO_2$) and then thawed. The tube was then frozen by liquid nitrogen, and was thawed. This process was repeated for a total of 3 times to allow a good mixing of $^{13}CO_2$ and $^{12}CO_2$. The tube was frozen again and the NMR valve was closed. After the tube was thawed, an HRMS analysis gave $^{13}CO_2$: $^{12}CO_2$ = 100.00 : 10.14. Thus the yield of CO_2 from the reaction was 0.010 mmol, or ca. 91% of $O{=}W(OSiMe_3)(CH_2SiMe_3)_3$ (**12**) from the reaction.

4.4.8. *Determination of Isotopomers of CO_2 from the Reaction of $(Me_3SiCH_2)_3(Me_3SiC{\equiv})W{\leftarrow}O{=}PMe_3$ (11) with $^{18}O_2$*

A Youngs NMR tube containing **11** (30 mg in toluene-d_8) was frozen in liquid nitrogen, and evacuated. Excess $^{18}O_2$ (>99% ^{18}O) was added, and the NMR tube was warmed to room temperature. After the ^1H NMR of the solution indicated that the reaction was complete, the gaseous products were analyzed by MS (Figures 4.3 and 4.4).

CHAPTER 5

Reactions of Tungsten Alkylidyne Complexes with Water

5.1. Introduction

Oxo ligands play a major role in the chemistry of metals, particularly the high valent, hard early transition metals.[38] With their large electronegativity, oxo ligands are effective to bring out the high oxidation states. Many early-transition-metal complexes are water-sensitive,[4b,39] and their reactions with H_2O usually lead to the formation of oxo complexes.[40-44] The nature of these reactions and their applications in, for example, the formation of microelectronic metal oxide materials[45] have attracted much recent attention.

Reactivities of early-transition-metal *organometallic* complexes toward water are of particular interest. Hillhouse and Bercaw reported that water reacts in a clean, stepwise manner with d^0 $Cp^*_2MH_2$ ($Cp^* = C_5Me_5$; M = Zr, Hf) to yield $Cp^*_2M(H)(OH)$, $(Cp^*MH)_2O$, $Cp^*_2M(OH)_2$, and finally $Cp^*_2M(OH)_2{\cdot}H_2O$, through the conversion of M-H bonds to M-O bonds accompanied by H_2 evolution.[40] Rosenthal and coworkers studied the reaction of d^2 $Cp_2Zr(THF)(\eta^2$-$Me_3SiC{\equiv}CSiMe_3)$ with H_2O, and found it to yield the zirconoxane complex $[Cp_2ZrC(SiMe_3){=}CH(SiMe_3)]_2O$.[41] Reactions of 1 equiv of H_2O with alkylidene complexes d^0 $Cp^*_2Ta(H)(=X)$ ($X = CH_2$, $C{=}CH_2$) yield XH_2 (CH_4, and $CH_2{=}CH_2$, respectively) and $Cp^*_2Ta(H)(=O)$.[42] Schrock, Lippard, Osborn and coworkers investigated the reactions of water with Group 6 neopentylidyne complexes, and

found that the reactions of H_2O with d^0 $(Bu^tCH_2)_3W{\equiv}CBu^t$ (**1**), $(Bu^tO)_3W{\equiv}CBu^t$, and $(Bu^tCH_2)_2Mo(=CHBu^t)(=NBu^t)$ gave $W_2O_3(CH_2Bu^t)_6$,[43a,44a] $[NEt_4][WO_3(CH_2Bu^t)]$,[44a] and $[\{Mo(=NBu^t)(CH_2Bu^t)_3\}_2(MoO_4)]$,[44b] respectively, and CMe_4. Legzdins and coworkers reported that the reactions of H_2O/O_2 with d^4 $Cp^*M(NO)(CH_2SiMe_3)_2$ (M = Mo, W) afford $Cp^*M(=O)_2(CH_2SiMe_3)$.[44c]

We reported in Chapter 4 that the reaction of O_2 with d^0 $(Me_3SiCH_2)_3(Me_3SiC{\equiv})W{\leftarrow}O{=}PMe_3$ (**11**) surprisingly yields a siloxide $O{=}W(OSiMe_3)(CH_2SiMe_3)_3$ (**12**). We have also found that the reactions of H_2O with $(Me_3SiCH_2)_3W{\equiv}CSiMe_3$ (**4a**), *or* **11** unexpectedly yielded CH_4 and **12** (Scheme 5.1). As in the reaction of O_2 with **11**, one -$SiMe_3$ group undergoes an unusual migration in these reactions with H_2O to give the -$OSiMe_3$ ligand in **12**.[42,45] When **4a** reacted with D_2O, analysis of the methane isotopomers by high-resolution mass spectrometry (HRMS) revealed the formation of CD_4, CHD_3 and CH_2D_2. Our studies of these reactions with water are presented.

5.2. Results and Discussion

5.2.1. *Reaction of $(Me_3SiCH_2)_3W(\equiv CSiMe_3)$ (4a) with H_2O. Preparation of $O{=}W(OSiMe_3)(CH_2SiMe_3)_3$ (12) and Study of the CH_4 Formation*

We were surprised to find that, when 3.4 equiv of H_2O was added to $(Me_3SiCH_2)_3W{\equiv}CSiMe_3$ (**4a**) in THF-d_8, subsequent reaction afforded **12** in ca. 60% yield by NMR. HRMS analyses of the gaseous products using $^{13}CH_4$ as the calibration showed the formation of 1.7 equiv (excess) of CH_4 (Figure 5.1).

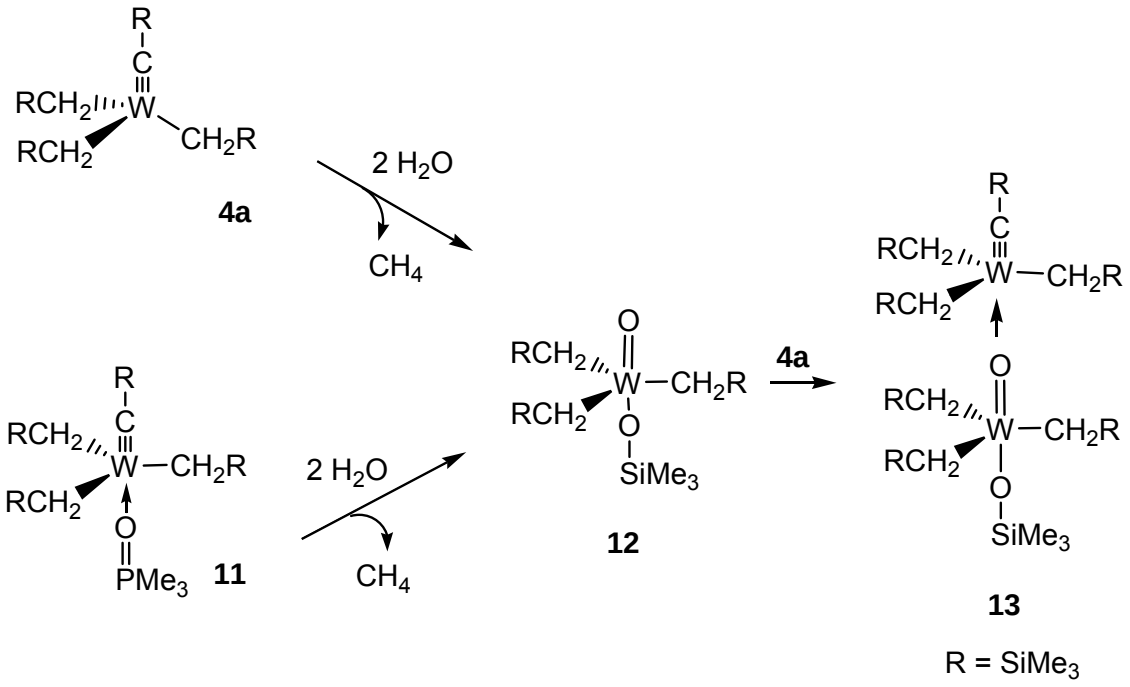

Scheme 5.1. The different routes to form **12** through reactions of H_2O.

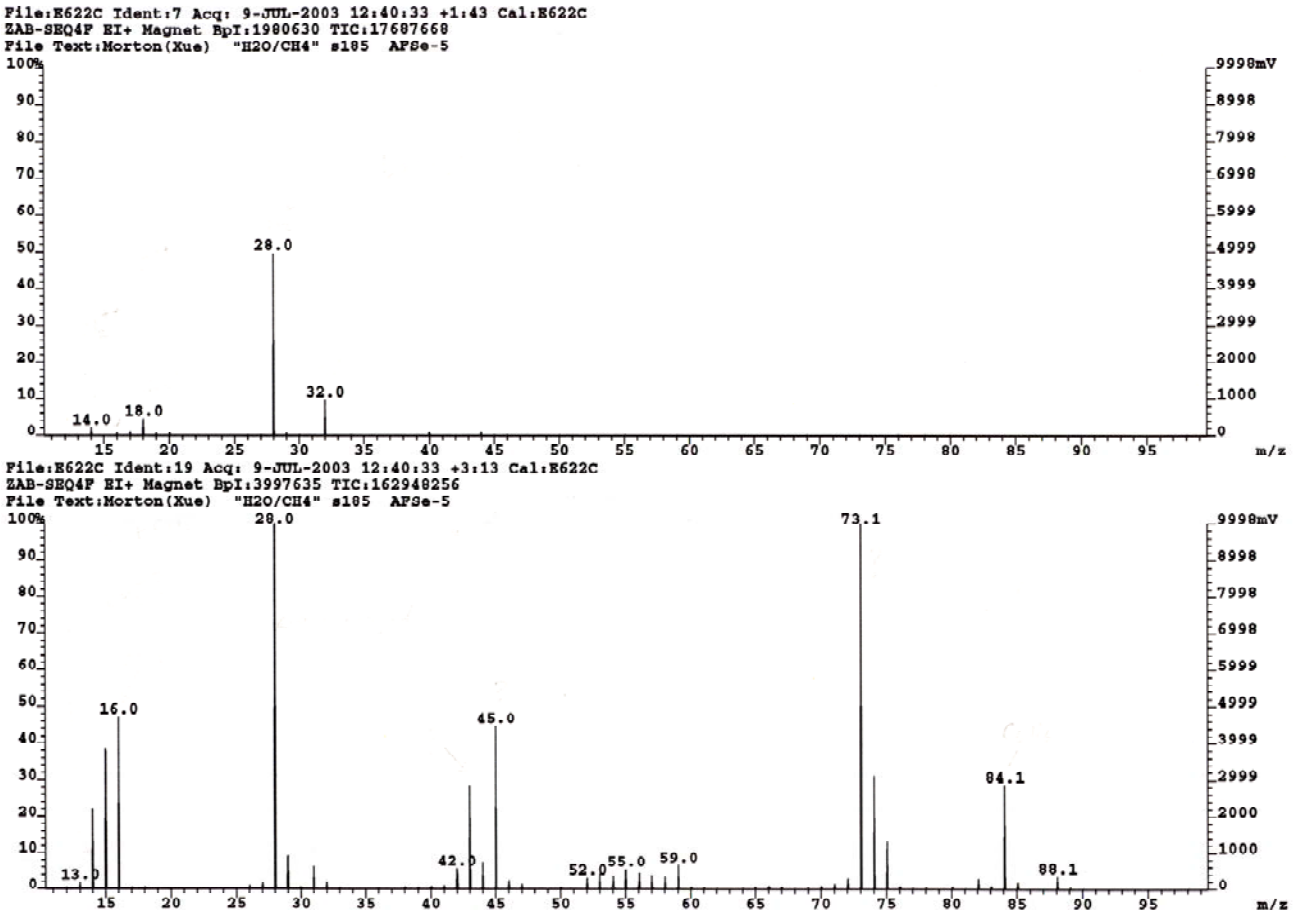

Figure 5.1. MS data of volatile products in the reaction of **4a** with H_2O.

12 was also found to decompose to CH_4 and unknown species in the presence of excess H_2O. It is thus likely that **12** reacted with the excess H_2O to yield additional CH_4.

5.2.2. *Reaction of $(Me_3SiCH_2)_3W(\equiv CSiMe_3)$ (4a) with D_2O*

In order to probe the mechanistic pathways in the formation of **12** and CH_4, $(Me_3SiCH_2)_3W{\equiv}CSiMe_3$ (**4a**) in THF-d_8 was added ca. 5 equiv of D_2O (99.9% D). An HRMS analysis of the methane isotopomers gave the following ratios of CH_4 : CH_3D : CH_2D_2 : CHD_3 : CD_4 = 0 : 3 : 100 : 19 : 32($\pm$ 5)% (Figure 5.2, Table 5.1). If the observation of CH_3D is ignored, as its HRMS signal is below the estimated error of 5%, the observations of CH_2D_2 and CHD_3 were surprising. ^2H NMR of the reaction of **4a** with D_2O revealed the formation of $O{=}W(OSiMe_3)(CH_{2-n}D_nSiMe_3)_3$ (**12-*d*$_n$**). The mechanistic pathway in the formation of **12** is not clear. In addition, **12** is likely decomposed by excess D_2O to give the methane isotopomers as well. However, the formation of CH_2D_2 and CHD_3, and the ^2H NMR studies are consistent with suggested pathways in Scheme 5.2 (Figure 5.3). The first step involves the addition of D–OD to the W≡C– bond to give **A**. The migration of the second D atom in W–OD to the W=CD– bond affords the tetraalkyl W oxo intermediate **C**. In addition to this pathway, **A** apparently undergoes an unexpected α-hydrogen migration from a $W–CH_2–$ to the W=CD– bond to yield **B** containing a W=CH– bond. Similar α-hydrogen migrations have been reported.[14,18,19c,22a,b] Subsequent D migration

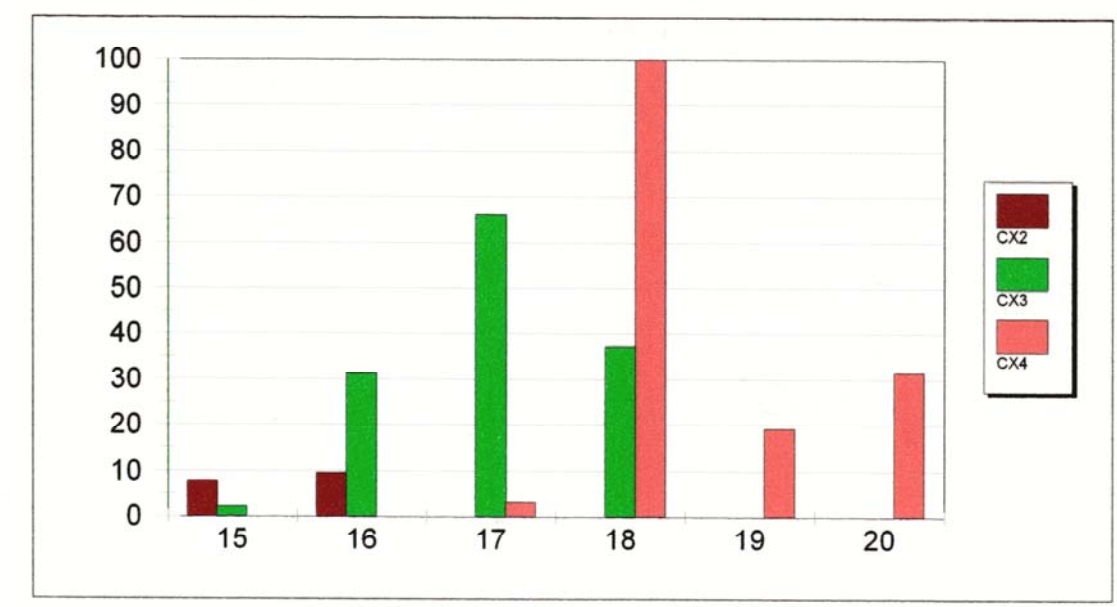

Figure 5.2. The HRMS mass spectrum for the methane isotopomers in the 15-20 Dalton region. Isotopomers of methylene (CX_2), methyl (CX_3) and methane (CX_4) are given in blue, black, green and red colors, respectively. $^{16}OH_2$ and $^{18}OH_2$ and their fragments are omitted for clarity.

Table 5.1. List of HRMS peaks and their intensities in the 15-20 Dalton region.

Calculated				Observed	
Chemical Species	Mass	#H	#D	Mass	Rel. %
CHD	15.0219	1	1	15.0216	7.8
CH_3	15.0235	3	0	15.0232	2.1
^{16}O	15.9949			15.9949	1.3
CD_2	16.0282	0	2	16.0282	9.6
CH_2D	16.0298	2	1	16.0299	31.3
CH_4	16.0313	4	0		
^{16}OH	17.0027			17.0027	2.0
CHD_2	17.0360	1	2	17.0361	66.2
CH_3D	17.0376	3	1	17.0378	3.1
$^{16}OH_2$	18.0106			18.0106	8.9
CD_3	18.0423	0	3	18.0424	37.3
CH_2D_2	18.0439	2	2	18.0440	100.0
^{18}OH	19.0070			19.0070	3.5
CHD_3	19.0501	1	3	19.0501	19.3
$^{18}OH_2$	20.0148			20.0148	13.2
CD_4	20.0564	0	4	20.0564	31.5

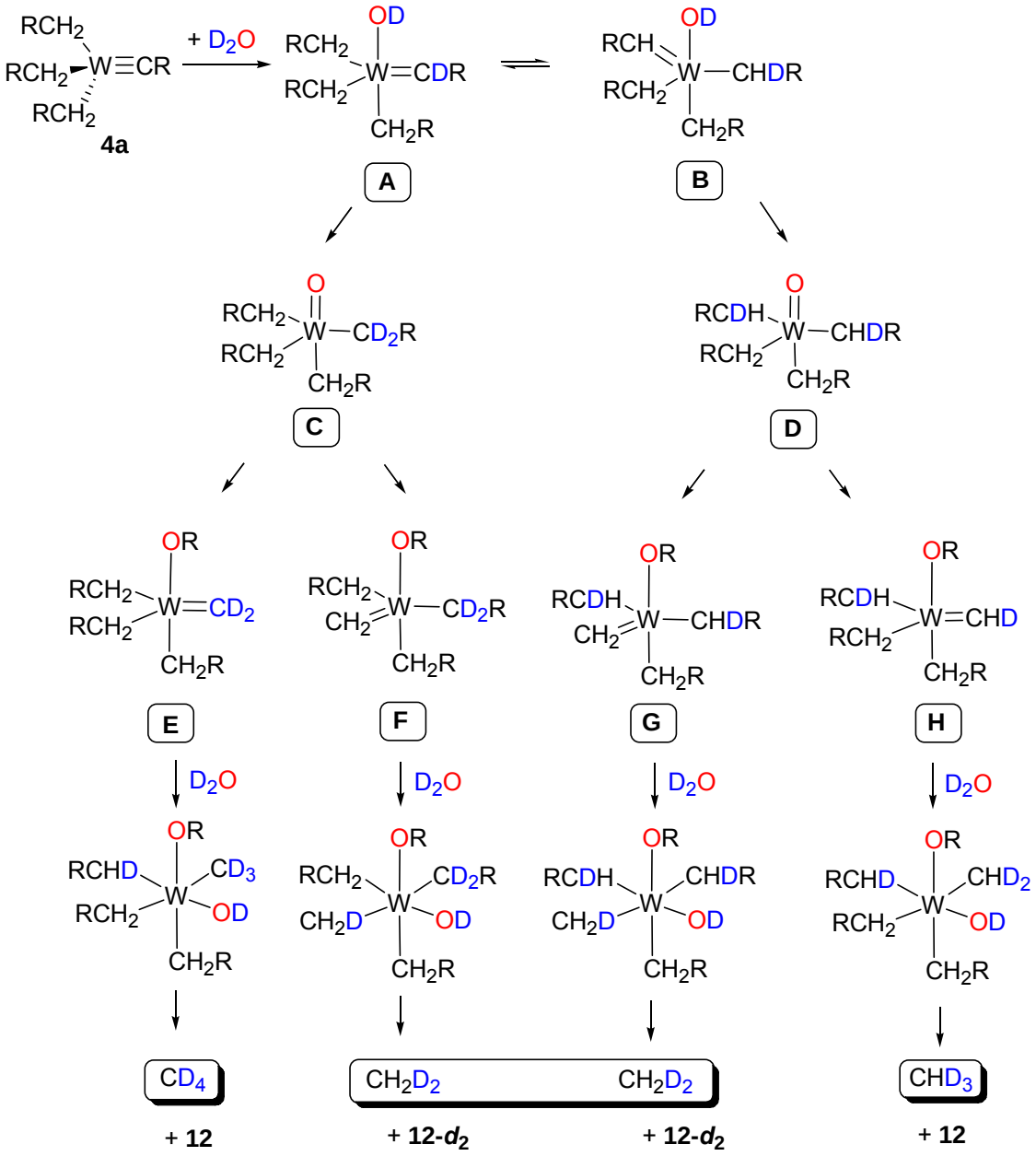

Scheme 5.2. Reaction of D_2O with **4a** and the formation of methane isotopomers.

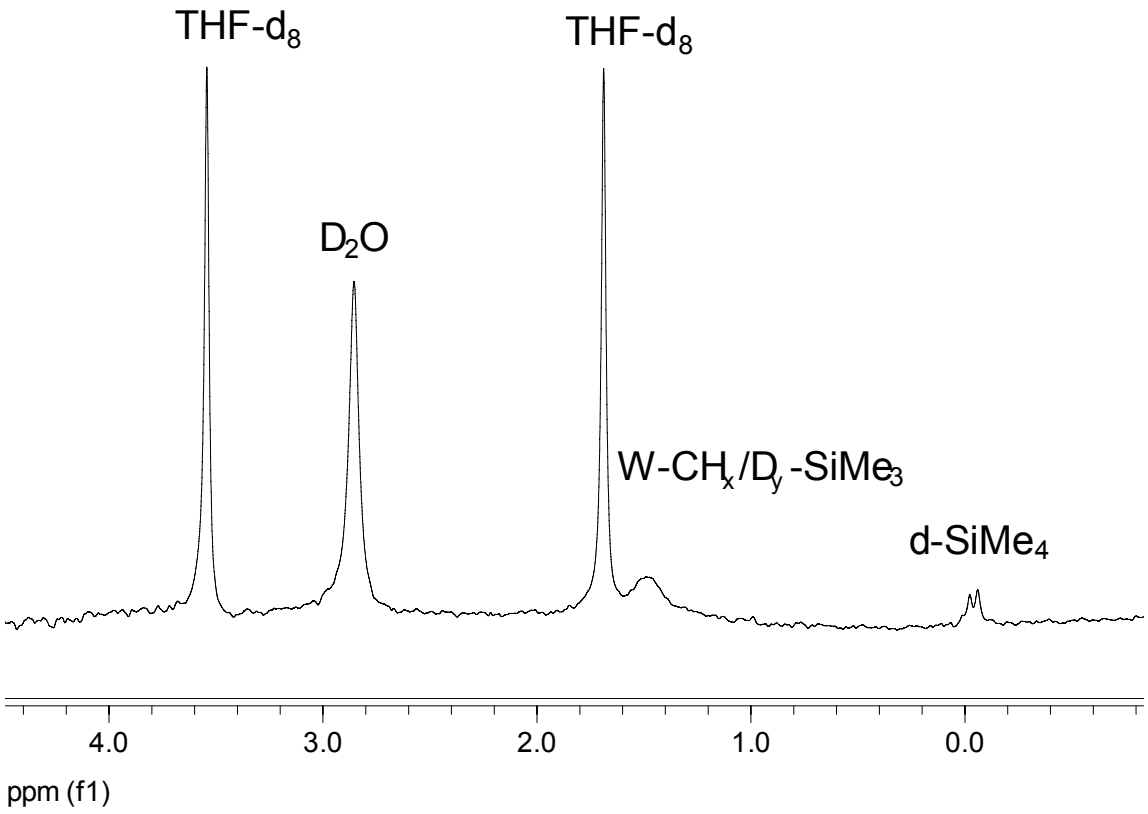

Figure 5.3. ^{2}H NMR spectrum of the α-H region in **12**. Non-deuterated THF solvent was used with one drop of THF-d_8 as reference.

from W–OD to the W=CH– bond yields **D**. The $–SiMe_3$ group in *one* of these alkyl ligands in **C** and **D** undergoes the C–Si bond cleavage and migration to the oxo ligand to give **E**/**F** and **G/H**, respectively, containing a methylene ligand ($W=CD_2–$ in **E**, $W=CH_2–$ in **F**/**G**, or W=CHD– in **H**), which subsequently reacts with D_2O to yield the methane isotopomers.

It is interesting to note that the reactions of H_2O with $(Bu^tCH_2)_3W{\equiv}CBu^t$ (**1**), $(Bu^tO)_3W{\equiv}CBu^t$, and $(Bu^tCH_2)_2Mo(=CHBu^t)(=NBu^t)$ give neopentane CMe_4 and oxo complexes $W_2O_3(CH_2Bu^t)_6$,[43a,44a] $[NEt_4][WO_3(CH_2Bu^t)]$,[44a] and $[\{Mo(=NBu^t)(CH_2Bu^t)_3\}_2\text{-}(MoO_4)]$,[44b] respectively. The alkylidene intermediate $(Bu^tCH_2)_3W(=CDBu^t)(OD)$ in the reaction of **1** with D_2O does not undergo α-hydrogen migration.[44a] Reactions of H_2O/O_2 with d^4 $Cp^*M(NO)(CH_2SiMe_3)_2$ (M = Mo, W) afford $Cp^*M(=O)_2(CH_2SiMe_3)$,[44c] and no $–SiMe_3$ migration to the oxo ligands was observed. It is not clear why the unusual $–SiMe_3$ migration occurs in the current reaction of **4a** with H_2O.

5.2.3. *Reaction of $(Me_3SiCH_2)_3(Me_3SiC{\equiv})W{\leftarrow}O=PMe_3$ (11) with H_2O*

$(Me_3SiCH_2)_3(Me_3SiC{\equiv})W{\leftarrow}O=PMe_3$ (**11**) was found to react with H_2O to give $O=W(OSiMe_3)(CH_2SiMe_3)_3$ (**12**). This reaction is, however, much slower than that of phosphine oxide-free $(Me_3SiCH_2)_3W{\equiv}CSiMe_3$ (**4a**), the parent compound of **11**, with H_2O. The reaction of **4a** with H_2O is completed in ca. 1 hour. In the reaction of **11** with 8 equiv of H_2O, ^1H NMR monitoring of the mixture

revealed that, after 5 days, only a small amount of **11** had reacted to give only 6% of **12**. A large amount of **11** remained in the mixture.

It is not clear how water reacts with the phosphine oxide complex **11**. At least two pathways are possible: (a) direct attack of **11** by a water molecule, while $(Me_3SiCH_2)_3W{\equiv}CSiMe_3$ (**4a**) is coordinated to the tungsten center; (b) dissociation of the $O{=}PMe_3$ from the metal center to give $(Me_3SiCH_2)_3W{\equiv}CSiMe_3$ (**4a**) which, as discussed earlier in this chapter, undergoes hydrolysis to give the products. Ligands such as phosphine oxides coordinate to metal centers through 2e, dative bonds to give adducts. Such bonding is known to be reversible. In other words, equilibria among the metal complexes, ligands and their adducts such as that in Scheme 5.1 for **11**, $(Me_3SiCH_2)_3W{\equiv}CSiMe_3$ (**4a**), and the adduct $(Me_3SiCH_2)_3(Me_3SiC{\equiv})W{\leftarrow}O{=}PMe_3$ (**11**) slow the reaction to form complex **12**.

If **11** reacts directly with H_2O, the slowness of the reaction of **11** with H_2O is perhaps not surprising, given the fact that it is coordinated by a phosphine oxide ligand. This coordination provides at least two electrons to the tungsten center so it is less electron deficient and has less drive to coordinate to water. The coordination also blocks the tungsten atom from attack by the water molecule to begin the hydrolysis reaction.

A more likely pathway in the hydrolysis of **11** is that the $O{=}PMe_3$ ligand dissociates from **11** through the equilibrium in Scheme 5.3 to give **4a**, which then reacts with H_2O to give **12**. The kinetics of the $O{=}PMe_3$ dissociation from **11** may be slow, and this leads to the small overall rate of the reaction of **11** with H_2O. In

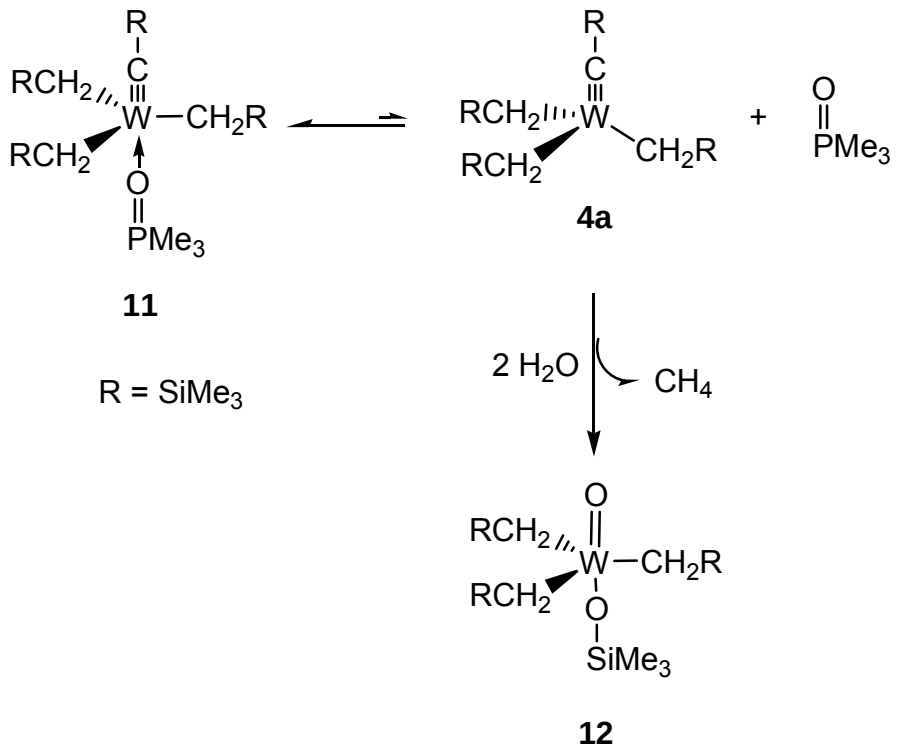

Scheme 5.3. Formation of **12** from the reaction of **11** with H_2O.

addition, both $O{=}PMe_3$ and H_2O compete for the small amount of newly formed **4a**, further reducing the yield of **12**.

5.3. Concluding Remarks

The formation of the novel siloxide **12** demonstrates rich chemistry in the reactions of d^0 complexes with H_2O. The presence of β-silicon atoms in **4a** and **11** is a critical factor in the observed unique reactivities here. As in the reaction of **11** with O_2, the silyl migration in the reactions of **4a** and **11** with H_2O is perhaps driven by the oxophilicity of silicon.

5.4. Experimental Section

5.4.1. *General Procedures*

All manipulations were performed under a dry nitrogen or argon atmosphere with the use of either a glovebox or standard Schlenk techniques. Solvents were purified by distillation from potassium benzophenone ketyl. NMR solvents were dried and stored over 5 Å molecular sieves. NMR spectra were recorded on Bruker AC-250 and AMX-400 Fourier transform spectrometers. ^1H and ^{13}C NMR spectra were referenced to solvents (residual protons in the ^1H spectra). ^{29}Si chemical shifts were referenced to $SiMe_4$. $(Me_3SiCH_2)_3W{\equiv}CSiMe_3$ (**4a**) was prepared from $WCl_3(OMe)_3$ and $ClMgCH_2SiMe_3$ using a procedure similar to that for the preparation of $(Me_3CCH_2)_3W{\equiv}CCMe_3$.[15h] **11** was prepared by the procedure in Chapter 4. $^{13}CH_4$ (99% ^{13}C) was purchased from Cambridge Isotope Laboratories, Inc. (Andover, Massachusetts) and used as received.

5.4.2. *Preparation of $(Me_3SiCH_2)_3(Me_3SiC{\equiv})W{\leftarrow}O{=}W(OSiMe_3)(CH_2SiMe_3)_3$ (13) via the Reaction of 4a with H_2O.*

While a solution of $(Me_3SiCH_2)_3W{\equiv}CSiMe_3$ (**4a**, 183 mg, 0.345 mmol) in THF (ca. 5–10 mL) at room temperature was stirred, H_2O (14 µL, 0.777 mmol) was added *via* syringe. An immediate color change from yellow to reddish-orange was observed upon addition of water. Stirring continued at room temperature for approximately 1 hour. All volatiles were then removed *in vacuo.* In a separate flask, $(Me_3SiCH_2)_3W{\equiv}CSiMe_3$ (**4a**, 183 mg, 0.345 mmol) was added dropwise to the first Schlenk flask. The mixture was filtered, and the filtrate was placed in the freezer at –30 °C to give crystals of $(Me_3SiCH_2)_3(Me_3SiC{\equiv})W{\leftarrow}O{=}W(OSiMe_3)(CH_2SiMe_3)_3$ (**13**, 46.5 mg, 12.5% yield). When the reaction was conducted in THF-d_8 in a Youngs NMR tube, the yield of **12** was ca. 60% as estimated by NMR. CH_4 was observed in the MS analysis of the gases in the headspace of the Youngs tube.

5.4.3. *Quantitative Determination of CH_4 Yielded from the Reaction of $(Me_3SiCH_2)_3W{\equiv}CSiMe_3$ (4a) with H_2O*

In a Youngs NMR tube, $(Me_3SiCH_2)_3W{\equiv}CSiMe_3$ (**4a**, 105 mg, 0.197 mmol) and 4,4'-dimethylbiphenyl (5.3 mg, 0.029 mmol) were dissolved in THF-d_8 (0.4 mL). H_2O (ca. 12 mg, 0.67 mmol) was added, and the NMR lid was closed immediately. The NMR tube was placed in an NMR spectrometer, and the reaction was monitored by ^1H NMR spectroscopy. The reaction was essentially

complete within 30 min to give O=W(OSiMe$_3$)(CH$_2$SiMe$_3$)$_3$ (**12**) (0.118 mmol, 60% yield based on **4a**). On a calibrated vacuum line with a volume of 170.7 mL, 0.0893 mmol of $^{13}CH_4$ (0.0127 atm) was introduced. The Youngs tube containing the product, attached to the line previously, was opened and allowed to mix with the $^{13}CH_4$ gas in the manifold for approximately 15 min. The Youngs tube was frozen by liquid nitrogen to condense the CH_4 gas ($^{13}CH_4$ and CH_4) and then thawed. The tube was then frozen by liquid nitrogen, and was thawed. This process was repeated for a total of 3 times to allow a good mixing of $^{13}CH_4$ and $^{12}CH_4$. The tube was frozen again and the NMR lid was closed. After the tube was thawed, an HRMS analysis gave a ratio of $^{13}CH_4$: $^{12}CH_4$ was found to be 27.55 : 100.00. Thus the yield of CH_4 from the reaction was 0.323 mmol, or ca. 164% yield from **4a**. It was found in a separate test that the product **12** reacted with H_2O to yield CH_4 as well. In other words, 1 equiv of **4a** reacts with excess H_2O to yield at least 2 equiv of CH_4. It is reasonable to assume that, in the current case, the excess H_2O (69%) reacted with the product **12**, producing additional CH_4 and lowering the yield of **12**.

5.4.4. *Reaction of (Me$_3$SiCH$_2$)$_3$W≡CSiMe$_3$ (4a) with D$_2$O*

4a (30 mg, 0.057 mmol) in THF-d_8 (ca. 0.5 mL) at room temperature was transferred to a Youngs NMR tube. D_2O (ca. 5 μL, 0.28 mmol) was added *via* syringe in a glove box. An immediate color change from yellow to reddish-orange was observed upon addition of D_2O. ^1H NMR spectra of the solution confirmed formation of O=W(OSiMe$_3$)(CH$_{2-n}$D$_n$SiMe$_3$)$_3$ (**12-*d*$_n$**) in solution. A

separate ^{2}D NMR study of this reaction is reported below. Studies with high-resolution mass spectrometry (HRMS) were conducted shortly after D_2O was added.

5.4.5. *^{2}H NMR Studies of the Reaction of $(Me_3SiCH_2)_3W{\equiv}CSiMe_3$ (4a) with D_2O*

4a (50 mg, 0.094 mmol) in THF (ca. 0.5 mL) at room temperature was transferred to a Youngs NMR tube. D_2O (ca. 5 µL, 0.28 mmol) was added *via* syringe in a glove box. A ^{2}H NMR spectrum at −10 °C showed a broad peak at 1.55 ppm attributable to –CH*D*SiMe$_3$ and –C*D*$_2$SiMe$_3$.

5.4.6. *The Analysis of Volatile Products by Mass Spectrometry (MS) and High-Resolution Mass Spectrometry (HRMS)*

Electron-ionization mass spectrometry (EI-MS, 70 eV) was conducted on a VG ZAB-EQ double focusing mass spectrometer for the analysis of CO_2 and CH_4. In the HRMS studies, the instrument was tuned to a resolution ($M/\Delta M \approx$ 12000) sufficient to discriminate between the various isotopomers of CH_xD_y ($x + y = 4$) and the EI-fragmentation products produced from them (Table 5.1). The sample gas was introduced through a needle valve to produce a registered source pressure of ca. 10^{-6} mbar. Vapor of H_2O (ca. 90% ^{18}O, 10% ^{16}O) was introduced through a separate inlet and used as the mass-calibration standard, thus allowing assignment of peaks to the CH_xD_y isotopomers (Table 5.1).

5.4.7. *Reaction of $(Me_3SiCH_2)_3(Me_3SiC{\equiv})W{\leftarrow}O{=}PMe_3$ (11) with H_2O*

H_2O (ca. 5 μL, 0.28 mmol) was added *via* syringe to $(Me_3SiCH_2)_3(Me_3SiC{\equiv})W{\leftarrow}O{=}PMe_3$ (**11**, 22 mg, 0.035 mmol) in toluene-d_8 (ca. 0.5 mL) at room temperature in a glove box. The solution was monitored for 5 days by ^{1}H NMR. A small amount of **11** had reacted to give 6% of the expected $O{=}W(OSiMe_3)(CH_2SiMe_3)_3$ (**12**), and a large amount of unreacted **11** was observed in solution.

5.4.8. *Decomposition of 12 by H_2O*

12 was found to react with H_2O and decompose to CH_4 and other unknown products. H_2O (ca. 2 μL, 0.11 mmol) was added *via* syringe to a J. R. Youngs NMR tube containing **4a** (50 mg, 0.094 mmol) and the reaction mixture was monitored by ^{1}H NMR spectroscopy. The sample was checked to ensure all starting material had reacted, and then all volatiles were removed *in vacuo*. Another aliquot of H_2O (ca. 2 μL, 0.11 mmol) was added to the reaction mixture dissolved in THF-d_8 in a J. R. Youngs NMR tube, and a ^{1}H NMR spectrum was taken to determine that **12** had fully decomposed to unknown products. The sample was submitted for MS analysis and CH_4 was found to be a product.

CHAPTER 6

Future Studies

Several new alkylidyne and *bis*(alkylidene) complexes have been prepared and characterized. They were found to undergo unusual exchanges and reactions with phosphines to give alkyl alkylidene alkylidyne complexes. Alkylidyne complexes were found to react with O_2 or H_2O, leading to the formation of a rare oxo siloxy complex.

Additional studies of the reactions of phosphines with alkylidyne complexes are needed to understand the nature of the α-hydrogen migration and abstraction reactions observed in Chapters 2 and 3, and to compare the differences between $-CH_2CCMe_3$ and $-CH_2SiMe_3$ ligands. Isolation of phosphine-oxide analogs of *bis*-phosphine, alkyl alkylidene alkylidyne complexes **8** and **9** might provide suitable crystals for elemental analysis and for the determination of the structures of the alkyl alkylidene alkylidyne complexes through X-ray crystallography. Studies with phosphines other than those used in this dissertation could provide a more comprehensive picture of the nature of the reactions reported in Chapters 2 and 3.

High-κ metal oxides have been used as microelectronic materials for CVD. Additional studies with Group VI metal alkylidene and imido complexes with oxygen could provide additional mechanistic information. Preliminary studies revealed that the reaction of **4a** or **3** with oxygen and water occurred to

give crystalline, trimeric complexes containing W(VI), bridging and terminal oxo ligands, and alkyl ligands. Isolation and full characterization of these complexes might provide insight into the nature of the reactions of alkylidyne complexes with O_2. Preliminary studies of the reaction of **4a** with oxygen transfer agents, such as pyridine-oxide and trimethylamine-oxide yield the siloxy complex **12**. This new reaction may provide a rich new area in which to study the nature of oxygen atom transfer reactions involving alkylidyne complexes. Investigation of the mechanism and kinetic studies would provide insight into the mechanism of formation of **12**.

An extension of the reactions of water with alkylidyne complexes may involve their controlled reactions with primary alcohols. Preliminary investigations revealed that ethanol reacted with **4a** to give perhaps an alkylidene product (based on the ^{1}H NMR spectrum), and this reaction is worth pursuing. Studies in this area might provide an avenue for precursors for microelectronic metal oxide materials.

REFERENCES

1. (a) See, e.g., *Metal-Dioxygen Complexes*, Special Issue, *Chem. Rev.* **1994**, *94*, Issue 3. (b) Holm, R. H. *Chem. Rev*. **1987**, *87*, 1401.
2. (a) Fischer, E. O.; Maasbol. A. *Angew. Chem., Int. Ed.* **1964**, *3*, 580. (b) Fischer, H., Kreissl, F. R., Schubert, U., Hofmann, P., Dotz, K. H., Weiss, K. *Transition Metal Carbene Complexes*, 1984, VCH Publishers: Weinheim.
3. (a) Schrock, R. R. *J. Organomet. Chem.* **1986**, *300*, 249. (b) Schrock, R. R. *J. Am. Chem. Soc.* **1974**, *96*, 6796. (c) Schrock, R. R.; Fellmann, J. D. *J. Am. Chem. Soc.* **1978**, *100*, 3359.
4. (a) Elschenbroich, C.; Salzer, A. *Organometallics: A Concise Introduction*, 2nd ed, 1992, VCH Publishers: Weinheim, Chapter 14. (b) Crabtree, R. H. *The Organometallic Chemistry of the Transition Metals*, 3rd ed.: Wiley, New York, 2001.
5. See, e.g., (a) Schrock, R. R. *Acc. Chem. Res*. **1979**, *12*, 98. (b) Nugent, W. A.; Mayer, J. M. *Metal-Ligand Multiple Bonds*; Wiley: New York, 1988. (c) Schrock, R. R. *Acc. Chem. Res.* **1986**, *19*, 342. (d) Fischer H., Kreissl, F. R., Schrock, R. R., Schubert, U., Hofmann, P., Weiss, K. *Carbyne Complexes*, 1988, VCH Publishers: Weinheim.
6. Greenwood, N. N.; Earnshaw, A. *Chemistry of the Elements*, 2nd ed., Butterworth and Heinemann, Oxford, UK, 1997.
7. (a) Simandi, L. I. *Catalytic Activation of Dioxygen by Metal Complexes*, Kluwer: Amsterdam, 1992. (b) Sawyer, D. T. *Oxygen Chemistry*, Oxford University Press: Oxford, UK, 1991. (c) Martell, A. E.; Sawyer, D. T. *Oxygen Complexes and Oxygen Activation by Transition Metals*, Plenum:

New York, 1987. (d) Chanon, M.; Julliard, M.; Santamaria, J.; Chanon, F. *New J. Chem.* **1992**, *16*, 171. (e) King, R. B. *Encyclopedia of Inorganic Chemistry*, Vol. 2, Wiley: New York, 1994. (f) Pauling, L; Coryell, C. D. *Proc. Natl. Acad. Sci. USA*, **1936**, *22*, 210.

8. (a) Frankland, E. *Ann*. **1853**, *85*, 347. (b) Frankland, E. *J. Chem. Soc.* **1862**, *15*, 363. (c) Demuth, R., Meyer, V. *Ber*. **1890**, *23*, 394.
9. (a) Zucchini, U.,Albizzati, E., Giannini, U. *J. Organomet. Chem*. **1971**, *26*, 357. (b) Brindley, P. B., Hodgson, J. C. *J. Organomet. Chem*. **1974**, *65*, 57.
10. (a) Blackburn, T. F.; Labinger, J. A.; Schwartz, J. *Tetrahedron Lett.* **1975**, *16*, 3041. (b) Labinger, J. A.; Hart, D. W.; Seibert, W. E.; Schwartz, J. *J. Am. Chem. Soc.* **1975**, *97*, 3851. (c) Gibson, T. *Organometallics* **1987**, *6*, 918. (d) Brindley, P. B.; Scotton, M. J. *J. Chem. Soc. Perkin II* **1981**, 419. (e) Van Asselt, A.; Santarsiero, B. D.; Bercaw, J. E. *J. Am. Chem. Soc.* **1986**, *108*, 8291. (f) Coughlin, E. B.; Bercaw, J. E. *Organometallics* **1992**, *11*, 465. (g) Tilley, T. D. *Organometallics* **1985**, *4*, 1452.
11. (a) Lubben, T. V.; Wolczanski, P. T. *J. Am. Chem. Soc.* **1987**, *109*, 424. (b) Lubben, T. V.; Wolczanski, P. T. *J. Am. Chem. Soc.* **1985**, *107*, 701. (c) Wang, R.-J.; Folting, K.; Huffman, J. C.; Chamberlain, L. R.; Rothwell, I. P. *Inorg. Chim. Acta* **1986**, *120*, 81. (d) Gibson, V. C.; Redshaw, C.; Walker, G. L. P.; Howard, J. A. K.; Hoy, V. J.; Cole, J. M.; Kuzmina, L. G.; De Silva, D. S. *J. Chem. Soc., Dalton Trans.* **1999**, 161. (e) Brindley, P. B.; Hodgson, J. C. *J. Organomet. Chem.* **1974**, *65*, 57. (f) Kim, S.-J.; Jung, I. N.; Yoo, B. R.; Cho, S.; Ko, J.; Kim, S. H.; Kang, S. O. *Organometallics* **2001**, *20*, 1501.

(g) Schaverien, C. J.; Orpen, A. G. *Inorg. Chem.* **1991**, *30*, 4968. (h) Adam, W.; Metz, M.; Prechtl, F.; Renz, M. *Synthesis* **1994**, 563. (i) Adam, W.; Putterlik, J.; Schuhmann, R. M.; Sundermeyer, J. *Organometallics* **1996**, *15*, 4586. See also, (j) Vetter, W. M.; Sen, A. *Organometallics* **1991**, *10*, 244. (k) Van Asselt, A.; Trimmer, M. S.; Henling, L. M.; Bercaw, J. E. *J. Am. Chem. Soc.* **1988**, *110*, 8254. (l) Mansilla, N.; Rheinwald, G.; Lang, H. *J. Organomet. Chem.* **2000**, *602*, 72. (m) Schaverien, C. J. *J. Chem. Soc., Chem. Comm.* **1991**, 458.

12. (a) Senzaki, Y.; Hamilton, R. F.; Reid, K. G.; Hobbs, C. C.; Hedge, R. I.; Tiner, M. J. *Mater. Res. Soc. Symp. Proc.* **2000**, *606,* 13. (b) Son, K.-A.; Mao, A. Y.; Sun, Y.-M.; Kim, B. Y.; Liu, F.; Kamath, A.; White, J. M.; Kwong, D. L.; Roberts, D. A.; Vrtis, R. N. *Appl. Phys. Lett.* **1998**, *72*, 1187. (c) Niimi, H.; Johnson, R. S.; Lucovsky, G.; Massoud, H. Z. *Proc. Electrochem Soc.* **2000**, *2000-2*, 487. (d) Chiu, H.-T.; Wang, C.-N.; Chuang, S.-H. *Chem. Vap. Deposition* **2000**, *6*, 223.
13. Scott, J. F. *Annu. Rev. Mater. Sci.* **1998**, *28*, 79.
14. Morton, L. A.; Zhang, X-H.; Wang, R.; Lin, Z.; Wu, Y-D.; Xue, Z-L. *J. Am. Chem. Soc.* **2004,** *126*, 10208.
15. (a) Clark, D. N.; Schrock, R. R. *J. Am. Chem. Soc*. **1978**, *100*, 6774. (b) Schrock, R. R.; Clark, D. N.; Sancho, J.; Wengrovius, J. H.; Rocklage, S. M.; Pedersen, S. F. *Organometallics* **1982**, *1*, 1645. (c) Mayr, A.; Hoffmeister, H. *Adv. Organomet. Chem.* **1991**, *32*, 227. (d) Hua, F.; Mowat, W.; Skapski, A. C.; Wilkinson, G. *J. Chem. Soc., Chem. Commun.* **1971**,

1477. (e) Mowat, W.; Wilkinson, G. *J. Chem. Soc., Dalton Trans.* **1973**, 1120. (f) Kim, H. P.; Angelici, R. J. *Adv. Organomet. Chem.* **1987**, *27*, 51. (g) Andersen, R. A.; Chisholm, M. H.; Gibson, J. F.; Reichert, W. W.; Rothwell, I. P.; Wilkinson, G. *Inorg. Chem*, **1981**, *20*, 3934. (h) Schrock, R. R.; Sancho, J.; Pederson, S. F. *Inorg. Synth.* **1989**, *26*, 45.

16. (a) Schrock, R. R. *J. Am. Chem. Soc.* **1974**, *96*, 6796. (b) Schrock, R. R.; Fellman, J. D. *J. Am. Chem. Soc.* **1978**, *100*, 3359. (c) Li, L.; Hung, M.; Xue, Z. *J. Am. Chem. Soc.* **1995**, *117*, 12746. (d) Schrock, R. R. *Acc. Chem. Res.* **1979**, *12*, 98. (e) Schrock, R. R. in *Reactions of Coordinated Ligands*, P. S. Braterman, Ed.; Plenum: New York, 1986. (f) *Advances in Metal Carbene Chemistry*, Schubert, U. Ed.; *NATO ASI Series*, Series C, Vol. *269*, 1989. (g) Aguero, A.; Osborn, J. A. *New J. Chem.* **1988**, *12*, 111. (h) Schrock, R. R. *Acc. Chem. Res.* **1990**, *23*, 158. (i) Warren, T. H.; Schrock, R. R.; Davis, W. M. *J. Organomet. Chem.* **1998**, *569*, 125. (j) Feldman, J.; Schrock, R. R. *Prog. Inorg. Chem*. **1991**, *39*, 1.

17. (a) Rothwell, I. P. *Polyhedron* **1985**, *4*, 177. (b) *Comprehensive Organometallic Chemistry* G. Wilkinson, F. G. A. Stone, and E. W. Abel, Eds.; Pergamon: New York, 1982, Vol. 3, Ch. 25 by J. A. Labinger; Vol. 8, Ch. 54 by R. H. Grubbs. (c) *Comprehensive Organometallic Chemistry II*, E. W. Abel, F. G. A. Stone, and G. Wilkinson Eds.; Pergamon: New York, 1982, Vol. 5, Ch. 2 by D. E. Wigley and S. D. Gray; Ch. 5 by M. J. Winter and S. Woodward.

18. (a) Caulton, K. G.; Chisholm, M. H.; Streib, W. E.; Xue, Z. *J. Am. Chem. Soc.* **1991**, *113*, 6082. (b) Xue, Z.; Caulton, K. G.; Chisholm, M. H. *Chem. Mater.* **1991**, *3*, 384. (c) Xue, Z.; Chuang, S.–H.; Caulton, K. G.; Chisholm, M. H. *Chem. Mater.* **1998**, *10*, 2365.

19. (a) Edwards, D. S.; Biondi, L. V.; Ziller, J. W.; Churchill, M. R.; Schrock, R. R. *Organometallics* **1983**, *2*, 1505. (b) LaPointe, A. M.; Schrock, R. R. *Organometallics* **1995**, *14*, 1875. There is no H/D scrambling among the neopentyl and neopentylidene ligands in $Re(\equiv CBu^t)(=CHBu^t)(CD_2Bu^t)_2$ at 80 °C in toluene-d_8. (c) LaPointe, A. M.; Schrock, R. R.; Davis, W. M. *J. Am. Chem. Soc.* **1995**, *117*, 4802.

20. (a) Schrock, R. R. *Chem. Rev.* **2002,** *102*, 145. (b) Schrock, R. R. *Dalton Trans*. **2001**, 2541. (c) Feldman, J.; Schrock, R. R. *Prog. Inorg. Chem.* **1991**, *39*, 1. (d) Aguero, A.; Osborn, J. A. *New J. Chem.* **1988**, *12*, 111. (e) Mayr, A.; Hoffmeister, H. *Adv. Organomet. Chem.* **1991**, *32*, 227. (f) Kim, H. P.; Angelici, R. J. *Adv. Organomet. Chem.* **1987**, *27*, 51. (g) Mowat, W.; Wilkinson, G. *J. Chem. Soc., Dalton Trans.* **1973**, 1120. (h) Andersen, R. A.; Chisholm, M. H.; Gibson, J. F.; Reichert, W. W.; Rothwell, I. P.; Wilkinson, G. *Inorg. Chem.* **1981**, *20*, 3934. (i) Li, L.; Hung, M.; Xue, Z. *J. Am. Chem. Soc.* **1995**, *117*, 12746. (j) Xue, Z.; Li, L.; Hoyt, L. K.; Diminnie, J. B.; Pollitte, J. L. *J. Am. Chem. Soc.* **1994**, *116*, 2169.

21. For d^n type carbenes and carbynes, see, e.g., Refs. 5b, 5d, 15c and 15f, and (a) Trnka, T. M.; Grubbs, R. H. *Acc. Chem. Res.* **2001**, *34*, 18. (b) Schrock, R. R.; Hoveyda, A. H. *Angew. Chem, Inter. Ed.* **2003**, *42*, 4592.

(c) Pollagi, T. P.; Manna, J.; Stoner, T. C.; Geib, S. J.; Hopkins, M. D*. NATO ASI Series C* **1993**, *392*, 71. (d) Yong, B. S.; Nolan, S. P. *Chemtracts* **2003**, *16*, 205. (e) Doyle, M. P. *Pure Appl. Chem.* **1998**, *70*, 1123.

22. (a) Chen, T.; Wu, Z.; Li, L.; Sorasaenee, K. R.; Diminnie, J. B.; Pan, H.; Guzei, I. A.; Rheingold, A. L.; Xue, Z. *J. Am. Chem. Soc.* **1998**, *120*, 13519. (b) Choi, S.; Lin, Z.; Xue, Z. *Organometallics* **1999**, *18*, 5488. (c) Chen, T.-N.; Zhang, X.-H.; Wang, C.-S.; Wu, Z.-Z.; Li, L.-T.; Sorasaenee, K. R.; Diminnie, J. B.; Pan, H. J.; Guzei, I. A.; Rheingold, A. L.; Wu, Y.-D.; Xue, Z.-L. *Organometallics* **2005**, *24,* 1214. (d) Wu, Z.; Cai, H.; Yu, Y.-X.; Blanton, J. R.; Diminnie, J. B.; Pan, H.-J. Xue, Z.-L. *Organometallics* **2002**, *21*, 3973.
23. (a) Fellmann, J. D.; Schrock, R. R.; Rupprecht, G. A. *J. Am. Chem. Soc.* **1981**, *103*, 5752. (b) Fellmann, J. D.; Rupprecht, G. A.; Wood, C. D.; Schrock, R. R. *J. Am. Chem. Soc.* **1978**, *100*, 5964. (c) Diminnie, J. B.; Hall, H. D.; Xue, Z. *J. Chem. Soc.*, *Chem. Commun*. **1996**, 2383. (d) Diminnie, J. B.; Xue, Z. *J. Am. Chem. Soc.* **1997**, *119*, 12657. (e) Diminnie, J. B.; Blanton, J. R.; Cai, H.; Quisenberry, K. T.; Xue, Z. *Organometallics* **2001**, *20*, 1504.
24. Churchill, M. R.; Youngs, W. J. *Inorg. Chem.* **1979**, *18*, 1930.
25. The liquid sample of **5a-b** was shipped overnight in an insulated container with dry ice for elemental analysis. The sample was analyzed immediately upon arrival. Repeated attempts to get elemental analysis of **5a-b** afforded the following data: Calcd. C 43.10; H 7.99; P 4.63; Found C 48.47, 48.53; H 7.79, 7.80; P 4.22, 4.18.

26. See, e.g., Espenson, J. H. *Chemical Kinetics and Reaction Mechanism*; 2nd Ed., McGraw-Hill: New York, 1995, pp. 46-49.

27. Morse, P. M.; Spencer, M. D.; Wilson, S. R.; Girolami, G. S. *Organometallics* **1994**, *13*, 1646.

28. (a) This technique utilizes phase cycling to suppress unwanted signals, unlike other techniques which apply ^{13}C broad-band decoupling. HMQC demonstrates the sensitivity advantage of the inverse detection method. (b) ^{1}H-gated-decoupled-^{13}C experiments allow for full NOE-enhancement and give a fully coupled ^{13}C spectrum. (c) Braun, S.; Kalinowski, H.-O.; Berger, S. *150 and More Basic NMR Experiments. A Practical Course*. 2nd Ed., Wiley-VCH: Weinheim, 1998, pp. 384-387.

29. (a) Frisch, M. J.; Trucks, G. W.; Schlegel, H. B.; Scuseria, G. E.; Robb, M. A.; Cheeseman, J. R.; Montgomery, J. A.; Vreven, Jr., T.; Kudin, K. N.; Burant, J. C.; Millam, J. M.; Iyengar, S. S.; Tomasi, J.; Barone, V.; Mennucci, B.; Cossi, M.; Scalmani, G.; Rega, N.; Petersson, G. A.; Nakatsuji, H.; Hada, M.; Ehara, M.; Toyota, K.; Fukuda, R.; Hasegawa, J.; Ishida, M.; Nakajima, T.; Honda, Y.; Kitao, O.; Nakai, H.; Klene, M.; Li, X.; Knox, J. E.; Hratchian, H. P.; Cross, J. B.; Adamo, C.; Jaramillo, J.; Gomperts, R.; Stratmann, R. E.; Yazyev, O.; Austin, A. J.; Cammi, R.; Pomelli, C.; Ochterski, J. W.; Ayala, P. Y.; Morokuma, K.; Voth, G. A.; Salvador, P.; Dannenberg, J. J.; Zakrzewski, V. G.; Dapprich, S.; Daniels, A. D.; Strain, M. C.; Farkas, O.; Malick, D. K.; Rabuck, A. D.; Raghavachari, K.; Foresman, J. B.; Ortiz, J. V.; Cui, Q.; Baboul, A. G.; Clifford, S.; Cioslowski,

J.; Stefanov, B. B.; Liu, G.; Liashenko, A.; Piskorz, P.; Komaromi, I.; Martin, R. L.; Fox, D. J.; Keith, T.; Al-Laham, M. A.; Peng, C. Y.; Nanayakkara, A.; Challacombe, M.; Gill, P. M. W.; Johnson, B.; Chen, W.; Wong, M. W.; Gonzalez, C.; Pople, J. A. *Gaussian 03*, Revision B.03, Gaussian, Inc., Pittsburgh PA, 2003. (b) Hay, P. J.; Wadt, W. R. *J. Chem. Phys.* **1985**, *82*, 299. (c) Ehlers, A. W.; Böhme, M.; Dapprich, S.; Gobbi, A.; Höllwarth, A.; Jonas, V.; Köhler, K. F.; Stegmann, R.; Veldkamp, A.; Frenking, G. *Chem. Phys. Lett.* **1993**, *208*, 111. (d) Andrae, D.; Haeussermann, U.; Dolg, M.; Stoll, H.; Preuss, H. *Theor. Chim. Acta* **1990**, *77*, 123.

30. (a) Murdzek, J. S.; Schrock, R. R. in Ref. 5d, pp. 155-164. (b) Schrock, R. R.; Sancho, J.; Pederson, S. F. *Inorg. Synth.* **1989**, *26*, 44.
31. Diminnie, J. B.; Hall, H. D.; Xue, Z. *Chem. Comm*. **1996**, 2383.
32. (a) Toreki, R.; Schrock, R. R. *J. Am. Chem. Soc*. **1992**, *114*, 3367. (b) Toreki, R.; Vaughan, G. A.; Schrock, R. R.; Davis, W. M. *J. Am. Chem. Soc.* **1993**, *115*, 127.
33. Wood, C. D.; McLain, S. J.; Schrock, R. R. *J. Am. Chem. Soc.* **1979**, *101*, 3210.
34. (a) *The Activation of Dioxygen and Homogeneous Catalytic Oxidation*, Barton, D. H. R., Martell, A. E.; Sawyer, D. T. Eds, Plenum: New York, 1993. (b) Theopold, K. H.; Reinaud, O. M.; Blanchard, S.; Leelasubeharoen, S.; Hess, A.; Thyagarajan, S. *ACS Symp. Ser.* **2002**, *823*, 75. (c) *Advances in Catalytic Activation of Dioxygen by Metal Complexes*. *Catalysis by Metal Complexes*, **2003**, *26* (Simándi, L. I. Ed,). (d) Que, L.,

Jr.; Tolman, W. B. *Angew. Chem. Inter. Ed.* **2002**, *41*, 1114. (e) *Metal Catalyzed Oxidations of Organic Compounds*, Sheldon, R. A.; Kochi, J. K., Academic Press: New York, 1981.

35. Veige, A. S.; Slaughter, L. M.; Lobkovsky, E. B.; Wolczanski, P. T.; Matsunaga, N.; Decker, S. A.; Cundari., T. R. *Inorg. Chem*. **2003**, *42*, 6204.
36. See, e.g., (a) Feinstein-Jaffe, I.; Gibson, D.; Lippard, S. J.; Schrock, R. R.; Spool, A. *J. Am. Chem. Soc.* **1984**, *106*, 6305. (b) Feng, S. G.; Luan, L.; White, P.; Brookhart, M. S.; Templeton, J. L.; Young, C. G. *Inorg. Chem.* **1991**, *30*, 2582. (c) Blosch, L. L.; Abboud, K.; Boncella, J. M. *J. Am. Chem. Soc.* **1991**, *113*, 7066.
37. The electronegativities of C and Si are 2.55 and 1.90, respectively.
38. Shriver, D.; Atkins, P. *Inorganic Chemistry*, 3rd ed., W. H. Freeman and Co.: New York, pp. 296-297.
39. See also reviews on organometallics in aqueous solution: (a) Darensbourg, D. J. in *Aqueous-Phase Organometallic Catalysis*, Cornils, B. and Herrmann, W. A. Eds., 2nd ed.: Wiley-VCH, 2004. (b) Roundhill, D. M. *Adv. Organomet. Chem.* **1995**, *38*, 155.
40. Hillhouse, G. L.; Bercaw, J. E. *J. Am. Chem. Soc.* **1984**, *106,* 5412.
41. Rosenthal, U.; Ohff, A.; Michalik, M.; Goerls, H.; Burlakov, V. V.; Shur, V. B. *Organometallics* **1993**, *12*, 5016.
42. van Asselt, A.; Burger, B. J.; Gibson, V. C.; Bercaw, J. E. *J. Am. Chem. Soc.* **1986**, *108,* 5347.
43. See, e.g., (a) Feinstein-Jaffe, I.; Gibson, D.; Lippard, S. J.; Schrock, R. R.;

Spool, A. *J. Am. Chem. Soc.* **1984**, *106*, 6305. (b) Feng, S. G.; Luan, L.; White, P.; Brookhart, M. S.; Templeton, J. L.; Young, C. G. *Inorg. Chem.* **1991**, *30*, 2582. (c) Blosch, L. L.; Abboud, K.; Boncella, J. M. *J. Am. Chem. Soc.* **1991**, *113*, 7066.

44. (a) Feinstein-Jaffe, I.; Pedersen, S. F.; Schrock, R. R. *J. Am. Chem. Soc.* **1983,** *105*, 7176. (b) Schoettel, G.; Kress, J.; Fischer, J.; Osborn, J. A. *J. Chem. Soc. Chem. Comm.* **1988**, 914. (c) Legzdins, P.; Phillips, E. C.; Rettig, S. J.; Sanchez, L.; Trotter, J.; Yee, V. C. *Organometallics* **1988**, *7*, 1877.

45. See, e.g., (a) Lim, B. S.; Rahtu, A.; Gordon, R. G. *Nature Mater.* **2003**, *2*, 749. (b) Hausmann, D. M.; de Rouffignac, P.; Smith, A.; Gordon, R.; Monsma, D. *Thin Solid Films* **2003**, *443*, 1. (c) Gordon, R. G.; Becker, J.; Hausmann, D.; Suh, S. *Chem. Mater.* **2001**, *13*, 2463. (d) Smith, R. C.; Ma, T.; Campbell, S. A.; Gladfelter, W. L. US Patent Application, 2003, 20030092287. (e) Baum, T. H.; Xu, C.; Hendrix, B. C.; Roeder, J. F. PCT International Application 2002, WO 2002079211.

APPENDIX

Table A1. Atomic coordinates ($\times 10^4$) and equivalent isotropic displacement parameters ($Å^2 \times 10^3$) for **3b**. *U*(eq) is defined as one third of the trace of the orthogonalized U_{ij} tensor.

	x	y	z	*U*(eq)
W(1)	3333	6667	9210(1)	59(1)
P(1)	3333	6667	11286(4)	63(1)
C(1)	3840(20)	8228(18)	11950(20)	99(8)
C(2)	5036(11)	8174(11)	9337(15)	70(4)
Si(1)	6694(4)	8485(3)	9184(7)	65(1)
C(3)	7440(20)	9410(20)	7903(16)	103(8)
C(4)	7670(20)	9428(19)	10394(17)	105(8)
C(5)	6733(14)	6956(11)	9130(20)	112(6)
C(6)	2560(30)	6480(40)	7679(14)	69(10)
Si(2)	3333	6667	6288(4)	64(1)
C(7)	4730(20)	6450(30)	6460(30)	44(10)
C(8)	3910(40)	8350(20)	5840(50)	310(110)
C(9)	2260(30)	5570(40)	5210(30)	101(18)

Table A2. Bond distances (Å) for **3b**.

Bond	Distance	Bond	Distance
W(1)-C(2)#1	1.964(12)	Si(2)-C(9)#2	1.854(15)
W(1)-C(2)	1.964(12)	Si(2)-C(9)#1	1.854(15)
W(1)-C(2)#2	1.964(12)	Si(2)-C(9)	1.854(15)
W(1)-C(6)#2	2.041(18)	Si(2)-C(6)#1	1.889(19)
W(1)-C(6)#1	2.041(19)	Si(2)-C(6)#2	1.889(19)
W(1)-C(6)	2.041(18)	Si(2)-C(8)#2	1.874(16)
W(1)-P(1)	2.514(5)	Si(2)-C(8)	1.874(16)
P(1)-C(1)#1	1.86(2)	Si(2)-C(8)#1	1.874(16)
P(1)-C(1)#2	1.86(2)	Si(2)-C(7)	1.858(15)
P(1)-C(1)	1.86(2)	Si(2)-C(7)#2	1.858(15)
C(2)-Si(1)	1.860(13)	Si(2)-C(7)#1	1.858(15)
Si(1)-C(4)	1.871(13)	C(7)-C(8)#1	0.84(7)
Si(1)-C(3)	1.861(13)	C(7)-C(9)#2	1.62(6)
Si(1)-C(5)	1.879(10)	C(7)-C(6)#2	1.98(4)
C(6)-C(6)#1	1.48(4)	C(8)-C(7)#2	0.84(7)
C(6)-C(6)#2	1.48(4)	C(8)-C(9)#1	1.06(7)

Table A2. Continued

Bond	Distance	Bond	Distance
C(6)-Si(2)	1.889(19)	C(9)-C(8)#2	1.06(7)
C(6)-C(7)#1	1.98(4)	C(9)-C(7)#1	1.62(6)

Symmetry transformations used to generate equivalent atoms:

#1 -x+y,-x+1,z #2 -y+1,x-y+1,z

Table A3. Bond angles (°) in **3b**.

Bond	Angle	Bond	Angle
C(2)#1-W(1)-C(2)	119.39(15)	C(6)#2-W(1)-C(6)	42.5(11)
C(2)-W(1)-C(2)#2	119.39(14)	C(6)#1-W(1)-C(6)	42.5(11)
C(2)#1-W(1)-C(6)#2	71.1(8)	C(2)#1-W(1)-P(1)	85.5(5)
C(2)-W(1)-C(6)#2	98.7(14)	C(2)-W(1)-P(1)	85.5(5)
C(2)#2-W(1)-C(6)#2	112.7(11)	C(2)#2-W(1)-P(1)	85.5(5)
C(2)#1-W(1)-C(6)#1	112.7(11)	C(2)#1-W(1)-C(2)#2	119.39(15)
C(2)-W(1)-C(6)#1	71.1(8)	C(6)#2-W(1)-P(1)	155.3(6)
C(2)#2-W(1)-C(6)#1	98.7(14)	C(6)#1-W(1)-P(1)	155.3(6)
C(6)#2-W(1)-C(6)#1	42.5(11)	C(6)-W(1)-P(1)	155.3(6)
C(2)#1-W(1)-C(6)	98.7(14)	C(1)#1-P(1)-C(1)#2	102.8(9)
C(2)-W(1)-C(6)	112.7(12)	C(1)#1-P(1)-C(1)	102.8(9)
C(2)#2-W(1)-C(6)	71.1(8)	C(1)#2-P(1)-C(1)	102.8(9)
C(1)#1-P(1)-W(1)	115.6(7)	C(6)#2-C(6)-W(1)	68.8(5)
C(1)#2-P(1)-W(1)	115.6(7)	Si(2)-C(6)-W(1)	128.4(12)
C(1)-P(1)-W(1)	115.6(7)	C(7)#1-C(6)-W(1)	143(2)
Si(1)-C(2)-W(1)	135.1(7)	C(9)#2-Si(2)-C(9)#1	76(2)
C(2)-Si(1)-C(4)	109.5(12)	C(9)#2-Si(2)-C(9)	76(2)
C(2)-Si(1)-C(3)	110.8(8)	C(9)#1-Si(2)-C(9)	76(2)
C(4)-Si(1)-C(3)	108.5(6)	C(9)#2-Si(2)-C(6)	160.5(16)

Table A3. Continued

Bond	Angle	Bond	Angle
C(2)-Si(1)-C(5)	111.2(6)	C(9)#1-Si(2)-C(6)	122(2)
C(4)-Si(1)-C(5)	108.0(7)	C(9)-Si(2)-C(6)	114.5(15)
C(3)-Si(1)-C(5)	108.7(7)	C(9)#2-Si(2)-C(6)#1	122(2)
C(6)#1-C(6)-C(6)#2	60.002(17)	C(9)#1-Si(2)-C(6)#1	114.5(15)
C(6)#1-C(6)-Si(2)	66.9(6)	C(9)-Si(2)-C(6)#1	160.5(16)
C(6)#2-C(6)-Si(2)	66.9(6)	C(6)-Si(2)-C(6)#1	46.1(12)
C(6)#1-C(6)-C(7)#1	123.1(13)	C(9)#2-Si(2)-C(6)#2	114.5(15)
C(6)#2-C(6)-C(7)#1	87(3)	C(9)#1-Si(2)-C(6)#2	160.5(16)
Si(2)-C(6)-C(7)#1	57.4(9)	C(9)-Si(2)-C(6)#2	122(2)
C(6)#1-C(6)-W(1)	68.8(5)	C(6)-Si(2)-C(6)#2	46.1(11)
C(6)#1-Si(2)-C(6)#2	46.1(11)	C(6)#1-Si(2)-C(8)#2	128(2)
C(9)#2-Si(2)-C(8)#2	108.8(10)	C(6)#2-Si(2)-C(8)#2	106.1(19)
C(9)#1-Si(2)-C(8)#2	85(3)	C(9)#2-Si(2)-C(8)	85(3)
C(9)-Si(2)-C(8)#2	33(2)	C(9)#1-Si(2)-C(8)	33(2)
C(6)-Si(2)-C(8)#2	83(2)	C(9)-Si(2)-C(8)	108.8(10)
C(6)-Si(2)-C(8)	106.1(19)	C(9)#1-Si(2)-C(7)#2	51.7(19)
C(6)#1-Si(2)-C(8)	83(2)	C(9)-Si(2)-C(7)#2	120.8(18)
C(6)#2-Si(2)-C(8)	128(2)	C(6)-Si(2)-C(7)#2	79.9(18)
C(8)#2-Si(2)-C(8)	112.1(17)	C(6)#1-Si(2)-C(7)#2	63.7(16)

Table A3. Continued

Bond	Angle	Bond	Angle
C(9)#2-Si(2)-C(8)#1	33(2)	C(6)#2-Si(2)-C(7)#2	108.9(12)
C(9)#1-Si(2)-C(8)#1	108.8(10)	C(8)#2-Si(2)-C(7)#2	108.4(11)
C(9)-Si(2)-C(8)#1	85(3)	C(8)-Si(2)-C(7)#2	26(2)
C(6)-Si(2)-C(8)#1	128(2)	C(8)#1-Si(2)-C(7)#2	132.6(11)
C(6)#1-Si(2)-C(8)#1	106.1(19)	C(7)-Si(2)-C(7)#2	118.8(4)
C(6)#2-Si(2)-C(8)#1	83(2)	C(9)#2-Si(2)-C(7)#1	120.8(18)
C(8)#2-Si(2)-C(8)#1	112.1(18)	C(9)#1-Si(2)-C(7)#1	109.9(10)
C(8)-Si(2)-C(8)#1	112.1(18)	C(9)-Si(2)-C(7)#1	51.7(19)
C(9)#2-Si(2)-C(7)	51.7(19)	C(6)-Si(2)-C(7)#1	63.7(16)
C(9)#1-Si(2)-C(7)	120.8(18)	C(6)#1-Si(2)-C(7)#1	108.9(12)
C(9)-Si(2)-C(7)	109.9(10)	C(6)#2-Si(2)-C(7)#1	79.9(18)
C(6)-Si(2)-C(7)	108.9(12)	C(8)#2-Si(2)-C(7)#1	26(2)
C(6)#1-Si(2)-C(7)	79.9(18)	C(8)-Si(2)-C(7)#1	132.6(11)
C(6)#2-Si(2)-C(7)	63.7(16)	C(8)#1-Si(2)-C(7)#1	108.4(11)
C(8)#2-Si(2)-C(7)	132.6(11)	C(7)-Si(2)-C(7)#1	118.8(4)
C(8)-Si(2)-C(7)	108.4(11)	C(7)#2-Si(2)-C(7)#1	118.8(4)
C(8)#1-Si(2)-C(7)	26(2)	C(8)#1-C(7)-C(9)#2	36(2)
C(9)#2-Si(2)-C(7)#2	109.9(10)	C(8)#1-C(7)-Si(2)	78.0(18)
C(9)#2-C(7)-Si(2)	64.0(12)	C(7)#2-C(8)-Si(2)	75.8(16)

Table A3. Continued

Bond	Angle	Bond	Angle
C(8)#1-C(7)-C(6)#2	118(2)	C(8)#2-C(9)-Si(2)	74.5(15)
C(9)#2-C(7)-C(6)#2	121.9(14)	C(9)#1-C(8)-Si(2)	72.4(15)
Si(2)-C(7)-C(6)#2	58.9(11)	C(8)#2-C(9)-C(7)#1	28(3)
C(7)#2-C(8)-C(9)#1	116(3)	C(7)#1-C(9)-Si(2)	64.2(11)

Symmetry transformations used to generate equivalent atoms:

#1 -x+y,-x+1,z #2 -y+1,x-y+1,z

Table A4. Anisotropic displacement parameters ($Å^2 \times 10^3$) for **3b**. The anisotropic displacement factor exponent takes the form: $-2\pi^2[h^2a^{*2}U_{11} + ... + 2hka^*b^*U_{12}]$.

	U_{11}	U_{22}	U_{33}	U_{23}	U_{13}	U_{12}
W(1)	73(1)	73(1)	31(1)	0	0	36(1)
P(1)	78(2)	78(2)	34(2)	0	0	39(1)
C(2)	94(6)	86(7)	53(9)	44(8)	4(6)	62(5)
Si(1)	80(2)	26(1)	76(2)	8(3)	-37(3)	16(2)
C(3)	71(11)	170(20)	82(8)	27(13)	5(9)	72(14)
C(4)	113(15)	59(11)	85(9)	1(9)	-24(12)	1(11)
C(5)	75(9)	76(9)	196(18)	-22(13)	42(19)	46(8)
C(6)	89(19)	120(30)	45(7)	16(19)	6(9)	80(20)
Si(2)	78(2)	78(2)	38(3)	0	0	39(1)

Table A5. Hydrogen coordinates ($\times 10^4$) and isotropic displacement parameters ($Å^2 \times 10^3$) for **3b**.

	x	y	z	*U*(eq)
H(1A)	3666	8107	12742	148
H(1B)	3362	8606	11623	148
H(1C)	4751	8797	11826	148
H(2A)	5003	8789	8821	84
H(2B)	5032	8503	10085	84
H(3A)	7355	10168	7888	154
H(3B)	7012	8876	7257	154
H(3C)	8343	9658	7889	154
H(4A)	7992	10336	10260	157
H(4B)	8382	9278	10498	157
H(4C)	7136	9165	11060	157
H(5A)	6198	6429	8524	168
H(5B)	6410	6497	9832	168
H(5C)	7610	7146	9020	168
H(6A)	2245	7074	7676	83
H(6B)	1811	5654	7676	83
H(7A)	4520	5623	6738	67

Table A5. Continued

	x	y	z	*U*(eq)
H(7B)	5135	6573	5749	67
H(7C)	5304	7092	6959	67
H(8A)	4274	8457	5119	469
H(8B)	3157	8413	5805	469
H(8C)	4518	8997	6326	469
H(9A)	2049	4752	5489	152
H(9B)	1499	5626	5140	152
H(9C)	2653	5697	4495	152

Table A6. Atomic coordinates ($\times 10^4$) and equivalent isotropic displacement parameters ($Å^2 \times 10^3$) for **11**. *U*(eq) is defined as one third of the trace of the orthogonalized U_{ij} tensor.

	X	y	z	*U*(eq)
C(1)	6791(7)	5740(9)	8323(6)	50(2)
C(2)	7870(4)	7663(6)	6970(4)	48(2)
C(3)	7984(5)	4246(6)	6889(5)	56(2)
C(4)	8409(4)	5930(7)	8145(4)	51(2)
C(5)	6139(6)	3123(9)	7884(5)	89(3)
C(6)	7377(5)	3208(11)	9043(7)	102(4)
C(7)	5852(10)	4203(13)	9481(8)	104(5)
C(8)	8060(14)	9386(19)	8347(13)	263(15)
C(9)	7763(10)	10518(11)	6801(11)	172(8)
C(10)	6532(6)	9112(9)	7591(18)	208(12)
C(11)	8370(10)	5343(18)	5306(7)	172(8)
C(12)	8958(10)	2804(12)	5753(9)	210(11)
C(13)	9593(7)	5070(20)	6514(9)	170(8)
C(14)	9809(5)	7248(10)	8707(6)	96(4)
C(15)	9674(6)	4367(12)	8850(7)	108(4)
C(16)	8732(7)	6051(12)	9883(5)	106(4)
C(17)	5951(11)	4353(13)	5591(8)	107(6)

Table A6. Continued

	X	y	z	*U*(eq)
C(18)	6042(6)	7053(12)	5408(7)	121(5)
C(19)	5138(6)	5994(10)	6564(6)	89(3)
O(1)	6657(5)	5842(7)	6637(5)	71(2)
P(1)	6010(1)	5829(2)	6103(1)	58(1)
Si(1)	6558(1)	4098(2)	8669(1)	58(1)
Si(2)	7549(1)	9158(2)	7442(5)	66(1)
Si(3)	8713(1)	4350(2)	6124(1)	64(1)
Si(4)	9152(1)	5915(3)	8886(1)	65(1)
W(1)	7654(1)	5895(1)	7488(1)	35(1)

Table A7. Bond distances (Å) for **11**.

Bond	Distance	Bond	Distance
C(1)-Si(1)	1.873(10)	C(15)-Si(4)	1.878(11)
C(1)-W(1)	2.115(11)	C(16)-Si(4)	1.878(11)
C(2)-Si(2)	1.860(8)	C(17)-P(1)	1.788(12)
C(2)-W(1)	2.097(7)	C(18)-P(1)	1.756(10)
C(3)-Si(3)	1.856(7)	C(19)-P(1)	1.760(10)
C(3)-W(1)	2.102(7)	O(1)-W(1)	2.307(8)
C(4)-Si(4)	1.842(8)	O(1)-P(1)	1.479(8)
C(4)-W(1)	1.763(8)	Si(1)-C(1)-W(1)	116.7(5)
C(5)-Si(1)	1.852(9)	Si(2)-C(2)-W(1)	120.4(4)
C(6)-Si(1)	1.855(9)	Si(3)-C(3)-W(1)	119.8(4)
C(7)-Si(1)	1.886(14)	P(1)-O(1)-W(1)	178.7(6)
C(8)-Si(2)	1.820(18)	W(1)-C(4)-Si(4)	175.7(5)
C(9)-Si(2)	1.846(13)	C(14)-Si(4)-C(4)	109.7(4)
C(10)-Si(2)	1.840(10)	C(14)-Si(4)-C(15)	109.5(6)
C(11)-Si(3)	1.856(13)	C(2)-W(1)-C(1)	119.5(3)
C(12)-Si(3)	1.801(12)	C(3)-W(1)-C(1)	118.3(3)
C(13)-Si(3)	1.871(14)	C(4)-W(1)-O(1)	179.5(3)
C(14)-Si(4)	1.856(9)		

Symmetry transformations used to generate equivalent atoms: #1 x, -y+1/2, z

Table A8. Bond angles (°) for **11**.

Bond	Angle	Bond	Angle
C(4)-Si(4)-C(15)	110.1(5)	C(11)-Si(3)-C(3)	109.7(5)
C(14)-Si(4)-C(16)	110.3(5)	C(12)-Si(3)-C(13)	106.6(9)
C(4)-Si(4)-C(16)	110.0(5)	C(11)-Si(3)-C(13)	109.0(9)
C(15)-Si(4)-C(16)	107.2(5)	C(3)-Si(3)-C(13)	111.1(5)
C(6)-Si(1)-C(5)	107.0(6)	O(1)-P(1)-C(18)	113.0(5)
C(6)-Si(1)-C(1)	113.5(5)	O(1)-P(1)-C(19)	114.5(5)
C(5)-Si(1)-C(1)	111.7(5)	C(18)-P(1)-C(19)	105.3(6)
C(6)-Si(1)-C(7)	107.6(6)	O(1)-P(1)-C(17)	111.1(7)
C(5)-Si(1)-C(7)	107.5(6)	C(18)-P(1)-C(17)	107.7(7)
C(1)-Si(1)-C(7)	109.3(5)	C(19)-P(1)-C(17)	104.7(7)
C(8)-Si(2)-C(10)	112.4(12)	C(4)-W(1)-C(2)	96.4(3)
C(8)-Si(2)-C(9)	107.7(10)	C(4)-W(1)-C(3)	96.6(4)
C(10)-Si(2)-C(9)	108.0(8)	C(2)-W(1)-C(3)	118.1(3)
C(8)-Si(2)-C(2)	109.2(5)	C(4)-W(1)-C(1)	97.3(4)
C(10)-Si(2)-C(2)	110.1(5)	C(2)-W(1)-O(1)	84.0(3)
C(9)-Si(2)-C(2)	109.3(7)	C(3)-W(1)-O(1)	83.5(3)
C(12)-Si(3)-C(11)	108.7(8)	C(1)-W(1)-O(1)	82.2(3)
C(12)-Si(3)-C(3)	111.6(5)		

Symmetry transformations used to generate equivalent atoms: #1 x, -y+1/2, z

Table A9. Anisotropic displacement parameters ($Å^2 \times 10^3$) for **11**. The anisotropic displacement factor exponent takes the form: $-2\pi^2[h^2a^{*2}U_{11} + ... + 2hka^*b^*U_{12}]$.

	U_{11}	U_{22}	U_{33}	U_{23}	U_{13}	U_{12}
C(1)	58(6)	46(5)	45(5)	-8(4)	17(4)	-2(4)
C(2)	49(4)	44(4)	49(4)	2(3)	3(3)	-5(3)
C(3)	63(5)	43(4)	61(5)	0(3)	22(4)	2(3)
C(4)	44(4)	70(5)	39(4)	8(4)	4(3)	-3(4)
C(5)	106(8)	75(6)	87(7)	15(5)	10(6)	-32(6)
C(6)	86(7)	97(8)	123(10)	70(7)	22(6)	23(6)
C(7)	107(12)	109(10)	96(9)	1(8)	53(9)	0(8)
C(8)	310(30)	203(19)	280(20)	-202(19)	-150(20)	144(19)
C(9)	227(18)	41(6)	250(20)	40(9)	99(15)	8(8)
C(10)	72(7)	71(6)	480(40)	-46(17)	100(20)	7(5)
C(11)	199(18)	246(19)	70(8)	60(10)	75(10)	82(15)
C(12)	290(20)	102(10)	233(18)	-51(10)	218(18)	-14(12)
C(13)	71(9)	320(20)	124(12)	-40(16)	43(9)	-55(13)
C(14)	67(6)	134(10)	86(7)	16(6)	-20(5)	-36(6)
C(15)	77(7)	163(12)	84(7)	43(8)	6(6)	47(7)
C(16)	114(9)	165(12)	40(5)	16(6)	-20(5)	-25(8)

Table A9. Continued

	U_{11}	U_{22}	U_{33}	U_{23}	U_{13}	U_{12}
C(17)	124(14)	112(11)	86(8)	-34(8)	-32(9)	-8(10)
C(18)	88(8)	166(12)	108(9)	77(9)	-29(7)	-37(8)
C(19)	73(7)	125(9)	68(6)	-9(6)	-4(5)	11(6)
O(1)	65(5)	85(5)	63(4)	5(4)	-21(4)	-10(4)
P(1)	50(1)	82(1)	44(1)	1(1)	-9(1)	-10(1)
Si(1)	54(1)	61(1)	58(1)	14(1)	19(1)	-1(1)
Si(2)	70(1)	41(1)	86(2)	6(3)	22(2)	2(1)
Si(3)	71(2)	63(2)	58(1)	-6(1)	31(1)	1(1)
Si(4)	50(1)	97(2)	47(1)	14(1)	-10(1)	-8(1)
W(1)	34(1)	38(1)	33(1)	0(1)	2(1)	-1(1)

Table A10. Hydrogen coordinates ($\times 10^4$) and isotropic displacement parameters ($Å^2 \times 10^3$) for **11**.

	x	y	z	*U*(eq)
H(1A)	6930	6247	8772	60
H(1B)	6342	6113	8105	60
H(2A)	8406	7729	6904	57
H(2B)	7654	7642	6452	57
H(3A)	8157	3640	7274	67
H(3B)	7541	3886	6651	67
H(5A)	6480	3075	7454	134
H(5B)	5680	3506	7715	134
H(5C)	6041	2282	8076	134
H(6A)	7216	2403	9245	153
H(6B)	7612	3690	9449	153
H(6C)	7727	3072	8628	153
H(7A)	5760	3369	9686	156
H(7B)	5394	4553	9284	156
H(7C)	6043	4741	9886	156
H(8A)	7714	9408	8774	395
H(8B)	8330	10173	8325	395
H(8C)	8404	8695	8419	395

Table A10. Continued

	x	y	z	*U*(eq)
H(9A)	8237	10875	6944	259
H(9B)	7381	11153	6855	259
H(9C)	7783	10234	6271	259
H(10A)	6386	9793	7931	311
H(10B)	6395	8313	7821	311
H(10C)	6283	9205	7100	311
H(11A)	8768	5873	5120	257
H(11B)	7964	5866	5482	257
H(11C)	8199	4802	4892	257
H(12A)	8525	2414	5526	315
H(12B)	9139	2283	6171	315
H(12C)	9341	2891	5366	315
H(13A)	9472	5775	6843	256
H(13B)	9899	5350	6090	256
H(13C)	9859	4439	6811	256
H(14A)	9981	7216	8179	144
H(14B)	10228	7177	9053	144
H(14C)	9558	8041	8798	144
H(15A)	9981	4344	8393	162

Table A10. Continued

	x	y	z	*U*(eq)
H(15B)	9324	3675	8836	162
H(15C)	9983	4290	9304	162
H(16A)	9115	6269	10251	159
H(16B)	8511	5253	10027	159
H(16C)	8355	6700	9882	159
H(17A)	6418	4184	5336	161
H(17B)	5560	4401	5209	161
H(17C)	5843	3681	5952	161
H(18A)	6092	7857	5667	181
H(18B)	5590	7047	5107	181
H(18C)	6462	6923	5070	181
H(19A)	5065	5301	6920	133
H(19B)	4749	5985	6180	133
H(19C)	5124	6783	6843	133

Table A11. Atomic coordinates ($\times 10^4$) and equivalent isotropic displacement parameters ($Å^2 \times 10^3$) for **13**. *U*(eq) is defined as one third of the trace of the orthogonalized U_{ij} tensor.

	x	y	z	*U*(eq)
C(1)	6667	3333	1544(2)	43(3)
C(2)	6391(5)	4261(5)	1181(1)	63(2)
C(3)	7706(4)	4766(4)	1860(1)	35(1)
C(4)	8866(5)	5961(5)	1514(1)	51(2)
C(5)	9398(5)	4575(5)	1686(1)	58(2)
C(6)	9757(5)	6303(5)	1923(1)	58(2)
C(7)	7283(4)	2455(4)	2447(1)	32(1)
C(8)	9140(4)	3833(5)	2228(1)	49(2)
C(9)	8910(5)	2043(5)	2425(1)	64(2)
C(10)	9180(4)	3733(5)	2671(1)	51(2)
C(11)	7504(4)	4564(4)	3040(1)	48(2)
C(12)	4575(6)	7420(6)	1331(1)	89(3)
C(13)	2262(4)	5223(4)	727(1)	38(1)
C(14)	245(5)	3582(5)	694(1)	90(3)
C(15)	752(4)	5486(5)	508(1)	49(2)
C(16)	643(5)	5286(6)	951(1)	77(2)

Table A11. Continued

	x	y	z	*U*(eq)
C(17)	3333	6667	9799(1)	30(2)
C(18)	4110(5)	7908(4)	9430(1)	50(2)
C(19)	2380(4)	5215(4)	10114(1)	34(1)
C(20)	3657(5)	4496(5)	9928(1)	52(2)
C(21)	1709(5)	3975(4)	9752(1)	52(2)
C(22)	1835(5)	3128(5)	10138(1)	64(2)
O(1)	6667	3333	2181(1)	33(2)
O(2)	6667	3333	2716(1)	31(2)
O(3)	3333	6667	464(1)	39(2)
O(4)	3333	6667	997(1)	50(2)
Si(1)	6667	3333	1274(1)	46(1)
Si(2)	8925(1)	5383(1)	1745(1)	37(1)
Si(3)	8637(1)	3032(1)	2443(1)	30(1)
Si(4)	6667	3333	2954(1)	29(1)
Si(5)	3333	6667	1242(1)	61(1)
Si(6)	970(1)	4908(1)	721(1)	45(1)
Si(7)	3333	6667	9528(1)	31(1)
Si(8)	2412(1)	4227(1)	9982(1)	37(1)

Table A11. Continued

	x	y	z	*U*(eq)
W(1)	6667	3333	1804(1)	26(1)
W(2)	6667	3333	2434(1)	21(1)
W(3)	3333	6667	717(1)	32(1)
W(4)	3333	6667	10056(1)	24(1)

Table A12. Bond distances (Å) for **13**.

Bond	Distance	Bond	Distance
C(1)-W(1)	1.775(11)	C(1)-Si(1)	1.846(11)
C(2)-Si(1)	1.871(6)	C(3)-Si(2)	1.872(6)
C(3)-W(1)	2.100(5)	C(4)-Si(2)	1.862(6)
C(5)-Si(2)	1.852(6)	C(6)-Si(2)	1.869(6)
C(7)-Si(3)	1.895(5)	C(7)-W(2)	2.098(5)
C(8)-Si(3)	1.857(6)	C(9)-Si(3)	1.856(6)
C(10)-Si(3)	1.866(6)	C(11)-Si(4)	1.851(6)
C(12)-Si(5)	1.848(8)	C(13)-Si(6)	1.880(6)
C(13)-W(3)	2.091(5)	C(14)-Si(6)	1.862(7)
C(15)-Si(6)	1.853(6)	C(16)-Si(6)	1.856(8)
C(17)-W(4)	1.756(9)	C(17)-Si(7)	1.859(10)
C(18)-Si(7)	1.873(6)	C(19)-Si(8)	1.854(6)
C(19)-W(4)	2.096(5)	C(20)-Si(8)	1.866(6)
C(21)-Si(8)	1.863(6)	C(22)-Si(8)	1.869(6)
O(1)-W(2)	1.735(6)	O(1)-W(1)	2.578(6)
O(2)-Si(4)	1.630(6)	O(2)-W(2)	1.924(6)
O(3)-W(3)	1.731(7)	O(4)-Si(5)	1.676(8)
O(4)-W(3)	1.913(8)	Si(1)-C(2)#1	1.871(6)
Si(1)-C(2)#2	1.871(6)	Si(4)-C(11)#1	1.851(6)

Table A12. Continued

Bond	Distance	Bond	Distance
Si(4)-C(11)#2	1.851(6)	Si(5)-C(12)#3	1.848(8)
Si(5)-C(12)#4	1.848(8)	Si(7)-C(18)#3	1.873(6)
Si(7)-C(18)#4	1.873(6)	W(1)-C(3)#1	2.100(5)
W(1)-C(3)#2	2.100(5)	W(2)-C(7)#2	2.098(5)
W(2)-C(7)#1	2.098(5)	W(3)-C(13)#4	2.091(5)
W(3)-C(13)#3	2.091(5)	W(4)-C(19)#4	2.096(5)
W(4)-C(19)#3	2.096(5)		

Symmetry transformations used to generate equivalent atoms:

#1 -x+y+1,-x+1,z #2 -y+1,x-y,z #3 -y+1,x-y+1,z

#4 -x+y,-x+1,z

Table A13. Bond angles (°) for **13**.

Bond	Angle	Bond	Angle
W(1)-C(1)-Si(1)	180.0	Si(2)-C(3)-W(1)	123.7(3)
Si(3)-C(7)-W(2)	119.0(3)	Si(6)-C(13)-W(3)	119.1(3)
W(4)-C(17)-Si(7)	180.000(1)	Si(8)-C(19)-W(4)	123.1(3)
W(2)-O(1)-W(1)	180.0	Si(4)-O(2)-W(2)	180.0
Si(5)-O(4)-W(3)	180.000(1)	C(1)-Si(1)-C(2)#1	110.0(2)
C(1)-Si(1)-C(2)#2	110.0(2)	C(2)#1-Si(1)-C(2)#2	109.0(2)
C(1)-Si(1)-C(2)	110.0(2)	C(2)#1-Si(1)-C(2)	109.0(2)
C(2)#2-Si(1)-C(2)	109.0(2)	C(5)-Si(2)-C(4)	107.9(3)
C(5)-Si(2)-C(3)	114.2(3)	C(4)-Si(2)-C(3)	108.6(3)
C(5)-Si(2)-C(6)	108.4(3)	C(4)-Si(2)-C(6)	110.6(3)
C(3)-Si(2)-C(6)	107.1(3)	C(8)-Si(3)-C(9)	109.7(3)
C(8)-Si(3)-C(10)	109.4(3)	C(9)-Si(3)-C(10)	109.4(3)
C(8)-Si(3)-C(7)	110.4(3)	C(9)-Si(3)-C(7)	106.8(3)
C(10)-Si(3)-C(7)	111.1(3)	O(2)-Si(4)-C(11)#1	108.6(2)
O(2)-Si(4)-C(11)	108.6(2)	C(11)#1-Si(4)-C(11)	110.3(2)
O(2)-Si(4)-C(11)#2	108.6(2)	C(11)#1-Si(4)-C(11)#2	110.3(2)
C(11)-Si(4)-C(11)#2	110.3(2)	O(4)-Si(5)-C(12)#3	109.2(3)
O(4)-Si(5)-C(12)	109.2(3)	C(12)#3-Si(5)-C(12)	109.7(3)
O(4)-Si(5)-C(12)#4	109.2(3)	C(12)#3-Si(5)-C(12)#4	109.7(3)

Table A13. Continued

Bond	Angle	Bond	Angle
C(12)-Si(5)-C(12)#4	109.7(3)	C(16)-Si(6)-C(15)	110.2(3)
C(16)-Si(6)-C(14)	109.8(4)	C(15)-Si(6)-C(14)	109.5(3)
C(16)-Si(6)-C(13)	110.4(3)	C(15)-Si(6)-C(13)	110.2(3)
C(14)-Si(6)-C(13)	106.7(3)	C(17)-Si(7)-C(18)#3	110.9(2)
C(17)-Si(7)-C(18)	110.9(2)	C(18)#3-Si(7)-C(18)	108.0(2)
C(17)-Si(7)-C(18)#4	110.9(2)	C(18)#3-Si(7)-C(18)#4	108.0(2)
C(18)-Si(7)-C(18)#4	108.0(2)	C(19)-Si(8)-C(21)	108.9(3)
C(19)-Si(8)-C(20)	112.7(3)	C(21)-Si(8)-C(20)	110.3(3)
C(19)-Si(8)-C(22)	108.7(3)	C(21)-Si(8)-C(22)	108.5(3)
C(20)-Si(8)-C(22)	107.6(3)	C(1)-W(1)-C(3)#1	100.45(15)
C(1)-W(1)-C(3)	100.45(15)	C(3)#1-W(1)-C(3)	116.79(9)
C(1)-W(1)-C(3)#2	100.45(15)	C(3)#1-W(1)-C(3)#2	116.79(9)
C(3)-W(1)-C(3)#2	116.79(9)	C(1)-W(1)-O(1)	180.000(1)
C(3)#1-W(1)-O(1)	79.55(15)	C(3)-W(1)-O(1)	79.55(15)
C(3)#2-W(1)-O(1)	79.55(15)	O(1)-W(2)-O(2)	180.000(1)
O(1)-W(2)-C(7)	92.33(14)	O(2)-W(2)-C(7)	87.67(14)
O(1)-W(2)-C(7)#2	92.33(14)	O(2)-W(2)-C(7)#2	87.67(14)
C(7)-W(2)-C(7)#2	119.84(2)	O(1)-W(2)-C(7)#1	92.33(14)
O(2)-W(2)-C(7)#1	87.67(14)	C(7)-W(2)-C(7)#1	119.84(2)

Table A13. Continued

Bond	Angle	Bond	Angle
C(7)#2-W(2)-C(7)#1	119.84(2)	O(3)-W(3)-O(4)	180.000(1)
O(3)-W(3)-C(13)#4	91.82(17)	O(4)-W(3)-C(13)#4	88.18(17)
O(3)-W(3)-C(13)	91.82(17)	O(4)-W(3)-C(13)	88.18(17)
C(13)#4-W(3)-C(13)	119.900(18)	O(3)-W(3)-C(13)#3	91.82(17)
O(4)-W(3)-C(13)#3	88.18(17)	C(13)#4-W(3)-C(13)#3	119.900(19)
C(13)-W(3)-C(13)#3	119.900(19)	C(17)-W(4)-C(19)#4	100.96(15)
C(17)-W(4)-C(19)	100.96(15)	C(19)#4-W(4)-C(19)	116.47(10)
C(17)-W(4)-C(19)#3	100.96(15)	C(19)#4-W(4)-C(19)#3	116.47(10)
C(19)-W(4)-C(19)#3	116.47(9)		

Symmetry transformations used to generate equivalent atoms:

#1 -x+y+1,-x+1,z #2 -y+1,x-y,z #3 -y+1,x-y+1,z

#4 -x+y,-x+1,z

Table A14. Anisotropic displacement parameters ($Å^2 \times 10^3$) in **13**. The anisotropic displacement factor exponent takes the form: $-2\pi^2[h^2a^{*2}U_{11} + ... + 2hka^*b^*U_{12}]$.

	U_{11}	U_{22}	U_{33}	U_{23}	U_{13}	U_{12}
C(1)	26(4)	26(4)	76(8)	0	0	13(2)
C(2)	81(6)	73(5)	39(4)	18(3)	0(4)	41(5)
C(3)	41(4)	28(3)	37(3)	-1(2)	1(3)	18(3)
C(4)	57(5)	49(4)	47(4)	17(3)	15(3)	27(4)
C(5)	51(5)	67(5)	67(5)	16(4)	22(3)	38(4)
C(6)	50(5)	43(4)	70(5)	9(3)	-2(3)	15(4)
C(7)	32(3)	29(3)	33(3)	-2(2)	-2(2)	15(3)
C(8)	40(4)	56(4)	47(4)	11(3)	11(3)	20(4)
C(9)	42(4)	50(5)	109(6)	7(4)	10(4)	30(4)
C(10)	33(4)	63(5)	42(4)	-3(3)	-6(3)	15(3)
C(11)	48(4)	44(4)	44(4)	-5(3)	-5(3)	18(3)
C(12)	85(7)	97(7)	80(6)	-11(5)	-26(5)	41(6)
C(13)	28(3)	27(3)	57(4)	1(3)	-3(3)	12(3)
C(14)	36(5)	33(5)	185(9)	15(5)	-15(5)	6(4)
C(15)	32(4)	46(4)	68(4)	2(3)	-1(3)	19(3)
C(16)	54(5)	96(7)	80(6)	17(5)	16(4)	37(5)

Table A14. Continued

	U_{11}	U_{22}	U_{33}	U_{23}	U_{13}	U_{12}
C(17)	24(3)	24(3)	41(6)	0	0	12(2)
C(18)	50(4)	45(4)	48(4)	13(3)	8(3)	19(4)
C(19)	28(3)	25(3)	41(3)	4(2)	1(2)	9(3)
C(20)	57(5)	53(4)	60(4)	-9(3)	-5(3)	39(4)
C(21)	60(5)	36(4)	45(4)	-2(3)	-9(3)	14(4)
C(22)	91(6)	36(4)	52(4)	4(3)	-7(4)	23(4)
O(1)	28(2)	28(2)	41(4)	0	0	14(1)
O(2)	28(2)	28(2)	39(4)	0	0	14(1)
O(3)	26(2)	26(2)	64(5)	0	0	13(1)
O(4)	41(3)	41(3)	68(5)	0	0	20(2)
Si(1)	55(1)	55(1)	28(2)	0	0	27(1)
Si(2)	33(1)	32(1)	42(1)	10(1)	6(1)	14(1)
Si(3)	26(1)	34(1)	34(1)	2(1)	1(1)	17(1)
Si(4)	31(1)	31(1)	27(1)	0	0	15(1)
Si(5)	64(2)	64(2)	55(2)	0	0	32(1)
Si(6)	25(1)	34(1)	70(1)	10(1)	5(1)	10(1)
Si(7)	32(1)	32(1)	30(2)	0	0	16(1)
Si(8)	45(1)	24(1)	36(1)	0(1)	-2(1)	14(1)

Table A14. Continued

	U_{11}	U_{22}	U_{33}	U_{23}	U_{13}	U_{12}
W(1)	25(1)	25(1)	28(1)	0	0	13(1)
W(2)	20(1)	20(1)	24(1)	0	0	10(1)
W(3)	23(1)	23(1)	49(1)	0	0	11(1)
W(4)	20(1)	20(1)	32(1)	0	0	10(1)

Table A15. Hydrogen coordinates ($\times 10^4$) and isotropic displacement parameters ($Å^2 \times 10^3$) in **13**.

	x	y	z	*U*(eq)
H(2A)	5774	4123	1228	95
H(2B)	6387	4253	1041	95
H(2C)	6871	4882	1226	95
H(3A)	7413	5148	1827	42
H(3B)	7808	4818	2000	42
H(4A)	9477	6247	1449	76
H(4B)	8706	6448	1543	76
H(4C)	8385	5488	1430	76
H(5A)	8974	4093	1595	87
H(5B)	9443	4273	1803	87
H(5C)	10022	4939	1628	87
H(6A)	9766	5994	2042	87
H(6B)	9542	6750	1949	87
H(6C)	10391	6638	1869	87
H(7A)	7055	2075	2565	38
H(7B)	7034	2013	2338	38
H(8A)	9819	4076	2221	74

Table A15. Continued

	x	y	z	*U*(eq)
H(8B)	9021	4358	2240	74
H(8C)	8842	3479	2111	74
H(9A)	8626	1678	2309	96
H(9B)	8655	1634	2538	96
H(9C)	9592	2307	2421	96
H(10A)	9864	4018	2665	76
H(10B)	8938	3314	2782	76
H(10C)	9016	4227	2683	76
H(11A)	8105	4810	2973	71
H(11B)	7604	4553	3179	71
H(11C)	7236	4969	3014	71
H(12A)	4981	7215	1271	133
H(12B)	4589	7359	1470	133
H(12C)	4799	8078	1298	133
H(13A)	2367	4902	618	46
H(13B)	2357	4950	846	46
H(14A)	378	3283	802	135
H(14B)	407	3392	574	135

Table A15. Continued

	x	y	z	*U*(eq)
H(14C)	-424	3387	694	135
H(15A)	94	5330	507	74
H(15B)	890	5258	389	74
H(15C)	1160	6168	516	74
H(16A)	1003	5972	961	115
H(16B)	786	5006	1060	115
H(16C)	-30	5075	950	115
H(18A)	3822	8291	9458	75
H(18B)	4176	7879	9291	75
H(18C)	4731	8189	9490	75
H(19A)	2446	5119	10252	40
H(19B)	1739	5117	10097	40
H(20A)	3972	5057	9847	78
H(20B)	3635	3962	9860	78
H(20C)	4006	4606	10048	78
H(21A)	1038	3672	9782	77
H(21B)	1825	3558	9670	77
H(21C)	1901	4566	9684	77

Table A15. Continued

	x	y	z	*U*(eq)
H(22A)	2172	3256	10260	96
H(22B)	1857	2613	10072	96
H(22C)	1180	2950	10163	96

VITA

Laurel Anne Morton (maiden name: Laurel Anne Ray) was born on July 12th, 1977 in Evansville, Indiana, to parents Anne Laurel and John Michael Ray. Her father was a high school biology and chemistry teacher, football coach, and later a public health and safety consultant; her mother was a high school mathematics teacher. She grew up on a small cattle farm in Spring City, Tennessee, with her three sisters. At age 10, she moved to Chattanooga, followed four years later by a move to Knoxville, Tennessee, where she attended Farragut High School and enjoyed her drafting, music and science classes. After graduation in May 1995, she enrolled at Tennessee Technological University in Cookeville, Tennessee, the next fall semester. During her first semester at Tennessee Tech, she met her future husband, colleague and best friend, Samuel A. Morton III. She studied chemistry at Tennessee Tech, and conducted her undergraduate research on synthesis of ionic liquids and their use in the extraction of radioactive metal ions from waste water under the direction of Professors Dale Ensor and Dan Swartling. She presented this work at the American Chemical Society (ACS) National Meeting in Anaheim, California, in March 1999. While at Tennessee Tech, she was awarded the F. U. Foster Memorial Chemistry Scholarship for her excellence in the ACS curriculum. She graduated in May 1999 with a Bachelor of science degree in chemistry and began her Ph.D. studies the next fall in the chemistry department at the University of Tennessee, Knoxville. On July 7th, 2001, she married Samuel

Morton III in Knoxville, Tennessee surrounded by family and friends. She studied the synthesis and characterization of novel early-transition-metal complexes and reactions of alkylidyne complexes with oxygen and water under the direction of Professor Zi-Ling (Ben) Xue. While at the University of Tennessee, she was elected by the graduate student body to the position of Vice-President of the Graduate Student Senate. As a fourth year student, Laurel received a departmental outstanding teaching award. In April 2005, she received the Chancellor's Award for Academic Achievement and Chancellor's Award for Professional Promise.